Tidal Farm Electric Energy Production in the Tagus River

José Maria Simões de Almeida de Sousa Ceregeiro

Thesis to obtain the Master of Science Degree in

Civil Engineering

Supervisors:

Prof. Manuel Guilherme Caras Atlas Duarte Pinheiro

Dr. Francisco Javier Campuzano Guillen

Examination Committee

Chairperson: Prof. Rodrigo de Almada Cardoso Proença de Oliveira

Supervisor: Prof. Manuel Guilherme Caras Atlas Duarte Pinheiro

Member of the Committee: Prof. Ramiro Joaquim de Jesus Neves

May 2019

Declaration

I declare that this document is an original work of my own authorship and that it fulfills all the requirements of the Code of Conduct and Good Practices of the Universidade de Lisboa.

Acknowledgements

Few words can truly convey just how grateful I am.

Firstly, I would like to thank my parents. Thank you for having provided me and my siblings with one of the best educations a person could ask for, both at home and in school. Thank you for motivating me and for granting me the freedom to choose whichever college degree I thought would make me happier. You are the reason why I am where I am, and I owe you everything. I'm certain that Life will make sure that your efforts payed off.

Secondly, to my younger brother and sister: thank you for validating my inner child and for making sure that there is never a dull moment at home.

Next, to my girlfriend: few people in this world see me for who I truly am, and you sit at the very top of the ones that know me best. Thank you for supporting me when I most needed it, for always being there for me and for being my best friend.

To my friends, both the ones I made during the course of my degree and the ones that came before that: thank you for being a safety net that I can always fall on, if needed, and for the company you gave, give and hopefully will keep on giving me.

I would also like to thank all those who made it possible for me to finish this work, namely my supervisors Prof.Manuel Duarte Pinheiro and Dr.Francisco Campuzano. To Prof. Manuel Pinheiro, thank you for taking me in and taking a chance on me when no one else would, and for guiding me throughout this whole time; to Dr.Francisco Campuzano (and by affiliation, to MARETEC), for agreeing to collaborate with me in my pursuit of assessing the Tagus' tidal energy potential, and without whom my journey would have been immeasurably more difficult. Thank you both for having read this thesis and amending its flaws, thus ensuring that I'm submitting the best version possible of my work.

Lastly, but certainly not least, to Prof. Manuela Juliano: thank you for our long Skype conversations and screen sharing. Even though the distance that separates us is large, I've felt a very close support, and without you this thesis would not have been the same.

Abstract

The exponential population growth and increasing world energy consumption has prompted the world to search for new forms of renewable energy that could curb our dependence on fossil fuels, in order to safeguard the world's environment from the looming threat of climate change. Tidal energy is arguably one of the most promising renewable solutions to replace and diversify part of the energy supply. This is due to the tide's high predictability and technological immaturity when compared to other renewable sources, as it is an untapped market with room for development. The main ambition of this work is to explore the viability of powering the river-side urban areas, namely Oeiras and Lisbon, through the Tagus estuary's tidal energy. Such is accomplished by modelling the Tagus estuary's hydrodynamics through MOHID, a water modelling software developed by MARETEC, at the Instituto Superior Técnico. Different simulations were made, for different river water discharges throughout the year, so as to determine the behavior of said tidal farm over the course of one year. To simulate the energy production that this solution would generate, two calculation modes were used – one through the use of theoretical equations to predict the energy production of a tidal farm, and the other through the use of MOHID's built-in tool to assess a tidal turbine's energy production. In the end, an economic assessment of such a solution is presented, based on current tidal energy costs.

Keywords: Tidal Energy; Tidal Energy Converter (TEC); Levelized Cost of Energy (LCOE); MOHID; Tidal turbine; Simulation

Resumo

O crescimento populacional e consequente aumento do consumo de energia mundial solicitou o Mundo a procurar novas formas de energias renováveis que pudessem reduzir a nossa dependência em combustíveis fósseis, de forma a salvaguardar o Ambiente da ameaça iminente das alterações climáticas. A energia das marés é uma das mais esperançosas soluções para substituir e diversificar parte do fornecimento de energia. Isto deve-se à elevada previsibilidade das marés e da imaturidade das soluções tecnológicas quando comparadas a outras fontes de energia renovável, dado que se trata de um mercado inexplorado com espaço para desenvolvimento. A ambição principal deste trabalho é explorar a viabilidade de alimentação das zonas urbanas ribeirinhas, nomeadamente Oeiras e Lisboa, através da energia das marés do estuário do Tejo. Tal é alcançado com a modelação da hidrodinâmica do estuário do rio Tejo através do MOHID, um software de modelação aquática desenvolvido pelo MARETEC, no Instituto Superior Técnico. Diferentes simulações foram feitas, para diferentes descargas do rio, para determinar o comportamento de uma hipotética "tidal farm" ao longo de um ano. Foram usados dois modos de cálculo para estimar a energia que esta solução produziria – um através do uso de equações teóricas para prever a produção de energia de um campo de aproveitamento de energia das marés, e outro através do uso de uma ferramenta incorporada no MOHID para determinar a produção de energia de uma turbina. No fim, uma avaliação económica de tal solução com base nos custos atuais de energia das correntes de marés é apresentada.

Palavras-chave: Energia das marés; Conversor da Energia das Marés (TEC); Custo Nivelado de Energia (LCOE); MOHID; Turbina das marés; Simulação

Table of Contents

List of Figures

List of Tables

List of Symbols and Acronyms

A – Water flow area

C_P – Rotor Power Coefficient

€ - Euro

kW – Kilowatt

kWh – Kilowatt hour

GW – Gigawatt

GWh – Gigawatt hour

h - Hours

m – Metres

m^2 – Square Metres

m/s – Metres per second

m^3/s – Cubic metres per second

P – Power

η_{PT} – Powertrain Efficiency

ρ – Water Density

s – Seconds

TW - Terawatt

TWh – Terawatt hour

U – Water Velocity

V_{msp} – Mean Spring Peak Velocity

AEP – Annual Energy Production

APL – Administração do Porto de Lisboa

Capex – Capital Expenditures

CNES – Centre National d'Études Spatiales

CO2 – Carbon Dioxide

EDP – Energias de Portugal

EIA – Energy Information Administration

EMEC – European Marine Energy Centre

EPA – Environmental Protection Agency

EU – European Union

FES2004 – Finite Element Solution, global tidal model version 2004

GHG – Greenhouse Gases

GIS – Geographical Information System

GUI – Graphical User Interface

HDF – Hierarchical Data Format

IRENA – International Renewable Energy Agency

IST – Instituto Superior Técnico

LCOE – Levelized Cost of Energy

MARETEC – Marine and Environmental Technology Research Centre

MEP – Monthly Energy Production

MOHID – Modelo Hidrodinâmico

NASA – North America Space Agency

O&S – Operation and Maintenance

OES – Ocean Energy Systems

Opex – Operational Expenditures

PCOMS – Portuguese Coast Operational Modelling System

PTO – Power Take-Off

R&D – Research and Development

SNIRH – Sistema Nacional de Informação de Recursos Hídricos

TEC – Tidal Energy Converter

US – United States of America

WOCE – World Open Circulation Experiment

WWTP – Waste Water Treatment Plants

ZH – Hydrographic Zero

Chapter 1

INTRODUCTION

1.1. Context and Motivation

According to the United Nations, the current world population of 7.55 billion people has a growth rate of 1.10 per cent per year, which means an additional 83 million people annually. This number is expected to grow to 9.21 billion by the year 2040, meaning a 22% increase (United Nations, 2017). The enlarging population is coupled with an increment in the world's energy consumption, which is evident in the US Energy Information Administration's report, dubbed the EIA's *International Energy Outlook 2017* (US Energy Information Administration, 2017a). This report projects a 28% increase in world energy consumption between 2015 and 2040, to a total of 216 thousand TWh.

Humanity's great technological, economic and social evolution over the last few decades was mainly due to the use of fossil fuels. As such, this increasing energy demand poses a difficult challenge, as it could directly correlate to an increase in the burning of fossil fuels in order to meet our needs. Such is one of the world's most important current problems: to generate enough clean energy to guarantee human consumption without harming the environment (Castro-Santos et al., 2015).

The looming threat of climate change caused by the burning of fossil fuels has prompted policy makers, such as governments and institutions, to adopt targets to limit carbon dioxide emissions and utilize energy from renewable sources, in order to transition to a sustainable, low-carbon economy (Frost et al., 2018)

Considering that the global energy demand is increasing, renewable energy resources will play an increasingly important role in the world's future, as they can produce limitless energy, unlike fossil fuels, which are bound to the amount of resources that the planet currently holds. Moreover, by reducing the dependence on fossil fuels, renewable energy resources effectively contribute to the achievement of greenhouse gases (GHG) emissions targets and allow for almost zero emissions of air pollutants (Panwar et al., 2011).

A major culprit for GHG emissions are cities. According to the United Nations (2012), cities are responsible for the emission of 50 to 60% of the world's total GHG and consume about 75% of the global primary energy. The fact that cities are such large consumers of electricity, and given that 40% of the world population lives within 100 km of the coast (United Nations, 2007), makes ocean energy a great contender as an alternative solution to mainstream renewable energy sources to power the urban coastal areas. This is only aggravated in the case of Portugal, where 93% of its population lives within 50 km from the sea (Eurostat, 2013).

Ocean energy is abundant, geographically diverse, renewable and, under favorable regulatory and economic conditions, it could meet 10% of the EU's power demand by 2050, which could avoid the equivalent of 276m tonnes of CO_2 emissions annually (Ocean Energy Forum, 2016). Ocean energy can be harvested in different manners: it can be through wave energy, through tidal stream energy (generated from the flow of water in narrow channels) and through tidal barriers (which exploits the difference in surface height in a dammed estuary or bay) (EU, 2014).

According to the Portuguese *Instituto Hidrográfico*, the tidal difference between high and low tides in continental Portugal is roughly 3 meters (Instituto Hidrográfico, 2000). In theory, this renders the application of tidal energy solutions in Portugal purposeless, as the tidal energy systems require a tidal range of 3 to 7 meters to ensure its economic viability (US Energy Information Administration, 2017b; Lyon et al., 2004). However, the Tagus estuary, one of the largest in Western Europe, has the unique feature of having a narrowing on the river's mouth. This allows for the Tagus estuary to act as a reservoir, holding water in during high tides, and releasing it during low tides. Thanks to the narrowing, the water undergoes a convergence effect, much like the Venturi effect, where it must go through a constricted section and thus increase its velocity. It is this effect that creates water currents that are potentially strong enough to power tidal energy turbines that can be used to provide electricity to the city of Lisbon.

Although it is in its infancy, tidal energy has the potential to be a significant renewable energy contributor, as studies indicate that the global resource is approximately 3 TW, of which only 1 TW is harvestable in coastal areas (IRENA, 2014). Tidal energy also has the unique advantage of being more predictable than wind, is hardly influenced by weather conditions and it is available at night, unlike solar energy. Despite this, tidal energy solutions have yet to break into the commercial marketplace, mainly due to its current costs.

Previous studies already covered the potential electric energy of tidal currents in different Portuguese estuaries, such as the Lima River Estuary (Rebordão, 2008), the Tagus River Estuary (Lopes de Almeida, 2008) and the Douro River Estuary (Abreu, 2010). There are, however, quite a few differences between this work and the ones stated. Firstly, each uses a different modelling software, namely ADCIRC, Matlab and MOHID, respectively. The inherent advantage that MOHID possesses over the other two computational models is that MOHID is a specialized water modelling software that also has coded in a module that allows for the analysis of water flow through a turbine, and how it affects the surrounding water flow that goes into downstream turbines, and how that impacts their electric energy production. Secondly, none of the works mentioned take into account the water velocity vertical discretization, meaning that a tidal turbine's true electric energy generation potential is not being assessed, as it is a submerged device. This means that the water velocity to be determined is the one that flows through a turbine, and not the one that flows on the surface, as is calculated in all those different works.

As such, this work hopes to present a comprehensive analysis of the actual electric energy potential of a tidal farm placed in the mouth of the Tagus estuary.

1.2. Objectives and Methodology

The main ambition of this thesis is to explore the viability of powering some of the Lisbon urban area through the Tagus' tidal energy. The objective is to estimate the electric energy potential of a tidal farm placed in the Tagus river estuary, in order to power some of our human needs and urban activities.

Firstly, an extensive review of what tides are and of the different tidal energy technologies is presented. In it, some of the tidal technology's obstacles are explained. Secondly, the MOHID software is elucidated, with a brief explanation of its composition. Then, the characterization of the Tagus estuary and the resulting software model boundary conditions inputs are enunciated. Last, but not least, the viability of powering the Lisbon urban area through the Tagus' tidal energy is discussed. The latter will be done so by assessing its potential, along with technological, economic, social and environmental indicators. With that in mind, the Tagus estuary's hydrodynamics will be assessed resorting to the MOHID software, in order to evaluate the estuary's potential of there being implemented a possible future tidal farm that produces electricity from the tidal action.

As such, a simulation model that represents the local tidal variation will be developed so that it is possible to estimate the energy that can be produced. In addition to the tidal variation, the model will also have to consider other water discharges that go into the estuary, such as water from the Tagus and Sorraia rivers. While tidal amplitude is fairly constant over the course of one year, the same cannot be said about the amount of water that the rivers contribute to the estuary throughout the year, as this value is far greater during the Winter months than the Summer months, which can result in different amount of produced electricity.

For this reason, three different scenarios will be conducted to compare how tidal energy production varies along the course of one year: 1) electricity production during a Summer month, with low river discharges; 2) electricity production during a Winter month, with high amounts of river discharges, and 3) electricity production during an average month, with the average river discharge rate.

As for the turbines used in the tidal farm themselves, they ought to be bi-directional, so as to take advantage of the reversible water currents in the estuary. Their technical characteristics and layout, however, will be specified further ahead in the thesis.

Other than the potential tidal energy that a tidal farm can harness from the Tagus estuary, such a project's feasibility will also be discussed, with regards to its economy (LCOE analysis) and technical limitations

This thesis will mainly encompass the modeling of the Tagus estuary's hydrodynamics through the use of the MARETEC's (an Instituto Superior Técnico's research center) in-house numerical model named MOHID (http://www.mohid.com; Neves, 2013). Having run the simulations, the data will be processed using Microsoft's Office Excel program in order to assess the amount of energy that a potential tidal farm placed on the Tagus' mouth would produce.

In addition to these two softwares, this work also makes use of *Surfer*: a three-dimensional surface and contour mapping software, in order to better visualize the results.

1.3. Structure of the thesis

This work is composed of six chapters and annexes.

The current chapter is destined to assess the theme's relevance, as well as the thesis' objectives and structure.

The 2nd Chapter focuses on the tidal energy itself: how it originates, what it is, which technologies can harness their energy and which are their limitations.

The 3rd Chapter contemplates the general overview of how the MOHID Software works and the auxiliary tools that are used when modelling the Tagus estuary.

The 4th Chapter is referent to the case study itself, namely the simulation results from the different scenarios of tidal energy production in the Tagus estuary. In it, a characterization of the estuary is made, and the results are shown.

The different results regarding the tidal farm's electric energy production capacity and its variability are discussed in the 5th Chapter, where an economic and technical assessment is also made with regards to a possible tidal farm's feasibility, according to its energy production.

Lastly, the 6th Chapter presents some final considerations and conclusions relative to the case study and the technology used in this thesis. Finally, some opportunities and possible future developments are presented.

The annexes include an overview of the different Tidal Energy Converter (TEC) Device developers throughout the world, the variation in water velocity and energy production between the various simulations made, for the distinct assessment areas, and for both assessment methods.

Chapter 2

TIDAL ENERGY

2.1. General Overview

Tidal energy is a form of hydropower that converts the energy from the natural rise and fall of the tides into electricity. Tides are a natural phenomenon that manifests itself through the rise and fall of sea levels caused by the combined effects of the gravitational forces exerted by the Moon, the Sun and the rotation of the Earth. This cyclical vertical movement of the sea levels is also accompanied by variable horizontal movements, designated by tidal currents (Owen, 2008).

The gravitational forces that the Sun and the Moon exert of the Earth's water mass are described by Newton's law of universal gravitation:

$$F = G\frac{m_1 m_2}{d^2} \tag{1}$$

Where F is the gravitational force acting between two objects $[N]$ (in this case, the Moon and the Earth or the Sun and the Earth), m_1 and m_2 are the masses of the objects $[kg]$, d is the distance between the center of their masses $[m]$ and G is the gravitational constant $[N.(m/kg)^2]$.

As was said before, both the Moon and the Sun cause tides, since both exert a gravitational pull of the Earth. However, even though the Sun has 27 million times more mass than the Moon, the gravitational pull that the Moon exerts on the Earth is 2.17 times greater than the one that the Sun exerts on the Earth. This is due to the fact that Newton's law of universal gravitation is inversely proportional to the square of the distance, and the Moon is much closer to the Earth than the Sun is (Hammons, 2011).

Because of the Moon's orbit around the Earth, this pulling effect from both the Moon and the Sun can either work in accordance or in opposition to one another, thus resulting in *spring tides* and *neap tides*, respectively. Spring tides occur when the Sun, the Moon and the Earth line up with each other, a configuration known as a syzygy, resulting in the sum of the Moon's and the Sun's gravitational pull on the Earth's water masses. This is when the tide's range is at its maximum, culminating in higher high-tides and lower low-tides. Neap tides on the other hand happen when the Moon and the Sun are perpendicular to each other, when viewed from the Earth. This causes the gravitational pull of each celestial body to alienate each other, causing less extreme tidal variation, meaning a lower high-tide and a higher low tide (Figure 1).

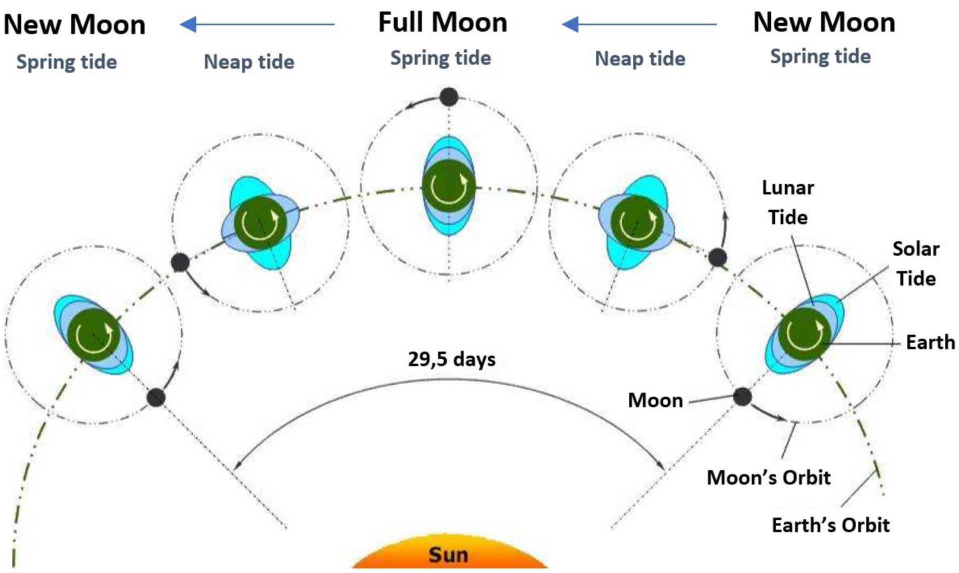

Figure 1 - Correlation of the tides with the phases of the Moon, and with the relative positions of the Earth, Moon and Sun. Source: (Abreu, 2010)

Given that the Moon orbits the Earth every 29.5 days, known as the lunar cycle, the time difference between spring tides and neap tides is normally 7 days, as they are in accordance with the phases of the Moon (Boyle, 2012).

Depending on the location of the planet, there can be three main types of tides when it comes to their daily frequency: semidiurnal, mixed and diurnal tides. Places with semidiurnal tides are characterized by having a tide period of 12 hours and 25 minutes, meaning that there are two high-tides and two low-tides every 24 hours and 50 minutes. This occurs because the Moon revolves around the Earth in the same direction that the Earth is rotating on its axis. Therefore, it takes the Earth an extra 50 minutes to "catch up" with the Moon every day. As such, when the Moon is directly above a landmass, the water around it is at high-tide. In contrast, 6 hours and 12.5 minutes later, when the landmass is "perpendicular" with the Moon, the water around it is at low-tide, and so on (O Rourke et al., 2010).

This is the tide experienced on the Portuguese coastline (as illustrated in Figure 2), as well as for most of the world.

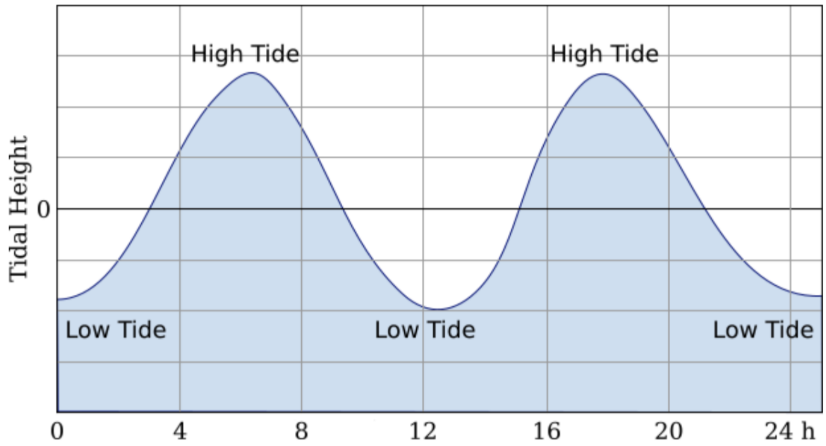

Figure 2 - Semidiurnal tide periodical behaviour (Willemsen 2018)

If the Earth was completely spherical and covered by oceans with no continents to block the water flow, there would be two high-tides and two low-tides per lunar day. However, in the real world, continents block the movement of water, complicating the tidal patterns. Due to this interference, tides can be mixed, meaning that the two high-tides and the two low-tides in a lunar day are of different heights. This type of tide can be found alongside the West coast of the USA, the Caribbean, in parts of Australia and in South East Asia. Diurnal tides on the other hand occur when there is so much continental interference that only one high-tide and one low-tide occur per lunar day. Diurnal tides can be found in the Gulf of Mexico (Willemsen, 2018).

In short, tidal amplitude is influenced by the lunar cycle (29.5 days) while the tidal frequency is influenced by the lunar day (24 hours and 50 minutes) and the geographical characteristics.

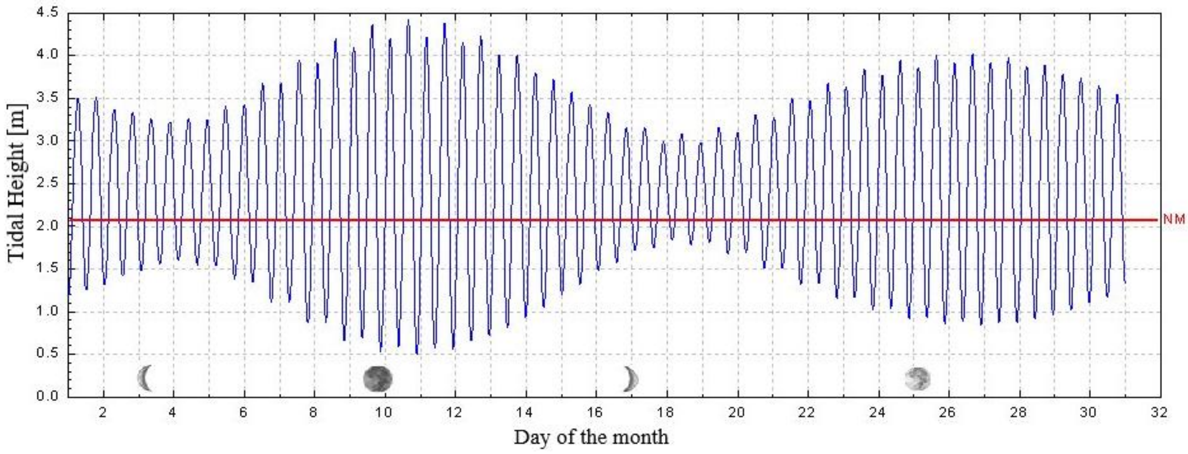

Figure 3 - Tidal profile in Lisbon, during September of 2018 (FCUL, 2018)

2.2. Technologies

Tidal energy consists of potential and kinetic components, thanks to the elevation in the water level and the resulting currents, respectively. Hence, tidal power technologies can be categorized into two main types: tidal range and tidal current technologies, which take advantage of the tide's potential and kinetic energy, respectively (O Rourke et al., 2010).

2.2.1. Tidal range concept and technologies

Tidal range technologies take advantage of the potential energy created by the difference in water levels through the use of tidal barrages. The principles of energy production of a tidal barrage are similar to that of a dam, except that a tidal barrage is built across a bay or estuary and that tidal currents flow in both directions (O Rourke et al., 2010). The available potential energy $[W]$ is given by the following equation:

$$P = \rho g Q H \tag{2}$$

Where ρ is the water density $[kg/m^3]$, g is the gravitational acceleration $[m/s^2]$, Q is the flow rate of water $[m^3/s]$ and H is the head height $[m]$.

Tidal barrages can be broken into single or double-basin systems. Single-basin systems consist of one basin and a barrage across a bay or estuary, and have three modes of operation: ebb, flood and two-way generation.

In one-way power generation at ebb tide, the reservoir is filled at flood tide and the valves are closed once the water has reached its highest level, thus trapping the water in the basin. From there, the turbine gates are kept closed up until the tide has receded (or ebbed) enough to develop a substantial hydrostatic head across the barrage (Prandle, 1984). The gates then open and the water is let flow through hydropower turbines that generate electricity for as long as the hydrostatic head is higher than the minimum level at which the turbines can operate efficiently (IRENA, 2014). An example of an ebb-tide tidal barrage is the *Annapolis* in Canada.

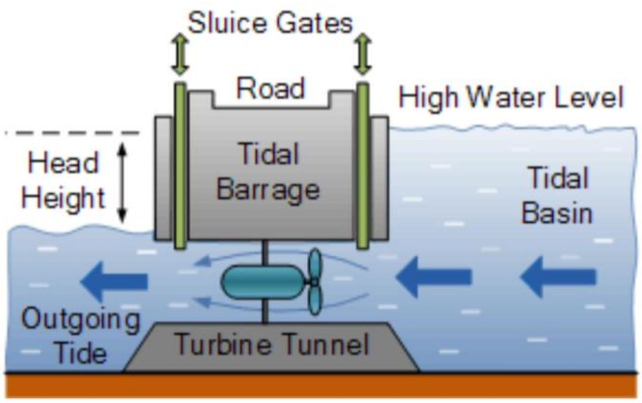

Figure 4 - Working principle of an ebb-generation tidal barrage

On the other hand, one-way power generation at flood tide works in the opposite way, where the valves are kept closed to isolate the reservoir while it is at its lowest level. Then, when the tide is high, the water flows from the sea to the reservoir via the turbines. Flood tide power generation is seen as a less favourable method of generating electricity due to environmental concerns of keeping the water levels in the reservoir at a low level for a long time (IRENA, 2014). The *Sihwa* barrage in South Korea is an example of a flood-tide tidal barrage, and is currently the largest tidal range barrage in the world, producing 552 GWh a year (IRENA, 2014).

Finally, a two-way power generation tidal barrage combines both flood and ebb phases of the tide to generate electricity. This has the advantage of increasing the period of power generation and of reducing the costs in generators since the power output is smaller (O Rourke et al., 2010). *La Rance* in France is a two-way tidal barrage and it produces 540 GWh a year (IRENA, 2014).

A double-basin system acts mostly like a single-basin system, the difference being that it consists of two basins: while the first is basically the same of an ebb generation single-basin system, the second basin acts a reservoir, allowing for an element of storage where water is pumped to, allowing for the delivery of electricity to match the need of consumers (O Rourke et al., 2010).

Although global tidal resources are largely unmapped, estimates place the global tidal range resources at 3TW, of which the technically harvestable resource, in nearshore areas, is 1TW (Charlier and Justus, 1993). However, given that the conventional tidal difference between high-tide and low-tide for the use of tidal barrages is 5-10 meters, that renders the application of this solution in Portugal purposeless, as the tidal difference in Portugal is roughly 3 meters (Instituto Hidrográfico, 2000). For this reason, this thesis will focus only on the tidal current potential of the Tagus estuary.

2.2.2. Tidal current concept and technologies

Unlike tidal range technologies, tidal current or tidal stream technologies make use of the tide's kinetic energy, converting it into electricity, in a manner similar to how wind turbines work (Rourke et al., 2009). The available kinetic energy $[W]$ of a tidal current is given by the following equation:

$$P = \frac{1}{2} A \rho U^3 \tag{3}$$

Where U is the velocity of the water flow $[m/s]$ through the specific area A $[m^2]$, and ρ is the water density $[kg/m^3]$. Due to the water's higher density when compared with the air, which is 832 times less dense, the blades can be smaller and turn more slowly than their wind counterparts, while also delivering a significant amount of power (O Rourke et al., 2010). Although not having been systematically mapped worldwide, the tidal current resources that are estimated to be harvestable in Europe are a minimum of 12 000 MW. However, tidal current technologies require the stream speed to be at least 1.5 meters per second $[m/s]$ in order for the turbines to work, thus tapping into these resources (IRENA, 2014).

As was stated before, an advantage for both tidal range and tidal current energy is that they are highly predictable, to the point where they can be predicted over several years. Furthermore, they are hardly influenced by weather conditions and are also able to generate electricity during day and night. Given that most tidal current structures are either floating or submerged, they also pose the unique advantage of having a low impact upon the surrounding landscape, both visually and spatially, as the land requirements are relatively low. All in all, these are all characteristics that are lacking in other forms of renewable energies, such as solar and wind power (IRENA, 2014).

There are several different tidal stream devices that convert the kinetic energy of free-flowing water into electricity, called Tidal Energy Converters (TEC), and they typically fall into four main categories:

A. Horizontal-Axis Turbine

Horizontal-axis turbines work similarly to wind energy converters, in the way that they exploit the lift that the fluid flow exerts on the blade, forcing the rotation of the turbine that is mounted on a horizontal axis (parallel to the direction of the water flow), which in turn is connected to a generator, converting mechanical energy into electrical energy (World Energy Council, 2016).

Despite resembling wind turbine generators, marine turbine designs must also consider factors such as reversing flows, cavitation and a harsher environment, such as salt-water corrosion, debris and having to endure greater forces due to the water's higher density. In order to overcome the reversing flows issue, horizontal-axis turbines can either turn 180º with each tide, or have rotor blades that accept flow from both directions (Lewis et al., 2011).

B. Vertical-Axis Turbine

The working principle of these turbines is similar to the one described above, except that the turbines are mounted on a vertical axis (perpendicular to the direction of the water flow).

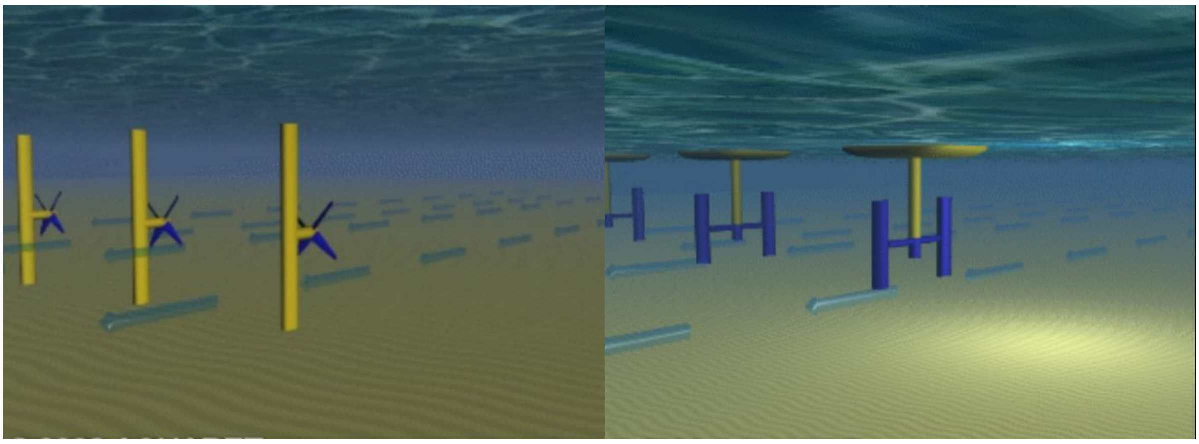

Figure 5 - Horizontal Axis Turbines (left) and Vertical Axis Turbines (right). Source: EMEC, n.d.

C. Enclosed Tips

Enclosed tips turbines are essentially horizontal-axis turbines that are encased in a Venturi tube type duct. This is made in order to accelerate and concentrate the fluid flow that goes through the turbines, taking advantage of the Venturi effect. This containment actually reduces the turbulence that turbines experience and facilitate the alignment of water flow that goes through them (World Energy Council, 2016).

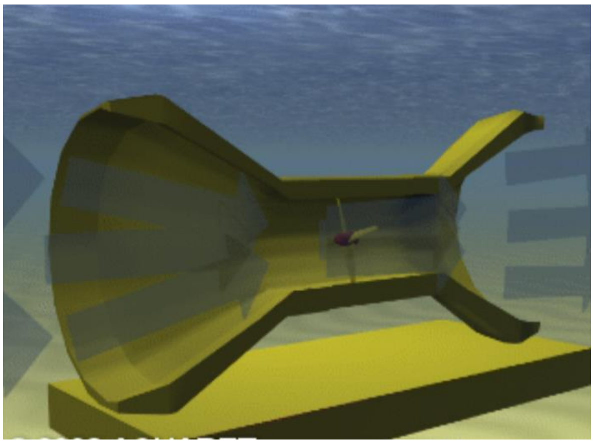

Figure 6 - Enclosed Tips Turbine. Source: EMEC, n.d.

D. Oscillating Hydrofoil

Oscillating hydrofoils consist of a blade called a hydrofoil (shaped like an airplane wing) located at the end of a swing arm. This allows them to move up and down as the tidal current flows on either side of the blade. This pitching motion (which prompted these devices to be also called "reciprocating devices") is used to pump hydraulic fluid through a motor, which in turn is converted to electricity through a generator. The advantage of oscillating hydrofoils is that the length of the blade is not constrained by the water depth, unlike horizontal and vertical-axis turbines. However, they require complex control systems to pitch the blades correctly (World Energy Council, 2016).

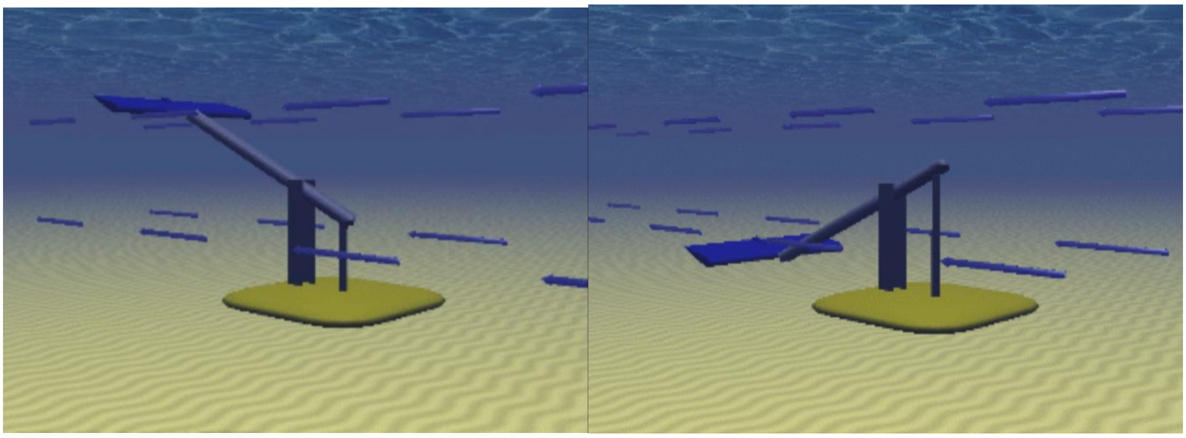

Figure 7 - Oscillating Hydrofoil pitching motion. Source: EMEC, n.d.

E. Other designs

There are several other designs that are in the research and development stage, the most prominent of which are the Archimedes Screw and the Tidal Kite. While the former is a variation of the Vertical-Axis Turbines, the latter is a kite carrying a turbine that "flies" in the tidal stream, forcing water to flow through the turbine (World Energy Council, 2016).

Annex 1 presents an extensive table containing a list of the tidal energy concepts known to EMEC – European Marine Energy Centre (http://www.emec.org.uk).

2.2.3. Tidal turbines technological aspects

Besides the energy-conversion method, there are other technological aspects to consider, as they can also determine the performance and costs of tidal current technologies, mainly how the devices are anchored, how they are placed amongst themselves and how to transfer the electricity produced back to shore.

When installing a tidal current turbine, there are three main support structures to be considered, all of which have to withstand the harsh environmental loads: the first is a gravity-based structure, that uses a large mass of concrete attached to the base of the structure to essentially sink it and achieve stability. The second option is through the use of piles, either made out of steel or concrete beams, to pin the structure to the seafloor. The third option would be to have a floating structure, usually moored to the seafloor using chains or wire (O Rourke et al., 2010).

The second technical aspect of tidal current technologies is their deployment in the form of farms or arrays. Given that individual turbines are limited in capacity, it is usual to deploy multi-row arrays of tidal turbines, in the form of a tidal farm in order to capture the full potential of tidal currents. However, each turbine has an impact of how the current flows, so the configuration in which they are placed to one another is an important factor to determine their potential energy output (IRENA, 2014).

Grid connection remains one of the critical aspects of tidal energy deployment because of their cost, putting many projects at risk (Krohn et al., 2013). In tidal current technology deployment, turbines need to be connected to each other. The array is then typically connected to an onshore substation through an export cable and eventually to the power grid (IRENA, 2014).

It is worth considering that not all TEC devices receive the same amount of research and development investment. Overall, the tidal energy sector shows significant convergence towards horizontal axis turbine technology, which receives 76% of all R&D efforts. As for the rest of the R&D investment, 4% goes into enclosed tips turbines, 2% into vertical axis turbines, another 2% into reciprocating devices, and the remaining 16% goes towards other solutions (Corsatea and Magagna, 2014). For this reason, this thesis will focus on the deployment of a tidal farm solution of an array of horizontal axis turbines on the Tagus estuary.

2.2.4. Horizontal Axis Turbine Solutions and performance

This subchapter aims to present a brief overview of the different horizontal axis turbine solutions, based on their rated power and foundation type. As was stated, there are three main ways by which a tidal turbine can be moored to the seafloor: gravity-based, piles and through a floating structure. A fourth, less common way of mooring a tidal turbine is via cables tethered to the seafloor, and it stays in place through its buoyancy.

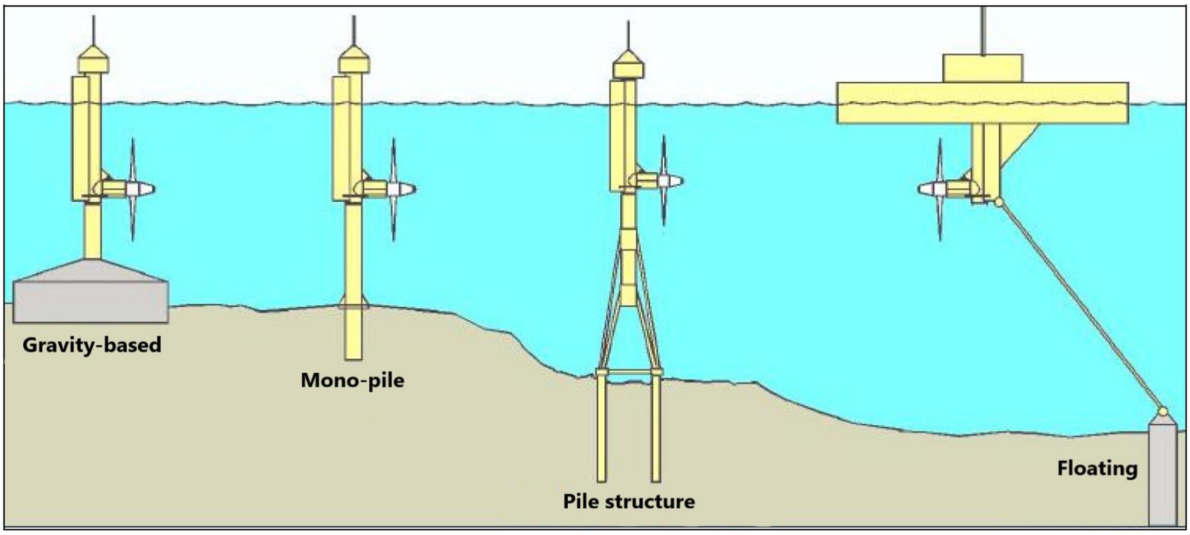

Figure 8 - Types of tidal turbines mooring solutions. Source: (Rebordão, 2008)

The following table sums up some of the existing solutions that could be implemented in the Tagus estuary. As the work progresses, a clearer picture of the Tagus' hydrodynamics is assessed, and it is expected that by the end of the thesis, a definitive answer regarding which is the optimal solution to be used shall be given.

Table 1 – Some existing horizontal axis tidal turbine solutions

Company	Device name	Mooring solution	Rotor Diameter [m]	Rated Power [MW]	Ref.
Andritz Hydro Hammerfest	HS1000	Gravity-based	21	1.0	[2]
Atlantis Resources Corp.	AR-1500	Gravity-based	18	1.5	[6]
Bourne Energy	TidalStar	Floating	6	0.05	[27]
Free Flow Power Corp.	Smart Turbine	Mono-pile	2.25	0.1	[33]
Hydra Tidal AS	Morild II	Floating	23	1.5	[36]
Magallanes Renovables	Magallanes Project	Floating	2x19	2.0	[53]
Mako Tidal Turbines	MAKO Tidal Turbines	Floating	-	-	[54]
Marine Current Turbines	SeaGen S	Mono-pile	2x(16-20)	1.2-2.0	[57]
	SeaGen U	Gravity-based	3x(16-20)	1.8-3.0	[57]
Marine Energy Corp	Current Catcher	Buoyancy	24x16	15	[58]
Nautricity Ltd	CoRMaT	Buoyancy	-	0.5	[93]
Nova Innovation Ltd	Nova M100	Gravity-based	9	0.1	[64]
Oceana Energy Company	TIDES	Gravity-based	2-18	>3	[68]
Ocean Flow Energy	Evopod	Floating	-	2.4	[67]
Renewable Devices Marine	Capricon 125	Buoyancy	-	1.25	[16]

Company	Device name	Mooring solution	Rotor Diameter [m]	Rated Power [MW]	Ref.
SABELLA SAS	D03	Gravity-based	3	0.03	[86]
SCHOTTEL	STG	Buoyancy	3-5	0.05-0.07	[88]
Scotrenewables	SR2000	Floating	2x16	2.0	[70]
SMD Hydrovision	TiDEL	Buoyancy	2x15	1.0	[84]
Sustainable Marine Energy	PLAT-O	Buoyancy	4x4	0.28	[92]
Tidal Energy Ltd	DeltaStream	Gravity-based	-	0.4	[59]
TidalStream Limited	Triton 3	Pile structure	3x20	3.0	[94]
Tocardo Tidal Turbines	UFS	Floating	-	1.5	[95]
Verdant Power	Free Flow System	Gravity-based	3x5	-	[102]
Water Wall Turbine Inc	WWT 2000	Floating	-	0.5-2.0	[105]

2.3. Tidal energy challenges

The deployment of TEC devices can have a wide array of benefits. However, they don't come without drawbacks, and being a relatively new technology means that they have a lot of uncertainties associated with them. As such, tidal energy devices need to overcome several challenges in order to become commercially competitive in the global energy market. These barriers can be specific to both the technology itself and their phase of development, which often overlap (Ocean Energy Forum, 2016). There are four key hurdles that tidal energy technologies need to overcome in order to be mass-deployed: technical, economic, socio-environmental and infrastructural barriers. In short, the challenge is to design a device that generates power reliably, cost-competitively, with acceptable socio-environmental impacts and that has the necessary infrastructure in place to enable mass rollout of the technology (IRENA, 2014a).

2.3.1. Technical barriers

Ocean energies have tremendous potential to be a major source of renewable energy in the future, thanks to the amount of energy potential contained in the planet's oceans. However, ocean energy technologies are still mostly at pre-commercial status, meaning that there are a number of technical areas, mainly in terms of resource, devices and array configurations, that need improving (IRENA, 2014a).

In terms of resource, mapping at the national level has not yet taken place for most countries. This poses a significant barrier to development, because the industry needs to know the characteristics of the local resource. In contrast, the industry also needs to improve its understanding of the resource's impact on power output and energy capture (IRENA, 2014a).

The three key challenges of a device design are reliability, survivability and installability, which is why improvements in device design are required for ocean energy technologies to reach commercial status. Having a similar operating principle to wind turbines gives horizontal-axis current turbines a developmental advantage when compared to other TEC technologies, thanks to the former's extensive operational experience. For this reason, Lewis et al. (2011) explain how they are bound to follow a similar development trajectory to wind turbines, with future current turbines likely to see advances in blade design, where the blades will swept larger areas (i.e., increasing the rotor diameter) in order to generate more power. Other necessary blade advances will include a reduction in blade erosion to improve durability (World Energy Council, 2016). Future tidal current designs are also expected to capitalize on lower installation costs, through the use of floating devices, whose mooring has lower installation and maintenance costs, unlike first-generation devices that consisted of bottom mounted designs (SI Ocean, 2013). Besides design, current turbines will also improve in efficiency, where threshold current velocities can be reduced in order to get turbines working and power take-off (PTO) systems can be lighter and more efficient, thus reducing overall weight, performance losses and maintenance frequency (Lewis et al., 2011; SI Ocean, 2013).

Lastly, there is the issue of there being limited experience in array development. Whilst the behavior of individual devices is well understood, their configuration in array formation remains uncertain. In the case of tidal stream arrays, one challenge comes in the form of understanding the impacts of wake effects of the yield of other current turbines that are downstream, as well as managing the practical complexities of inter-array underwater cabling (IRENA, 2014a).

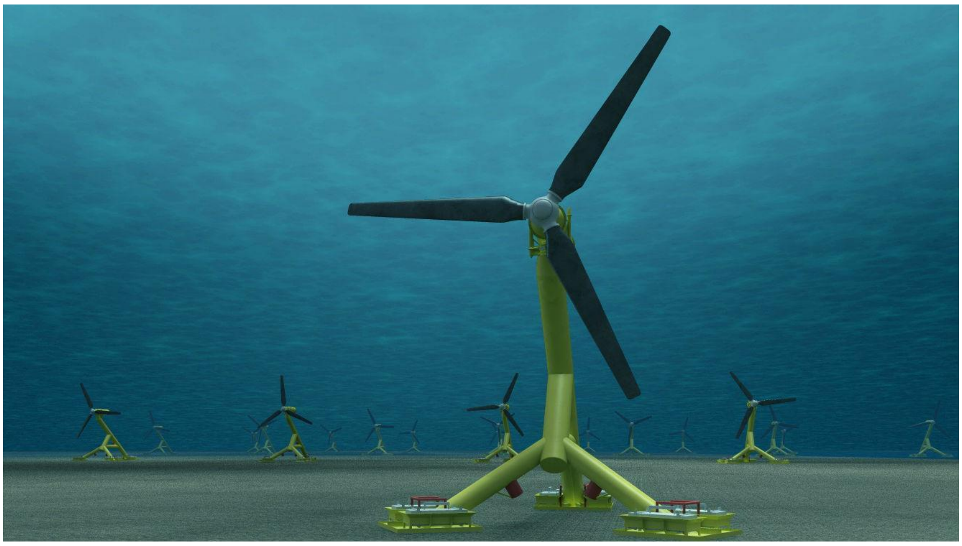

Figure 9 – Tidal-current farm array. Source: EMEC, n.d.

2.3.2. Economic and market barriers

Financial support is arguably the most important but also difficult challenge to overcome. No matter how well a technology works and how well a proof of concept performs, the determining factor in deploying a new renewable technology is its cost.

Traditionally, tidal energy has relied on government support, along with some involvement from venture capital and private equity investors for its development. The fact that tidal energy has to compete with already proven concepts and mature technologies such as wind and solar power also proves to be another barrier to funding (López et al., 2013). The reason for this is because investors are not interested in high-risk demonstration projects, whose primary benefits lie in learning and experience rather than financial returns.

Nowadays there is a wide range of power generating technologies that produce electricity from different sources, whether they are renewable or not. These can be quite distinct from one another over their physical principles or their operation. For instance: a solar photovoltaic (PV) system is drastically different from a biomass power plant. These differences are what causes the cost of power generation to be different from one another.

As such, the levelized cost of energy (LCOE) provides a common basis that allows for the comparison of the cost of energy coming from technologies that have different operating principles, unequal life spans, different size, capital cost, risk, return, capacities, among others. The LCOE is therefore an indicator of the minimum price at which electricity must be sold for a project to "break-even" (IRENA, 2018).

In short, the LCOE of a given technology is the ration of lifetime costs to lifetime electricity generation, both of which are discounted back to a common year using a discount rate that reflects the average cost of capital. This means that an electricity price above this value yields a greater return on capital, while a price below it would yield a loss on capital (EIA, 2018; IRENA, 2018).

$$LCOE = \frac{Lifetime\ cost\ (€)}{Lifetime\ energy\ production\ (kWh)} \tag{4}$$

A project's lifetime cost can be grouped into two main generic categories: *Capex* (capital expenditures), that include the initial upfront expenses, and *Opex* (operational expenditures), which are the operation and maintenance costs (O&M) (IEA, 2016). On tidal energy projects, these can be broken down into different components, as is shown in Table 2.

Table 2 - Cost categories for Capex and Opex. Source:(Jenne et al., 2015)

Capex	Opex
Development	Insurance
Infrastructure	Post installation environmental
Mooring/foundation	Marine operations
Device structural components	Shore-side operations
Power take-off	Replacement parts
Subsystem integration & profit margin	Consumables
Installation	-
Contingency	-

A study report commissioned by OES (Ocean Energy Systems) in 2015, aimed to present an industry averaged LCOE value for different ocean energy technologies, through averaging across a range of technology developers. In it, a tidal LCOE percentage breakdown by cost category for a commercial scale project is presented, as shown in Figure 10.

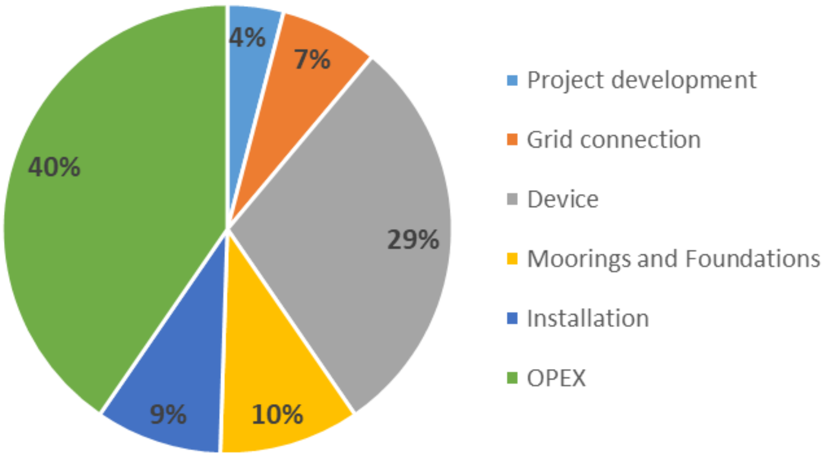

Figure 10 - Tidal LCOE percentage breakdown by cost category. Source: (OES, 2015)

In short, it can be stated that CAPEX costs represent 60% of a tidal farm deployment expenditure, while OPEX costs represent the other 40%. Of these 40%, a study made by Segura et al. (2017) suggests that a tidal farm's OPEX costs can be broken into the following categories:

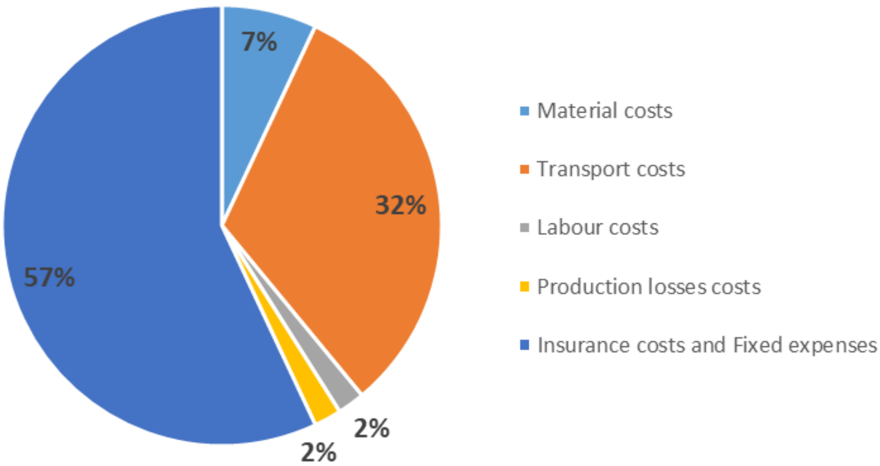

Figure 11 - Tidal farm's OPEX costs breakdown. Source: Segura et al. (2017)

On the other hand, a project's lifetime energy production is exactly that: the amount of energy that a project produces over the course of its lifetime.

All in all, there are several key inputs that go into the development of a renewable energy technology. For this reason, the LCOE varies by technology, country, operation principle, capital and operating costs and on the efficiency/performance of the technology (IRENA, 2018).

A good way of assessing the tidal energy development is by having it compared to other power generating technologies. As of now, the LCOE of ocean energy technologies are substantially higher than those of competing technologies because they are still in a pre-commercial stage, with scarce operational data and not taking advantage of economies of scale.

Table 3 - Global LCOE from renewable power generation technologies, 2010-2017. Source:(IRENA, 2018)

[USD/kWh]	2010	2017
Biomass	0.07	0.07
Geothermal	0.05	0.07
Hydro	0.04	0.05
Solar photovoltaic	0.36	0.10
Concentrating solar power	0.33	0.22
Offshore wind	0.17	0.14
Onshore wind	0.08	0.06
Fossil fuel cost range	0.05-0.17	

An early assessment of tidal energy's LCOE made in 2014 by IRENA placed at-the-time demonstration projects to be in the range of 0.25-0.47 €/kWh, while estimating that this value should be between 0.17-0.23 €/kWh by 2020. This high LCOE means that ocean energy technologies are currently unable to compete in the market without public sector intervention, although a significant cost reduction is expected in the long term (IRENA, 2014a).

While scaling-up tidal turbines offers potential for cost reduction, there are other areas that have cost reduction potential, which could be improved to deliver lower LCOE costs, namely foundations and moorings, power take off (PTO), the control systems, the electrical connection to the grid, the installation process and the operating and maintenance (O&M) costs (SI Ocean, 2013). However, the long-term pathway to cost reduction is difficult to predict. Although LCOE are expected to substantially reduce with scale, experience, learning and innovation, such cost reduction is largely dependent on deployment and investment rather than time. Policy makers are often hesitant to incentivize technologies that do not have a clear long-term pathway to grid integration, which gives this technology a high level of uncertainty with regards to deployment rates and cost reduction projections. Nonetheless, tidal current technologies are expected to be cost competitive with offshore wind by the mid-late 2020s (IRENA, 2014a).

A more recent study in tidal energy LCOE, however, forecasts an LCOE of 0.17 €/kWh for a tidal farm deployment of 100MW, 0.15 €/kWh by 200MW and 0.10 €/kWh by 1GW (Smart and Noonan, 2018).

This evidence is corroborated by Segura et al. (2017), who place an LCOE for a tidal energy project in a non-commercial stage (meaning higher risks and uncertainties) and for current TEC technology at 0.15 €/kWh, with values between 0.12-0.15 €/kWh being predicted. As the installed capacity is increased and more efficient technical advances are made, the LCOE values are expected to be around 0.09 €/kWh once the installed capacity increases to 1 GW, thus making it possible to obtain cost values similar to those of traditional renewable energy sources, whose values are between 0.05-0.10 €/kWh (see Table 3).

As such, an LCOE value of 0.15 €/kWh for a tidal farm deployment is assumed for the remainder of this thesis, for a considered service life of the tidal farm of 20 years (Det Norske Veritas AS, 2014).

2.3.3. Socio-environmental barriers

When considering that all forms of energy generation have an impact on the environment, tidal energy ranks among the ones with the least amount of negative impacts, given that it is a non-polluting renewable energy. This isn't to say there aren't environmental impacts. The ecological impacts of tidal current technologies are deemed as being less than the ones done by tidal range technologies. However, being an emerging technology, the nature and extent of environmental considerations remain uncertain, whether they are beneficial or adverse (Copping et al., 2013).

Given that tidal current energy is a new industry that involves both marine use and energy production, one challenge is that that could generate confusion over which jurisdiction of which regulating bodies they have to comply with, which can prove to be very complex and time-consuming. This in turn results in a lack of capacity from consenting bodies to approve ocean energy projects, resulting in long decision-making and deployment periods of time, which adds to the technology's high-risk and uncertain nature (IRENA, 2014a).

Another concern with ocean energy technologies is the fact that there can be a conflict of interests with coastal communities that engage in more traditional marine activities, such as the fishing industry, shipping routes, defense, tourism, recreation industry and environmental conservation, all of which can increase the risk of there being a public backlash towards these technologies, not only for functionality reasons, but also for factors such as visual impact of certain technologies (IRENA, 2014a).

2.3.4. Infrastructural barriers

There are several coastal regions that are unable to take advantage of the available energy resource provided by the ocean due to lack of the necessary infrastructure.

There are three issues when discussing the necessary infrastructure for the deployment of ocean energy systems: the first is the actual *in situs* infrastructure required to harness the ocean energy, namely the seabed electrical system, the submarine cable connection, the moorings, etc. The second is grid infrastructure, meaning the necessary connection to the electric grid in order to transfer the generated electricity to the market. This is often seen as an obstacle, as good ocean energy resources are often located in remote and sparsely populated areas (Magagna et al., 2014). The third issue is port infrastructure to provide the necessary help in offshore operations and maintenance (O&M) services (World Energy Council, 2016).

Thankfully, Portugal does have high voltage transmission lines available close to shore (IRENA, 2014), meaning that the grid infrastructure already exists. In the case of the Tagus estuary, there are several ports that could be used to aid in O&M services if a tidal farm were to be deployed, which covers the issue of port infrastructure. Supply over long distances also would not be an issue, since the tidal energy generated can power the nearby city of Lisbon.

Chapter 3

MOHID Software

There are currently several modelling softwares that are used to model anything from water basins' evapotranspiration, drainage, surface and underwater water-flow, etc., to rivers' flow depth velocities and flood zones, or even fluid dynamics overall. However, most softwares aim to tackle a specific issue and don't offer an interconnection between different problems. MOHID on the other hand is a hydrodynamic modelling software that has been developed through adding different modules, each responsible for handling a specific parameter, capable of interconnecting with each other in order to study various different water environments.

This, coupled with the fact that the software is open source, was a determining factor when choosing the software that would be used in modelling the Tagus estuary, and all its interveners, such as tidal action from the Atlantic Ocean, and water discharges from the Tagus and Sorraia rivers.

3.1. General Overview

MOHID is a three-dimensional water modelling system developed by MARETEC (Marine and Environmental Technology Research Centre; http://www.maretec.org) at the Instituto Superior Técnico – a branch of the University of Lisbon. Presently, it is organized in a hierarchical modular structure made up of over 60 modules, which add up to over 300 000 source code lines, capable of simulating complex environmental systems. The software is therefore divided into different modules, where each one can be seen as an independent mathematical model. Each module is therefore responsible for the management of a certain kind of information, which in turn will be communicated to other modules and the system will run under a single executable program (MARETEC, 2003).

MOHID is short for *Modelo Hidrodinâmico*, which translates to English as "Hydrodynamic Model". The reason for this is that when the model was first being created back in 1985, the sole purpose of the software was to be a two-dimensional tidal model, used to study estuaries and coastal areas using a classical finite-difference approach. As the system evolved, with more modules added to it, so did the name, evolving to its current denomination of MOHID Water Modelling System. The model is programmed in ANSI FORTRAN 95, which allows for it to be independent from the operating system in which it is executed and allows for the model to be used in any dimension: one, two or three dimensions (MOHID Wiki, 2018).

In order to convert the programming of systems into a numerical model, the analysis of the processes is placed according to the environment in which it occurs. This approach has created the system's current structure, divided into functional groups of hierarchical modules built on top of one or more databases. Such hierarchy can be seen in Figure 12.

Environmental systems are then assumed to be divided into three main compartments: air, water and land, which are run through two main core executable files, which can be found on the top of the pyramid:

- MOHID Water – three-dimensional numerical program to simulate surface water bodies;
- MOHID Land – numerical program to simulate hydrographic basin and aquifers.

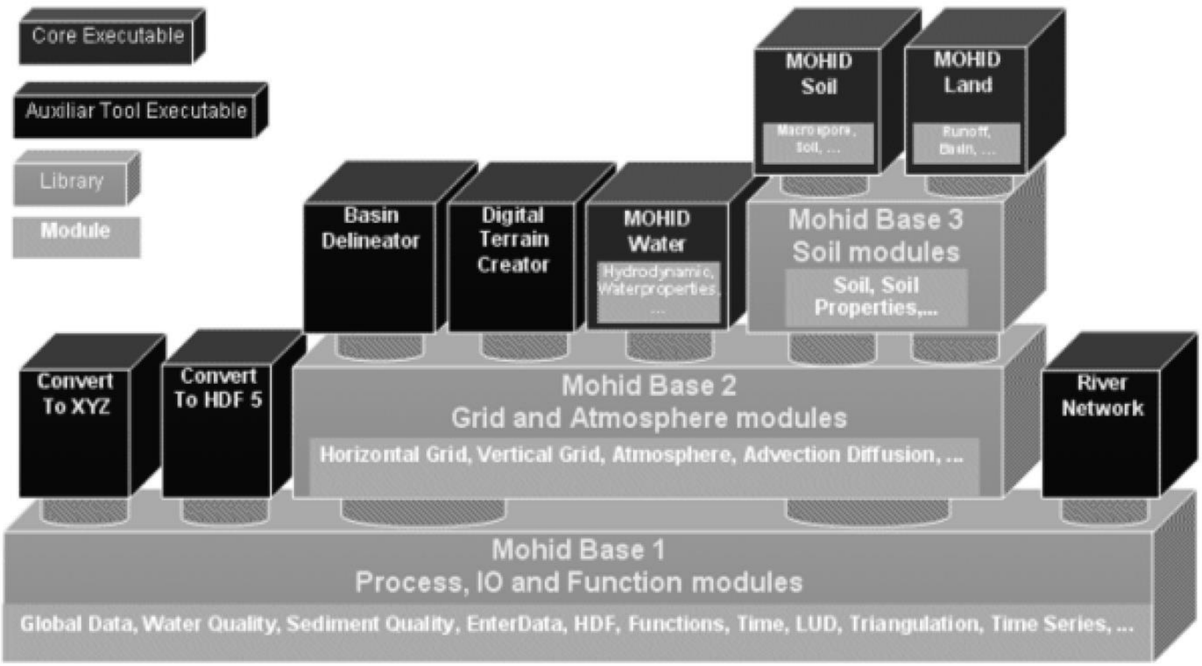

Figure 12 - Conception of the hierarchical interaction of the MOHID system (MOHID Wiki, 2018)

Another important feature of MOHID is the possibility to run nested models. This feature enables the study of local areas, obtaining the boundary conditions from the "father" model. Every model can have one or more nested child models, and the number of nested models that a simulation can have is only limited by the amount of the available of computing power (MARETEC, 2003).

For the purpose of this thesis, only the MOHID Water core file will be executed, given that the thesis only regards the simulation of water bodies flowing in and out of the Tagus estuary, and not how the water drains there. Given this, it is in the thesis' interest to contextualize how MOHID Water functions.

3.2. MOHID Water

MOHID Water is a three-dimensional numerical program used to simulate the main physical and biochemical properties of surface water bodies such as oceans, coastal areas, estuaries, reservoirs and rivers. The program is composed of a series of modules built on top of MOHID Base 1 and MOHID Base 2 (see Figure 12), which are mainly responsible for computing the water bodies' properties. The way it simulates each property is by using the finite element method, where it bases the model in finite volumes. The equations are therefore applied macroscopically in each and every grid cell volume, with respect to the divergence theorem, thus ensuring the conservation in the transport of the properties (MOHID Wiki, 2018).

The main MOHID system includes a baroclinic hydrodynamic module for the water column and the corresponding eulerian and lagrangian transport modules. The main model can also interact with some more specific modules that are used to simulate different properties in different scientific areas, such as sediment transport, water quality (dissolved oxygen, nitrogen and phosphorus, etc.), oil dispersion after an oil spill, discharges of marine outfalls, among other scenarios. However, only the modules that fall within the scope of this work are explored, as well as the support tools that are used to construct the model and also some considerations related to the developed model (MARETEC, 2003).

3.3. MOHID Modules

Seeing that the energy production from tidal turbines is mostly dependent on the water current velocity (see Equation (3)), it is safe to say that this is the primary parameter to determine, in order to assess a tidal farm's electrical output, and thus its viability.

As such, the Hydrodynamic Module is arguably the most important module that will be used, as it solves the primitive continuity and momentum equations for both the water's surface elevation and its 3D velocity field. This means that it computes the water velocity, as well as the water level and the water flux (MARETEC, 2003).

3.3.1. Module Hydrodynamic

As was stated, the MOHID's Hydrodynamic Module solves the primitive continuity and momentum equations for incompressible fluid flows in all three spatial directions, through the assumption of hydrostatic equilibrium, as well as the Boussinesq and Reynolds approximations (MARETEC, 2003). All the equations used by the Module are derived by taking into account these approximations, and they are as follows, adjusted to Cartesian coordinates:

$$\frac{\partial u}{\partial t}+u\frac{\partial u}{\partial x}+v\frac{\partial u}{\partial y}+w\frac{\partial u}{\partial z}-fv=-\frac{1}{\rho_r}\frac{\partial p}{\partial x}+\frac{\partial}{\partial x}\left(A_H\frac{\partial u}{\partial x}\right)+\frac{\partial}{\partial y}\left(A_H\frac{\partial u}{\partial y}\right)+\frac{\partial}{\partial z}\left(A_V\frac{\partial u}{\partial z}\right) \quad (5)$$

$$\frac{\partial v}{\partial t}+u\frac{\partial v}{\partial x}+v\frac{\partial v}{\partial y}+w\frac{\partial v}{\partial z}+fu=-\frac{1}{\rho_r}\frac{\partial p}{\partial y}+\frac{\partial}{\partial x}\left(A_H\frac{\partial v}{\partial x}\right)+\frac{\partial}{\partial y}\left(A_H\frac{\partial v}{\partial y}\right)+\frac{\partial}{\partial z}\left(A_V\frac{\partial v}{\partial z}\right) \quad (6)$$

$$\frac{\partial p}{\partial z}+\rho g=0 \quad (7)$$

$$\frac{\partial u}{\partial x}+\frac{\partial v}{\partial y}+\frac{\partial w}{\partial z}=0 \quad (8)$$

Where t represents time; u, v and w are the velocity components; f is the Coriolis parameter; p is pressure; ρ is water density; g is the gravitational acceleration; and A_H and A_V are the horizontal and vertical turbulent kinematic viscosity, respectively (Santos et al., 2004).

While the horizontal velocities – Equations 5 and 6 – are calculated based on the momentum equations, the free surface and vertical velocity – Equations 7 and 8 – are calculated based on the continuity equation. Each one of these equations, however, is explicitly applied to each control volume in a three-dimensional referential, in order to give rise to the model's entire hydrodynamic processes, such as current speed (Santos et al., 2004).

In order to simulate the evolution of the current velocity, the Hydrodynamic Module utilizes the information from the following modules:

- Module Geometry, to get the lateral areas and volumes of the model's finite volumes;
- Module InterfaceWaterAir, to get the processes that occur at the water-air interface, such as water fluxes (e.g. precipitation or evaporation) or wind stresses;
- Module InterfaceSedimentWater, to get the boundary conditions at the bottom of the water column, namely the bottom shear stress induced by currents;
- Module WaterProperties, to get the water density, which depends on salinity, temperature and pressure;

- Module Discharges, to get all the water discharges that flow into the estuary, besides the tides;
- Module OpenBoundary, to get the boundary conditions at the frontier with the open sea, namely water elevation and fluxes;
- Module Turbulence, to get the water viscosity, based on its flux and velocity.

Of these, while the Modules Geometry, WaterProperties and Turbulence are charged with computing the water mass characteristics, the remaining Modules (InterfaceWaterAir, InterfaceSedimentWater, Discharges and OpenBoundary) are responsible for determining the model's boundary conditions. Posteriorly, the more relevant Modules to building the model, and thus obtaining the water current velocities, are described.

3.3.2. Module Geometry

The Geometry Module computes the lateral areas and volumes of the finite volumes, based upon the surface elevation and the bathymetric data (MARETEC, 2003). In other words, it handles the vertical discretization of the water mass in MOHID. It does so by dividing the water column in different vertical coordinates, whether they are Sigma, Cartesian, Fixed Spacing, Harmonic, etc., depending on which one is more adequate for the case study at hand. The Module also allows for a subdivision of the vertical domain into different sub-domains, using different vertical coordinate systems (MOHID Wiki, n.d.), and that is exactly what is done in the thesis' model.

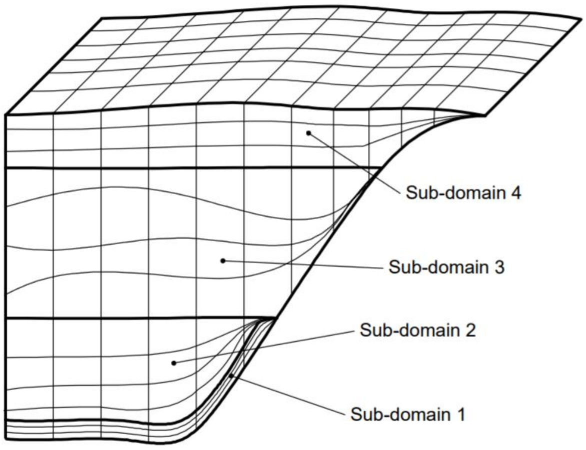

Figure 13 - Vertical discretisation with different coordinates domains (Fernandes, 2001)

It does so by dividing the water column into both Sigma and Cartesian coordinates, used to compute the surface and bottom layers, respectively. Sigma coordinates are convenient when the pressure gradient is barotropic, meaning that the pressure force is the same over the whole water column and the gradients' vertical velocity are mainly due to bottom friction. The Cartesian coordinates, on the other hand, are adequate when the flow is horizontal, which is what happens in systems with very low free surface gradient or in deep systems, where the baroclinic pressure is important (MOHID Wiki, n.d.).

3.3.3. Boundary Conditions

A model's boundary conditions can be either open or closed. While the former are usually used to define the interaction between the hydrodynamic module and other water masses (e.g. the hydrodynamics of an estuary when in contact with tidal action), the latter are used to define the coastline limits and the processes of exposure and disclosure of intertidal areas (Fernandes, 2001). The MOHID software has four modules that simplify the imposition of boundary conditions on a model: Discharges, InterfaceWaterAir, InterfaceSedimentWater and OpenBoundary.

- The Module Discharges is responsible for the input and output of water masses that are outside the scope of the computing domain, such as river discharges, effluent discharges, or water discharged from dams. These water masses can also carry properties associated to them, such as temperature, concentrations, salinity, etc.;
- The Module InterfaceWaterAir is responsible for the processes that occur at the water-air interface, such as computing wind shear stress, radiation balance, and heat and oxygen fluxes;
- The Module InterfaceSedimentWater is similar to the one described before, in the sense that it computes the boundary conditions at the bottom of the water column, instead of at the top. It does so by computing the shear stress as a boundary condition to the hydrodynamic module, caused by the bottom friction;
- Last but not least, the Module OpenBoundary provides with the model's open boundary condition, namely the adopted value for the average sea elevation/level and the tide's harmonic constituents.

As for the closed boundaries, or the land boundaries, these are placed in the model's grid data as non-compute areas, so that the program can assume these as impermeable areas that do not take part in the computing.

3.4. User Interface

A MOHID Water Modelling System model can be computed either simply through the use of executable files, or scripts, that execute a series of instructions contained in them, based on the given data files, or through the use of a graphical user interface. This graphical user interface is called MOHID Studio and, with it, one can use MOHID Numerical Engines from inside a user-friendly environment. It does so by managing all tasks required so as to prepare, execute and analyze the results of numerical simulations done by MOHID Numerical Engines (Braunschweig et al., 2012).

MOHID Studio is an all-in-one solution to the previous graphical user interfaces, which consisted of the MOHID GUI (graphical user interface used to handle the organization of the input and output files required by the MOHID numerical programs); the MOHID GIS (geographical information system which handled spatial and temporal variable data); the MOHID Postprocessor (graphical user interface which displayed data HDF files as animation on the screen); and the MOHID Time Series

Editor (graphical user interface that allowed the user to visualize time series data that was either required or produced by the MOHID numerical programs) (Braunschweig and Fernandes, 2005).

Therefore, MOHID Studio is an integrated system that allows for a user to manage and edit data files, create and launch simulations and analyze model results (Braunschweig et al., 2012).

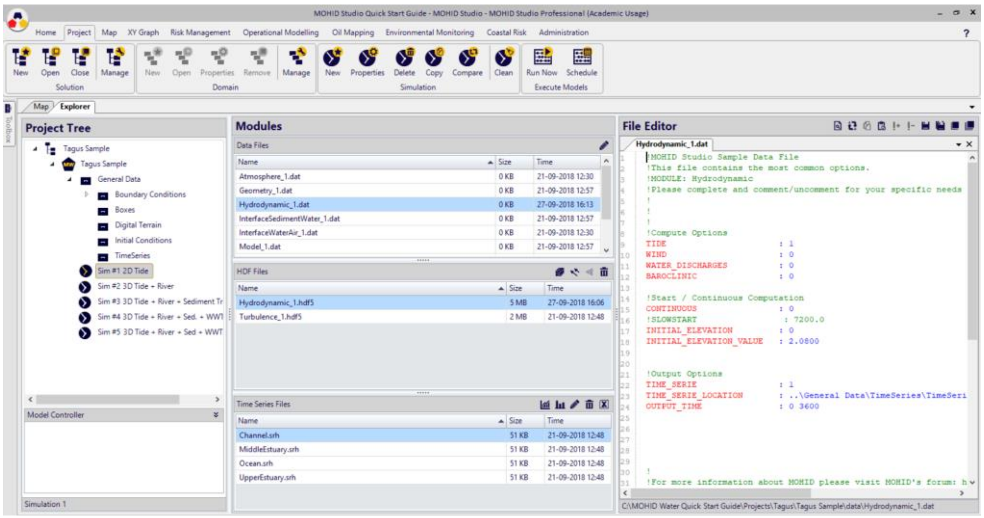

Figure 14 - MOHID Studio's main window

Similarly to how MOHID GUI used to organize projects, MOHID Studio does so by dividing them into three major units: (1) solutions; (2) domains and (3) simulations.

A solution is the upmost unit, and it groups together one or more domains. A domain is characterized by the geographic region that is being covered, the type of numerical model to use (MOHID Water, in this case) and the physical path on the disk where the files are stored. Lastly, a simulation is one execution of the numerical model over a given period of time (Braunschweig et al., 2012).

Data associated with projects is displayed in the "Explorer" window, which is divided into three main areas: (1) the Project Tree on the left, (2) the Modules window in the middle, where the files associated to a specific simulation are displayed, and (3) the File Editor on the right.

The Project Tree area is where a project's hierarchical structure – from solution to domain to simulations – is shown. The Modules window, on the other hand, is where the files associated to a specific simulation are displayed, both the input files (Data Files) and the output ones (HDF Files and Time Series Files). Data Files can be easily modified and saved by MOHID Studio, which is what is done in the File Editor area (Braunschweig et al., 2012).

After a simulation is executed, the list views containing HDF results and Time Series results are updated, and it is time to analyze the produced results. From them, the user has the ability to select which information it would like to display. MOHID has the capacity of producing several figures from the results, namely in terms of color, vectors, isolines, etc. The user can also visualize the results step-by-step, or under the form of continuous animations. HDF files can be loaded into the GIS map engine, where there are several ways of displaying the results, such as raster images and vector data.

Such data is displayed in the "Map" window, where it is divided into two main areas: (1) the Layers List on the left and (2) the Map Display on the right.

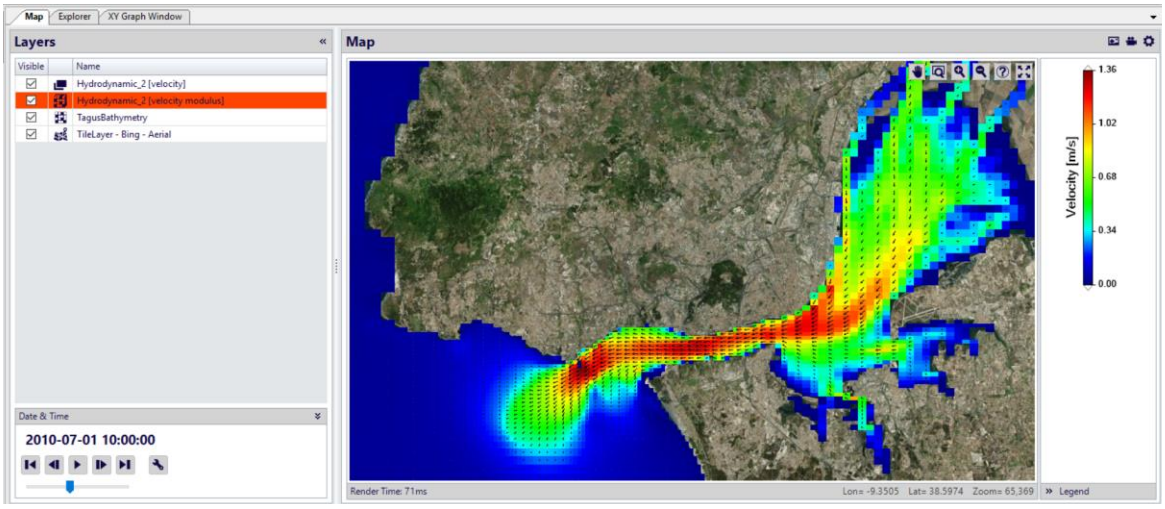

Figure 15 – MOHID Studio's Map window overview

Time Series files on the other hand can be loaded into the XY Graph engine, which produces a XY graph with the results. Such data is displayed in the "XY Graph" window, where it is divided into two main areas: (1) the Series List on the left and (2) the Graph Display on the right.

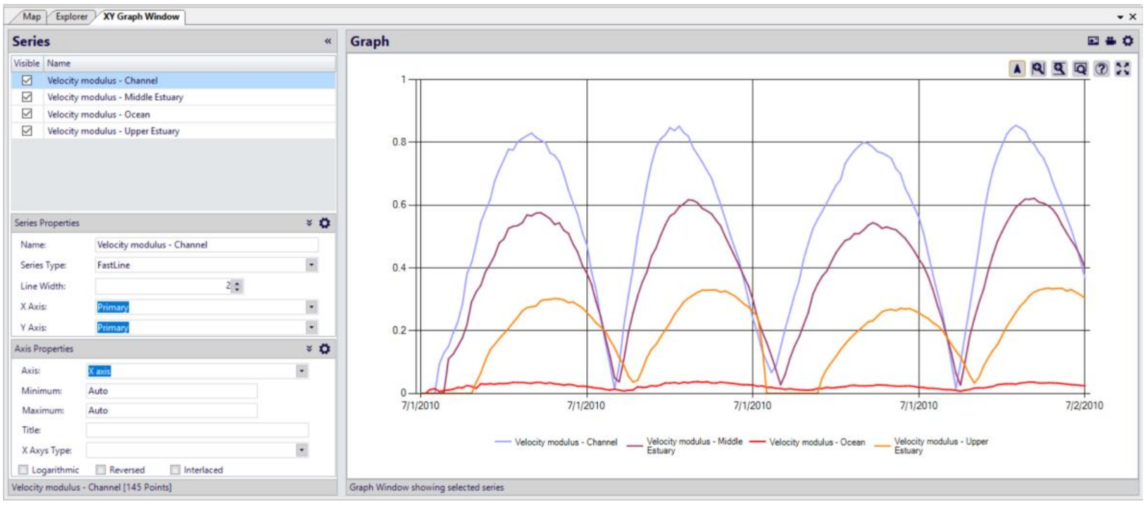

Figure 16 -MOHID Studio's XY Graph window overview

Chapter 4

CASE STUDY: Tagus River Estuary

4.1. General Overview

The Tagus is the longest river in the Iberian Peninsula. Its 1 100 kms drain the peninsula's third largest watershed, which has an area of roughly 81 310 km^2, accounting for 14% of the peninsula's total area. Of this, 32% is in Portuguese territory, while the remaining 68% is in Spain. The river empties into the Atlantic Ocean, through the Tagus estuary, which is the transition zone between the two (ARH Tejo, 2011).

The estuary is located beside the city of Lisbon and it is one of the largest in Western Europe. It has a total area of 320 km^2, of which 130 km^2 is intertidal area[1], and has a total length of 80km. The Tagus estuary (Figure 17) can be divided into 4 main sections (Portela, 1996):

- *The fluvial section* – It is correspondent to the river section that is still influenced by the tides. It is situated between Muge and Vila Franca de Xira, and is roughly 30 km long, with an average width of 600 m. The water here is characterized by being fresh, with a low salinity.
- *The upper section* – This is where there the estuary experiences a great transversal development, with it reaching a maximum width of 14.5 km. It is situated between Vila Franca de Xira and the Sacavém-Alcochete section, which accounts for a total of 20 km in length. This section is

[1] Meaning that water floods this much area during high tides.

characterized by having a lot of intertidal area, with a very low average water depth, where it does not go beyond 5 meters deep in some deeper grooves.

- *The middle section* – It consists of wide area, commonly referred to as “Mar de Palha”, situated between the Sacavém-Alcochete and the Praça do Comércio-Cacilhas sections. It is a 15 km long section with an average water depth of 5 meters, except for the navigation channels, which can be up to 30 meters deep.
- The lower section – This is the fourth and last section of the estuary. It corresponds to the estuary’s exit channel, with predominantly marine characteristics. It can be classified as a corridor 15 km long and 1.9 km wide on average and is placed between the sections of Praça do Comércio-Cacilhas and the river’s mouth, which marks the estuary’s conventional limit. It is also the section with the largest average water depth, reaching all the way up to 40 meters. The fact that the lower section of the estuary is much narrower than the adjacent water bodies – the Atlantic Ocean and the “Mar de Palha” – allows it for there to exist a phenomenon similar to that of the Venturi effect, where water flows through a constricted section of a pipe and therefore its velocity increases. It is this increase in water velocity that makes it possible for energy to be extracted from the estuary’s water currents, making it this thesis’ case study area.

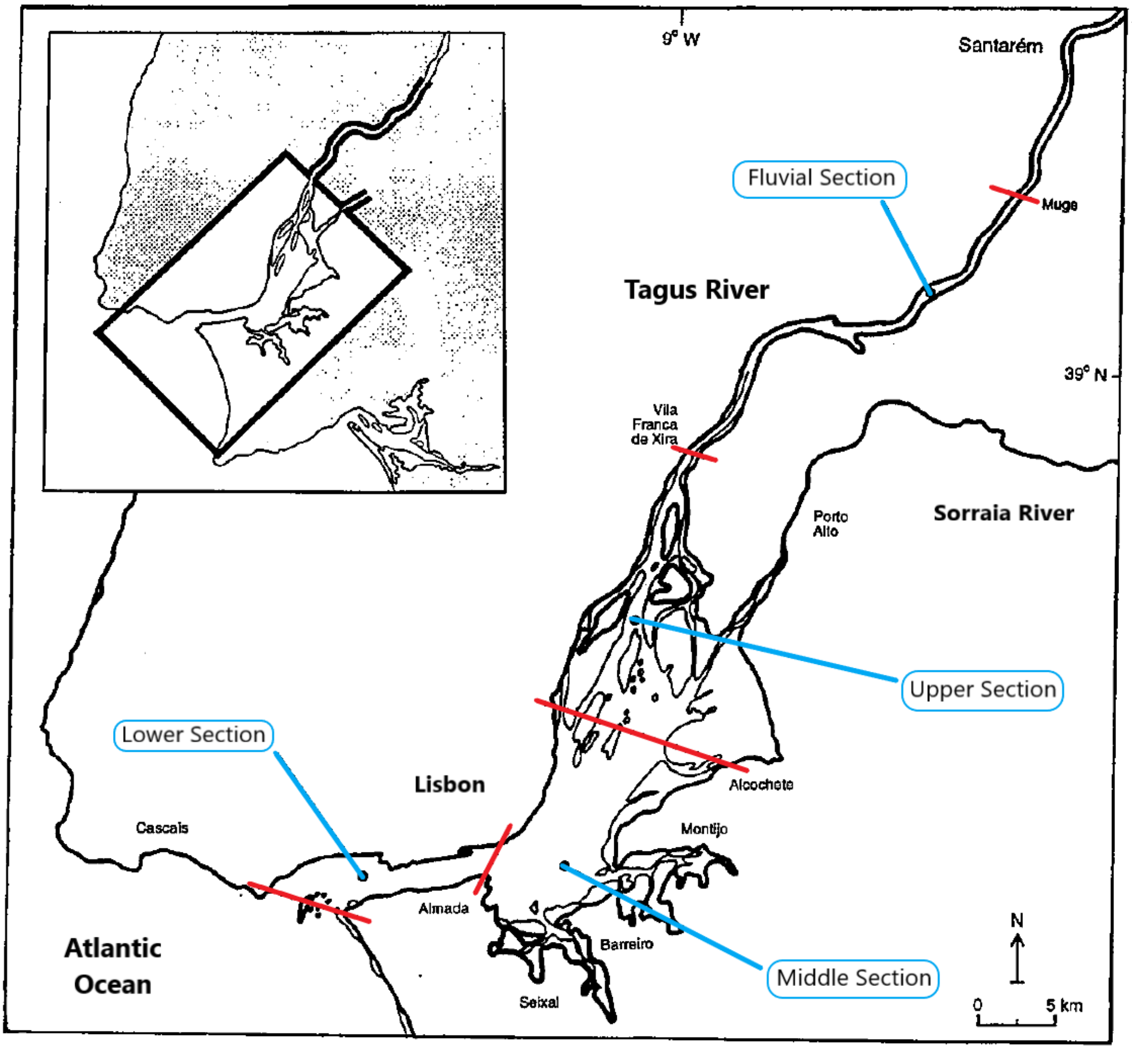

Figure 17 - Tagus Estuary. Source: (Portela, 1996)

When considering the water inputs into the estuary, there are 2 main sources: fresh water from the rivers and salt water from the tides.

While the main source of fresh water comes from the Tagus river, there are also some smaller contributions from other rivers, such as the Sorraia and Trancão rivers. As was stated before, the Tagus river is the longest in the Iberian Peninsula, draining an 81 310 km² watershed. As with any Iberian river, the Tagus shows a large seasonal and interannual variability, with a mean annual flow rate of roughly 350 m³/s, averaged between the years of 1973 to 2010 (Macedo, 2006).

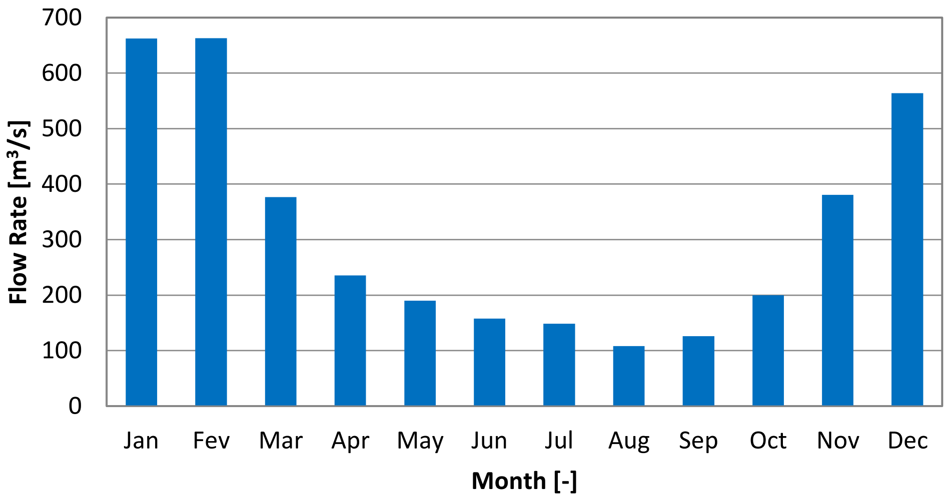

Figure 18 – Average monthly flow rate into the Tagus estuary from the Tagus river, between 1973-2010

In the case of exceptional flooding events, however, the resulting instantaneous peak flow rate can be upwards of 13 000 m³/s, as it was during an exceptionally rainy February in 1979, whose average monthly flow rate reached 3 730 m³/s (Macedo, 2006).

As for the other fresh water contributors, Portela (1996) estimates that the Sorraia river's mean annual flow rate is equivalent to around 8.5% of the Tagus' discharge, whereas the remaining effluents to the estuary (i.e. Trancão, Enguias, Moita, and several wastewater treatment plants (WWTP)) have a near negligible flow rate.

However, the main factor that determines the characteristics of the estuary's hydrodynamic regime is the salt water from the tides. The reason for this is because the average tidal water volume is immense when compared to the estuary's water volume at low tide. As was stated before, the tidal cycle in Portugal is semidiurnal, meaning that the estuary experiences two high-tides and two low-tides each day. According to the Portuguese Hydrographic Institute, the average values for the different tidal reference levels that occur in Lisbon (referenced to the Lisbon's charted depth) are presented in Table 4.

Table 4 - Average values for the different tidal reference levels in Lisbon, between 2010 and 2018

	Tide	Height [m]
HAT	Highest Astronomical Tide	4.28
MHWS	Mean High Water Springs	3.86
MHW	Mean High Water	3.43
MHWN	Mean High Water Neap	3.00
MSL	Mean Sea Level	2.20
MLWN	Mean Low Water Neap	1.42
MLW	Mean Low Water	0.98
MLWS	Mean Low Water Springs	0.54
LAT	Lowest Astronomical Tide	0.17

The estuary's water volume at low tide is 1 900 x 10^6 m^3 (ICNF, 2018). Given that the mean tidal range is roughly 2.45 meters, this means that an additional 600 x 10^6 m^3 of water is added to the estuary during an average high tide, all of which has to rush in and out through the estuary's 4^{th} section (see Figure 17) every 6 hours and 12.5 minutes. This makes up to roughly 26 850 m^3/s, which is the reason behind the powerful tidal currents that are generated (ICNF, 2018). The difference in water volume is so great that 40% of the estuary's surface is left emerged during low-tides, giving rise to the 130 km^2 of intertidal area mentioned beforehand.

While tidal amplitudes are fairly constant throughout the year, the same cannot be said about river discharges, with there being much more water flow during the Winter months than the Summer months. For this reason, the estuary holds a lot more water during the wetter months, meaning it also discharges more water and therefore there are stronger tidal currents. In order to have a general idea of the amount of energy a tidal farm can generate throughout the year, this thesis will contemplate 3 different scenarios, which will be elaborated ahead (Chapter 4.2.2):

1. Energy production during the driest month;
2. Energy production during an average month;
3. Energy production during the wettest month;

Furthermore, the tidal farm energy resource will be assessed in one of two different ways: according to data processing in the Excel, and through the use of a MOHID Module, named Module TURBINE. The latter was developed with the implementation of tidal turbines in a simulation model in mind, in order to assess their energy production (Balsells Badia, 2017). This comparison will be made so as to determine whether the TURBINE Module that was coded into the MOHID software is a good enough approximation to the industry's guidelines on how to assess tidal turbines energy potential, or not.

4.2. Modelling the MOHID Solution

In agreement with what was said, the MOHID software was used in order to study the hydrodynamics of the Tagus estuary under different scenarios. The Tagus estuary is considered to be the reference modelling system for MOHID Water, as it has been extensively modelled with MOHID in several different works (e.g. Portela (1996); Pina (2001); Leitão (2003); Braunschweig et al. (2003); Pina et al. (2004); Brito (2005); Fernandes (2005); Campuzano et al. (2012); Campuzano (2018)). Over the years, the estuary model has been increasingly perfected through many different works, making it redundant to calibrate it with measured data from the Tagus estuary in order to validate the results obtained from the simulation model.

In this work, the model's main goal is to assess which areas within the estuary have the greatest energy potential, meaning the highest current speeds, in order to ensure the most amount of energy is captured from the tidal currents. It is worth mentioning that the time step of the model was configured to be 10 seconds, meaning the simulation model is computing the estuary's hydrodynamics every 10 seconds. As for the model's output data time, however, this has been set to be 1 hour, as an output data time of 10 seconds would entail an incomprehensibly large amount of data, as there are 267 840 10-second instances in a month, whereas there are only 744 hours instead.

4.2.1. Bathymetry

The bathymetry defines the model's horizontal domain (computational grid and bathymetry values for each grid cell) and is the most essential information needed to run any MOHID Water simulation.

The model was set up with a 120x145 cells grid with a variable horizontal resolution, varying from 2km at the ocean open boundary and progressively reducing in size until the estuary mouth, where a 300m resolution can be found. Each cell contains a value referent to that area's bathymetry, which is obtained from a digital terrain data file in point format (XYZ).

The polygon defining the areas where the model will not calculate any values, and thus act as the model's land boundary condition, is provided in MOHID's XY format. These encompass the areas surrounding the Tagus estuary, namely the districts of Lisbon, Santarém and Setúbal (shown as a Google Earth projection – see the figure below).

As for the model's vertical discretization, it consists of a mixed 50-layer vertical geometry which is composed of a Sigma domain with 7 layers from the surface until 8.68m in depth, on top of a Cartesian domain of 43 layers, with increasing thickness towards the bottom (Campuzano, 2018).

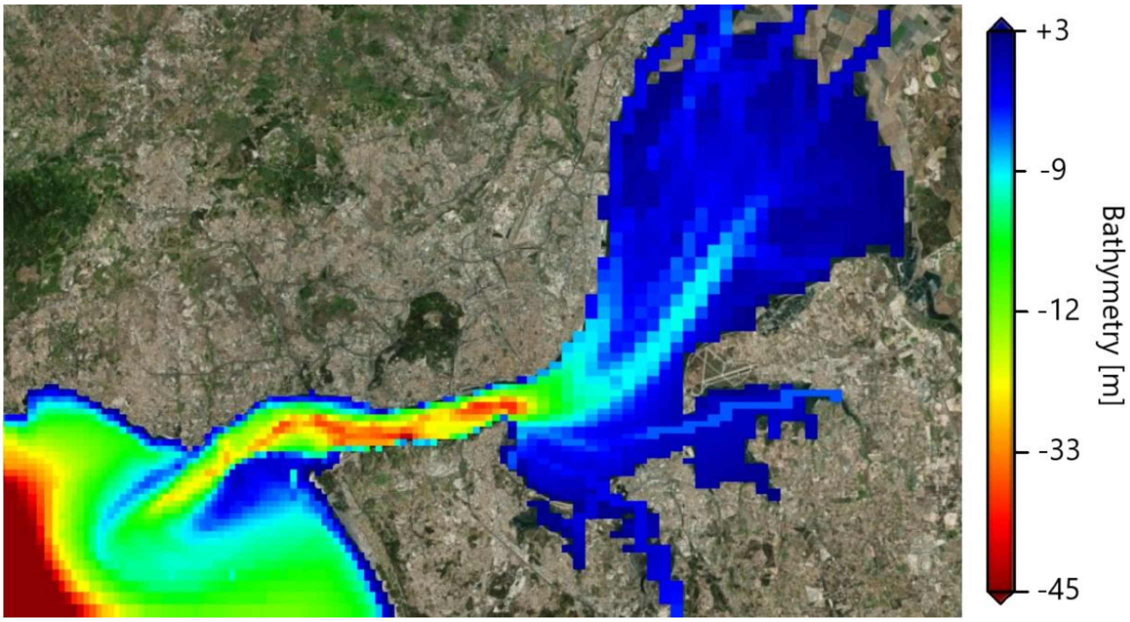

Figure 19 – Model's bathymetry zoomed in on the Tagus Estuary

4.2.2. River discharges

The Tagus river water flux imposed on the model was determined through the mean of the monthly water fluxes assessed on the Almourol hydrometric station, between the years of 1973 and 2010. This data can be accessed online, on the Portuguese National Water Resource Information System – Sistema Nacional de Informação de Recursos Hídricos (SNIRH).

This information shows that the Tagus river has a great variability in water flux throughout the year (as can be seen in Figure 18). In an effort to simplify the number of simulations to model, three different scenarios of monthly water discharge were adopted:

1. In the first simulation, the Tagus discharge is roughly that of the average driest month, meaning a continuous water flux of 110 m^3/s;
2. The second simulation contemplates the Tagus' mean monthly discharge of 350 m^3/s;
3. The third simulation looks into the wetter months by considering a water flux of 660 m^3/s;

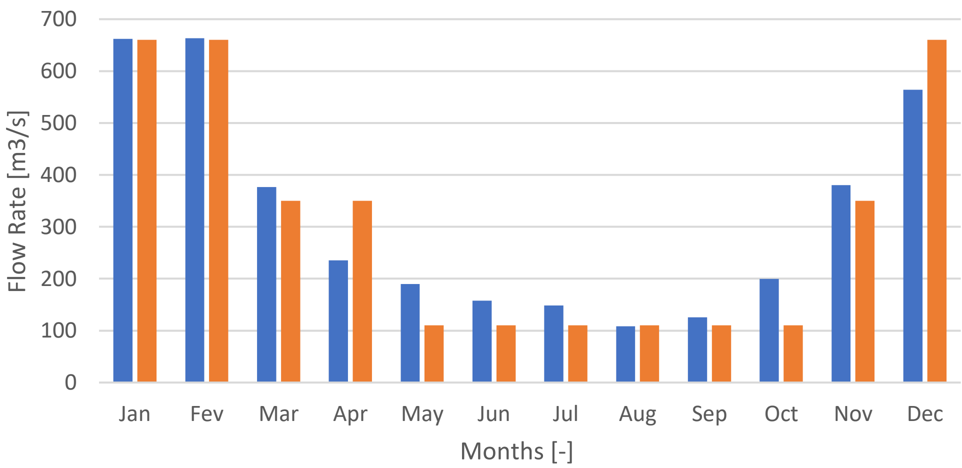

Figure 20 – Tagus river monthly flow (blue) and value considered for each month (orange)

For each and every one of the simulations, the water flux of the Sorraia river is also adjusted. While the Tagus river remains the single largest source of fresh water input into the model, Portela (1996) indicates that the Sorraia has a water flux roughly 8.5% that of the Tagus. As such, the water flux assumed for this river is adjusted accordingly, meaning a value of 9.50 m^3/s for the first simulation, 30 m^3/s for the second simulation and lastly, 56 m^3/s for the third simulation.

As for the other water discharge values (originated from the Trancão river and WWTPs - Waste Water Treatment Plants), these are assumed to be neglectable, given how the water flux that flows from these have very little representativity when compared to the Tagus river water flow.

4.2.3. Tidal Action

The tidal range found in the area has been obtained from data collected by the tidal gauge located in Cascais. This was done in order to have an overview of the tidal behavior so that it can be modelled as a boundary condition in the MOHID simulation model. As such, one year-long time series was used to investigate the seasonal variability, as well as the spring-neap tidal cycles in the area. Figure 21 shows the tidal range annual profile recorded at Cascais.

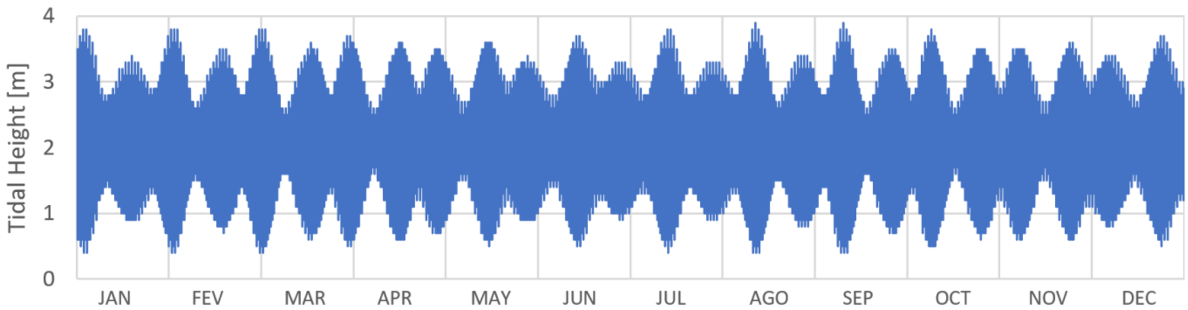

Figure 21 - Tidal height observed in Cascais during 2018. Source: (Instituto Hidrográfico, 2018)

Tidal records show a typical fortnightly cycle of spring/neap tides, with maximum ranges of about 3.50 m observed during the most energetic spring tides, and minimum ranges of roughly 0.80 m during the least energetic neap tides. For the purpose of this thesis, given how the tidal heights caused by the spring/neap cycles remain fairly consistent throughout the year, only the month that is representative of the average tidal range will be considered when modeling the MOHID solution, following the method of EMEC (2013).

Table 5 - Tidal range monthly mean values at Cascais

Month	Mean value [m]	Month	Mean value [m]
January	2.1683	July	2.0817
February	2.1019	August	2.1200
March	2.2217	September	2.1466
April	2.1569	October	2.1196
May	2.1000	November	2.1155
June	2.0621	December	2.0900
Average		**2.1237**	

Monthly tidal range averages (Table 5) show a peak tidal range during late Summer and reaches minimum values in early Autumn/Spring. However, the month that is representative of the average annual tidal range is August, meaning it will be the one to be used to estimate the average power density during the year. Figure 22 shows the tidal height variation in Cascais, during the month of August, in 2018.

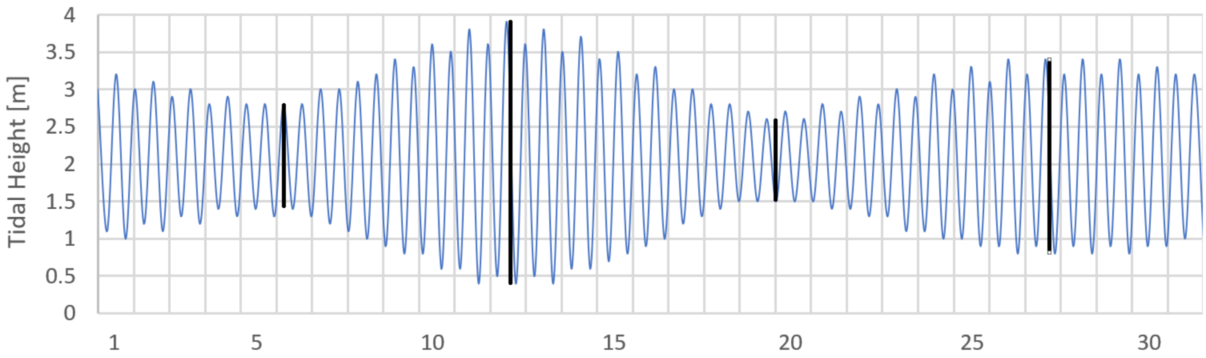

Figure 22 - August's monthly tidal profile in Cascais, 2018

It is possible to discern that the maximum tidal ranges that occur during the spring tides range from 3 to 3.5 m. This range is reduced by 60% during the most energetic neap tides and 70% during the weaker ones. These differences in tidal range translates directly into different current velocities on the river's mouth over the course of a month, with higher tidal variability resulting in higher current velocities, as more water must rush in and out of the estuary in the same amount of time.

The maximum water level variability takes place in the 11th – 13th, so it is expected for the maximum tidal velocities (and thus the maximum power output) to be reached around those days.

Figure 23 shows the daily tidal profile during the most energetic spring-tide period of the average month. As was stated beforehand, tides in Portugal are typically semidiurnal, showing two high/lows per day, with some differences in height between the two. This is caused by external factor such as changes of the declination of the Moon, the size, depth and topography of ocean basins, shoreline configuration and meteorological conditions (Physical Oceanography Group, 2010).

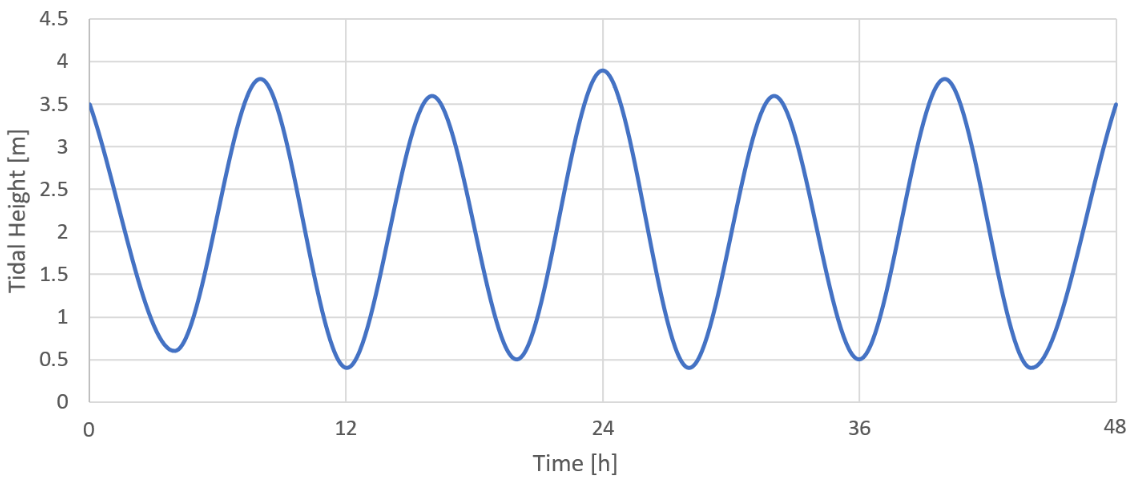

Figure 23 - Tidal profile on the days with the highest tidal amplitude

The tidal levels that were input on the simulation, which in turn act as one of the model's boundary conditions, were assessed through the Portuguese Coast Operational Modelling System, or PCOMS (Campuzano, 2018).

PCOMS is a forecast system based on the MOHID model which is continuously running in full operational mode, producing daily hydrodynamic results for the previous day and three-day forecasts for the Western Iberian Coast. The modelling system consists of two nested domains (domain 1 and domain 2), covering the Atlantic coast and its contiguous ocean (Campuzano, 2018).

The domain 1 barotropic model, with an approximately 5.4 km resolution, is forced with the FES2004 global tide solution along the Iberian ocean boundary (Campuzano, 2018). FES2004 (Finite Element Solution) presents a global solution to the tide's constituents. This program is based on a high-precision, finite-elements hydrodynamic model to provide tidal waves on a global scale. It does so by combining in-situ measurements from tide gauges datasets from WOCE (World Ocean Circulation Experiment) with altimetry data that has been acquired on the TOPEX/POSEIDON missions (joint satellite mission between NASA and CNES top map ocean surface topography) (AVISO+, n.d.). This way, by imposing the boundary points coordinates and an adopted average ocean water level of 2.08 meters, the tide's 14 components are calculated: M2, S2, K2, N2, 2N2, O1, P1, K1, Q1, Mf, Mtm, Mm, Msqm and M4.

The domain 2 model uses the information from the domain 1 and runs the MOHID model in full baroclinic mode, so as to attend to the differences in water salinity near the coastline, due to the different river discharges. It is also a 5.4 km resolution domain resultant of the downscaling of the Mercator-Océan PSY2V4 North Atlantic solution. In order to initialize the model's velocity, water level, temperature and salinity fields, and for continuous boundary conditions, the PCOMS system uses the available properties of the MERCATOR solution (Campuzano, 2018). The PCOMS system produces results with a 900 s time step that are used by nested models such as the Tagus estuary model as boundary conditions. With that resolution, the nested model is capable of reproducing daily variations of the spring and neap tides cycle (Campuzano et al. 2012).

As for the atmospheric boundary/conditions, the model is forced with information from the MM5 atmospheric forecast model for the west Iberian coast (including wind speed, air temperature, mean sea level pressure, surface humidity, cloud cover, downward long wave radiation and solar radiation) so as to adjust the tidal components to the occurring meteorological conditions (Pinto et al., 2012).

As such, PCOMS results can be used as ocean boundary conditions to different local models, bringing ocean forecasts to more specific areas.

As for the simulations that are done for this thesis, each model simulation contemplates an entire month worth of tidal action and river water flux, so as to be able to characterize the estuary's hydrodynamics during an entire lunar cycle of 29.5 days, encompassing both spring and neap tides.

4.2.4. Tidal Turbines

As was stated beforehand, this thesis will mainly look into the energy production of a hypothetical tidal farm made of horizontal-axis tidal turbines.

According to EMEC (n.d.), there are dozens of companies worldwide that are developing their own horizontal-axis tidal energy device. Given that no single tidal current technology is currently the ‘standard’ technology, EMEC (2013) states that a turbine with generic characteristics ought to be used in order to assess the available resources.

The following characteristics should be specified for the TECs:

- Maximum rotor diameter – The diameter is believed to be currently limited to 20-25 m for a standard horizontal axis turbine;
- Top clearance – the clearance between the sea surface at lowest astronomical tide (LAT) and the highest point of the turbine’s swept area. It is recommended that a minimum of 5 m top clearance should be considered, to allow for recreational activities (such as boats, swimmers, etc.) and to minimize turbulence and wave loading effects on the TECs, as well as damage from floating materials such as tree trunks coming from the river;
- Bottom clearance – clearance between the seabed and the lowest point of the turbine’s swept area. This value should be the greater of either 25% of the water depth, or 5 m. This is done in order to allow for the movement of potentially TEC-damaging materials along the seafloor, and to minimize turbulence and shear loading from the bottom boundary layer;
- Device spacing and geometry of array – the lateral spacing between devices ought to be two and a half times the rotor diameter (2.5d), whereas downstream spacing should be 10d. The devices should also be positioned in an alternating downstream arrangement, as shown in Figure 21.

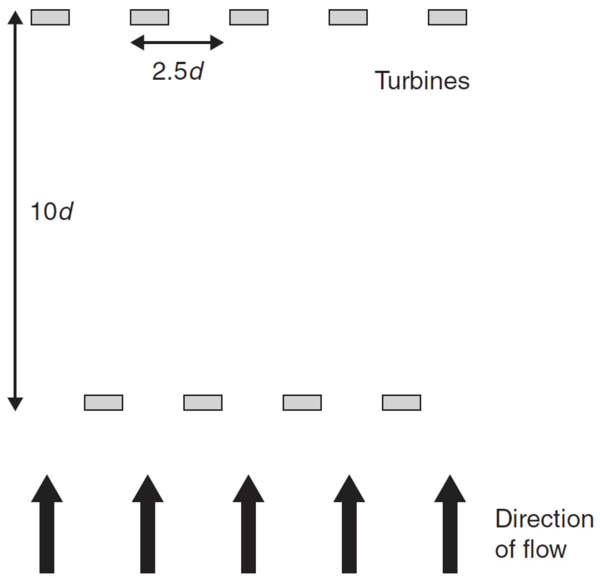

Figure 24 – Proposed device spacing and geometry of array. Source:(EMEC, 2013)

The available kinetic energy of a tidal current is given the Equation (3) described in 2.2.2:

$$P = \frac{1}{2} A \rho U^3 \tag{3}$$

The fact that the water velocity is cubed makes it the more determinant variable when assessing the currents' energy. According to the equation above, one can obtain the following graph:

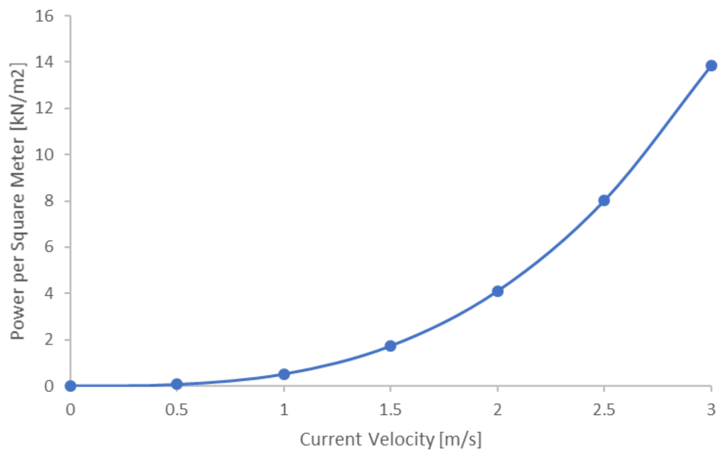

Figure 25 - Function of power output in terms of water velocity, per square meter

However, it is worth mentioning that not all the current's power is susceptible of being transferred to the TEC and transformed in electrical energy. One has to take into account the efficiency of all the mechanisms implicated in that transfer, such as the rotor power and the drive train efficiencies (Manwell et al., 2009). As such, Equation (3) can be defined as the following expression:

$$P_T = \frac{1}{2} A \cdot \rho \cdot C_P \cdot \eta_{PT} \cdot U^3 \tag{9}$$

Where η_{PT} is the powertrain efficiency (generator power/rotor power) and C_P is the rotor power coefficient.

The rotor power coefficient represents the ratio of actual electric power produced by a turbine divided by the total water current power flowing through the turbine at any given current speed. The theoretical maximum rotor power coefficient is given by *Betz' Law*. It states that no turbine can convert more than 16/27 (0.593) of the kinetic energy of the current into mechanical energy turning a rotor (Manwell et al., 2009).

Turbines extract energy by slowing down the water current. For a turbine to be 100% efficient, it would need to stop 100% of the water. However, in that case the rotor would have to be a solid disk, which wouldn't turn, and no kinetic energy would be converted. The opposite is also true: if a turbine were to have only one rotor blade, most of the water current would pass through the turbine's swept area with little to no dissipation. In the real world however, the rotor power coefficient limit is well below the *Betz Limit*, as it is also necessary to factor in the engineering requirements of a turbine, such as strength and durability (REUK, n.d.).

According to EMEC (2013), the rotor power coefficient can be considered to rise linearly from 0.38 at cut-in velocity to 0.45 at rated velocity. While the former is the minimum velocity required for device operation (necessary to produce the necessary torque to rotate the rotor), the latter is the current velocity at which the power output reaches the limit that the electrical generator is capable of.

As for the turbine's powertrain efficiency, it can be thought as an energy conversion chain, where each component is characterized by its efficiency. It represents the efficiency at which a turbine converts mechanical energy into electrical energy, and it is determined by the rotor efficiency, the generator efficiency and the electrical grid efficiency. All in all, the average powertrain efficiency can be considered to be 90% (EMEC, 2013).

4.3. Data Analysis

The first thing to consider when determining the best suited areas for implementing a tidal farm is to assess where the greatest energy potential is. In order to do so, the modelled simulation of the Tagus estuary with all the parameters mentioned beforehand was run three times, for three different scenarios of river water flow.

Figures 26 to 28 show the resulting average water velocity on the Tagus' mouth for the three different simulations with different river water discharges. These were done resorting to *Surfer*, a three-dimensional surface and contour mapping software, in order to better visualize the data

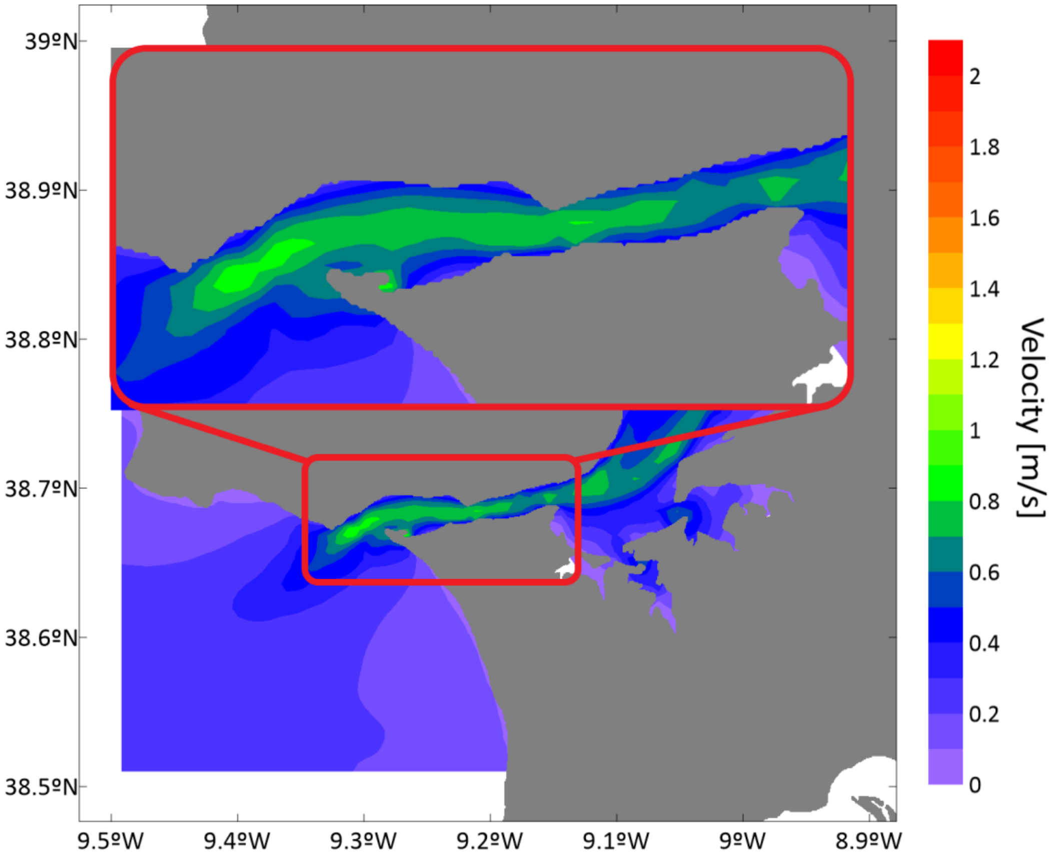

Figure 26 - Average water velocity for an average dry month discharge

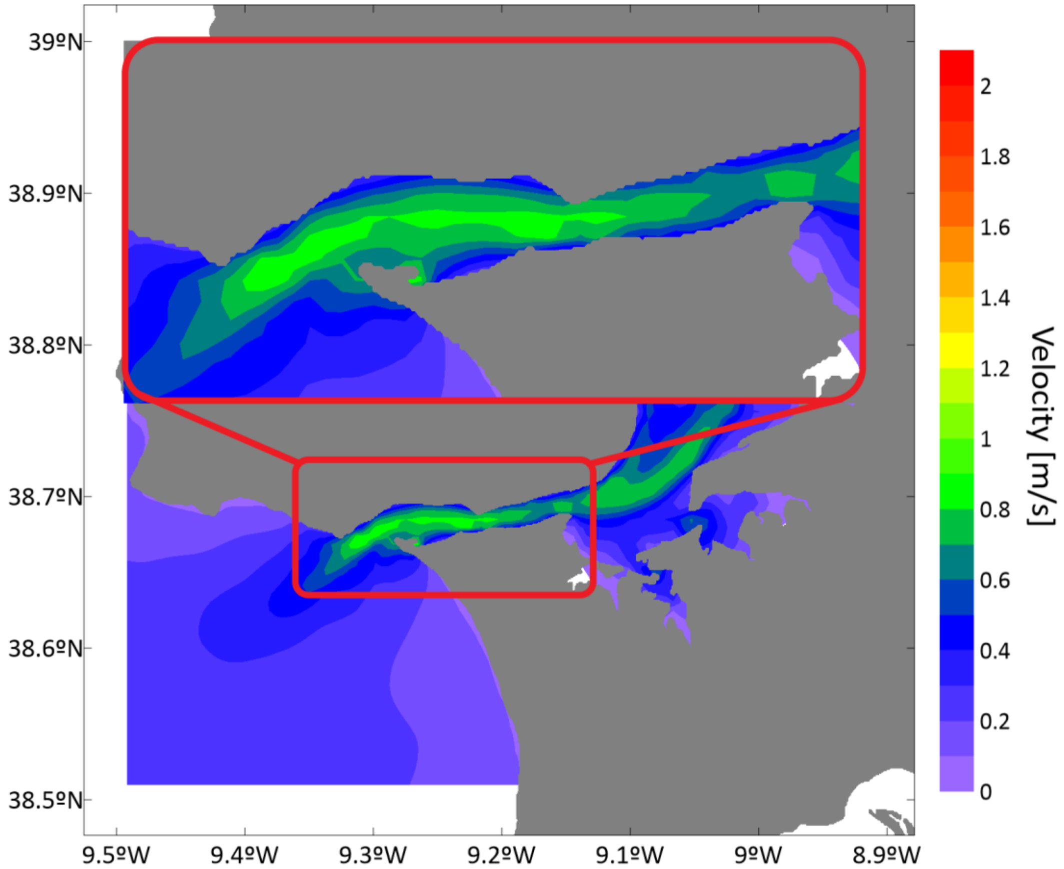

Figure 27 - Average water velocity for an average month discharge

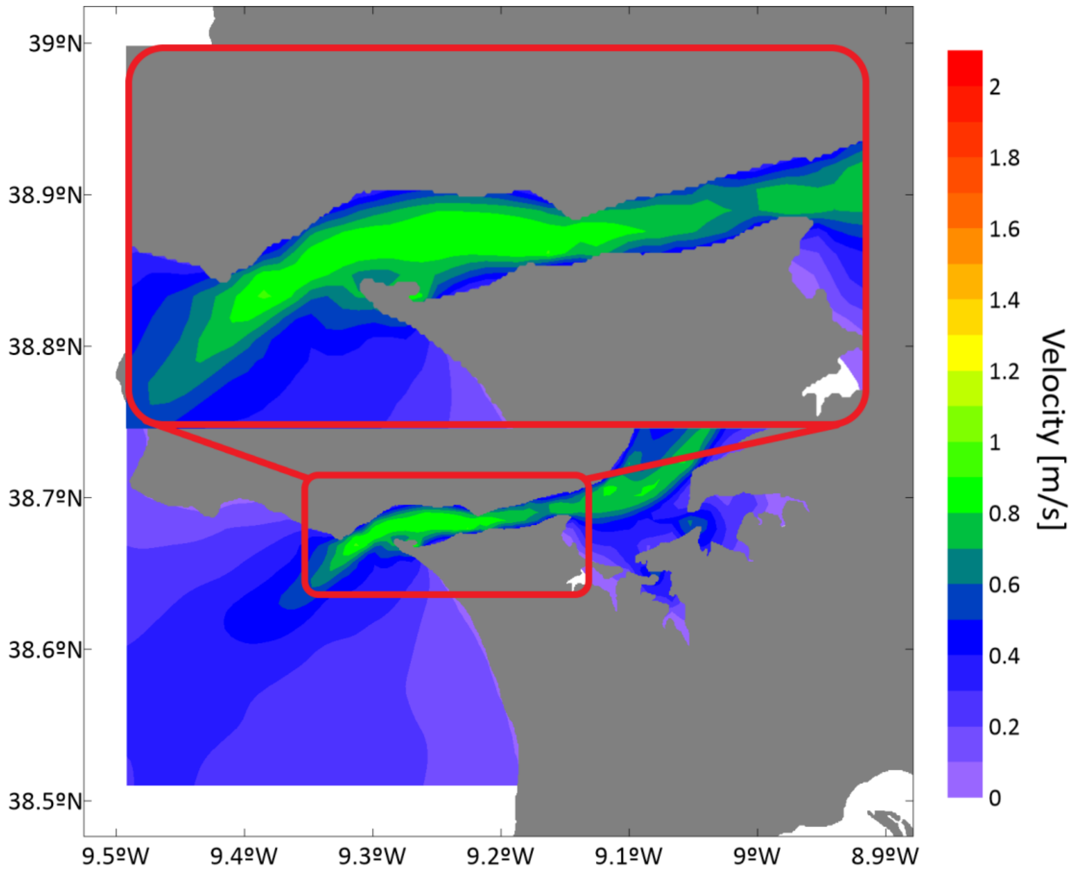

Figure 28 - Average water velocity for an average wet month discharge

It is worth mentioning that the images represented above are representative of the average water velocity overall. The fact that the water flow in the Tagus' mouth is bidirectional (flood and ebb tides) means that the water velocity and direction are always cancelling each other out in every single location, when trying to assess the average values. Therefore, the values portrayed are not representative of the average water velocity and direction during flood tides, nor during ebb tides.

Despite this, all three different scenarios show an average water direction flowing from the Tagus estuary towards the Atlantic Ocean, meaning that the average ebb tide has a higher average velocity than an average flood tide. This would in turn mean that it takes longer for the estuary to fill during a flood tide that it does to empty during an ebb tide, which makes sense, as the ebb tide is working in conjunction with the rivers' discharges in order to discharge the water into the Atlantic Ocean, while a flood tide has to work against the water flowing from the rivers.

It is also worth mentioning that the higher the river discharge, the higher the average water velocity throughout the channel into the estuary, as can be seen when comparing the information in each image. This makes sense, as a higher river discharge implies a larger amount of water that the estuary has to hold in before the ebb tide, thus causing higher current velocities.

In order to assess the locations with the highest energy potential, the fifty areas (model cells) with the highest energy density were highlighted:

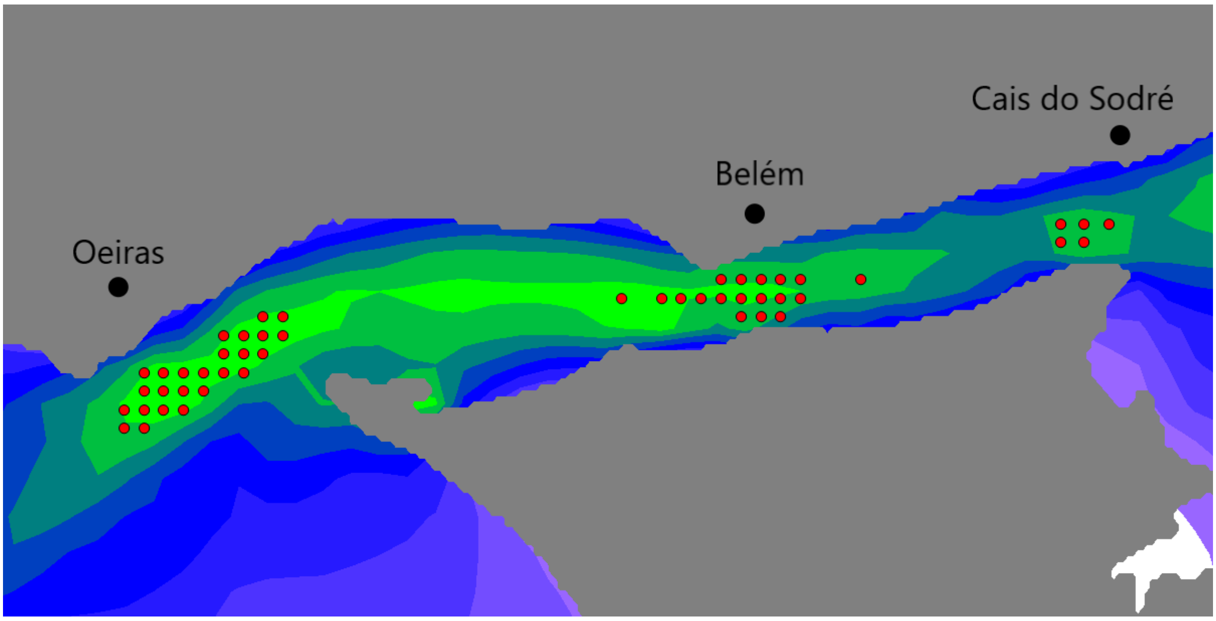

Figure 29 – Fifty areas (model cells) with the highest energy density during the average month simulation

The highlighted points remain largely unchanged for the other two simulations (dry and wet river discharges). Thus, there is a general trend between the three simulations that the locations with the highest energy potential are located within the regions of *Oeiras, Belém* and *Cais do Sodré*.

At this point, it is important to mention that the water channel that connects the Atlantic Ocean to the Tagus estuary is a vital waterway with a large economic importance to the city of Lisbon, as it allows the access of vessels such as cruise ships and cargo ships, which dock in the *Porto de Lisboa* (Lisbon Port). According to APL (2018) – *Administração do Porto de Lisboa*, over 11 million seaborne tonnes of goods and over 500 thousand seaborne passengers went through the Port of Lisbon in the year 2018 alone, meaning that they all had to access the Port via the estuary's channel.

As such, APL (n.d.) has set a mandatory approach navigation channel that goes through the water channel, from the Atlantic Ocean into the different Lisbon Port docks. This channel has to be 250 meters wide to allow for two-way vessel traffic and be dredged to -15.5 m (ZH), allowing for a 14 m service depth. This means that the approach channel allows for vessels with a maximum draught (the vertical distance between the waterline and the bottom of the ship's hull) of 14 meters.

Given the turbines' necessary top clearance of 5 meters (defined in Chapter 4.2.4), other minor vessels such as traffic passenger ships, water-taxis, yachts and recreational ships don't pose a threat to a potential tidal farm, as their draught is usually well below 5 meters.

Therefore, two energy-production assessments will be made:

1. Assuming there are no limits within the estuary channel where a tidal farm could be placed;
2. An exclusion zone made of the port's approach channel is taken into account, where a tidal farm cannot be built due to the movement of ships, which rules out several potential sites for implementing a tidal farm.

The comparison between these two assessments is done in order to compare the maximum theoretical energy that a turbine placed in the channel would produce, with the energy produced by a turbine placed in an area that does not interfere with the port's activity.

For the scope of this thesis, both assessments will determine the energy produced by a turbine in the highest energy density area of each of the regions with the highest energy potential mentioned above (*Oeiras, Belém* and *Cais do Sodré*).

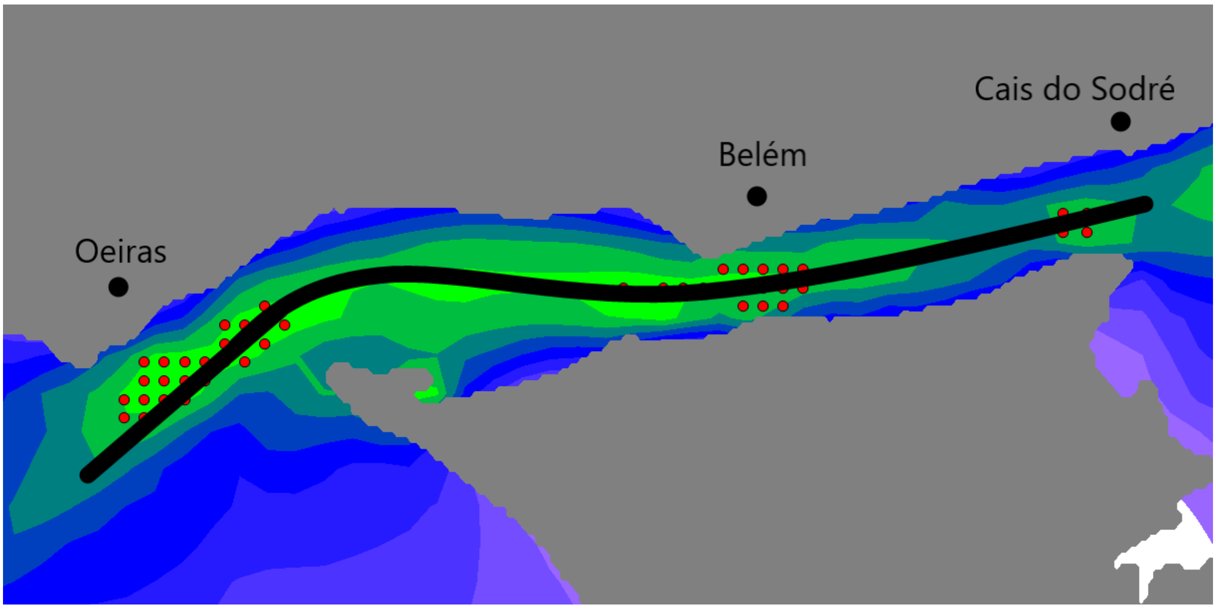

Figure 30 - Port of Lisbon's approach navigation channel (exclusion zone) over the previously highlighted areas

In both assessments, the area used to calculate the energy produced by a turbine is the one with the highest energy potential available in each of the three regions. The selected areas are presented in the following figure, where the points highlighted in red represent the areas with the maximum theoretical energy potential, and the ones in blue represent the areas with maximum energy potential when taking into account an exclusion zone brought by the port's approach channel.

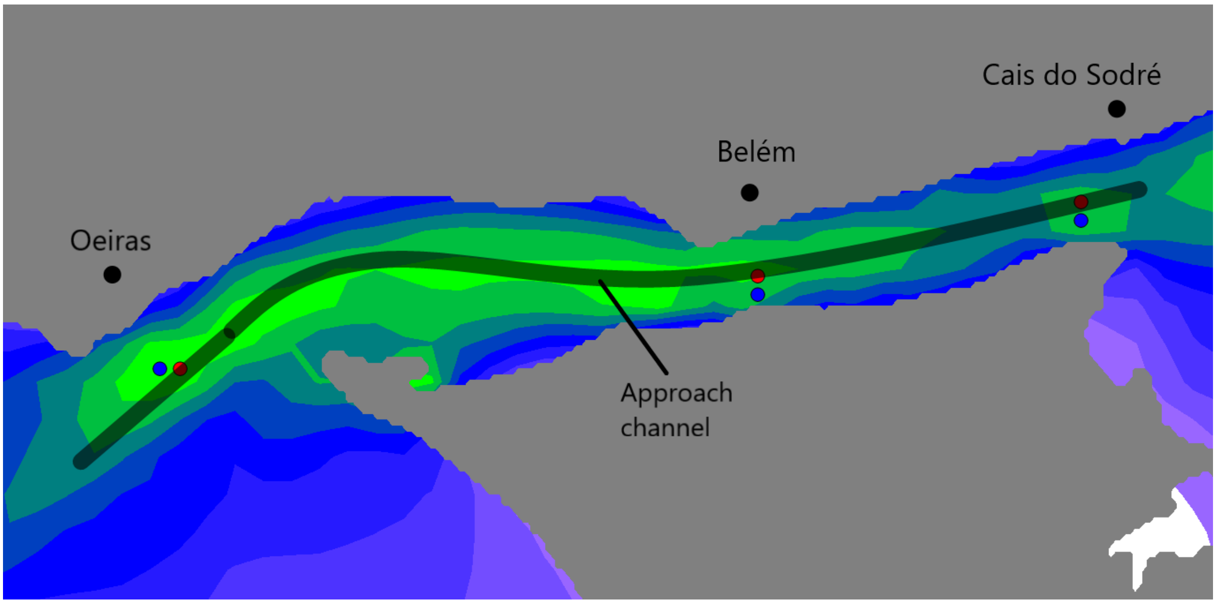

Figure 31 - Areas with the highest energy potential

The following table sums up the information regarding the current velocity of the highlighted points, where the potential energy produced by a turbine will be assessed:

Table 6 - Current velocity data of the highlighted areas of assessment

	Assessment w/o Exclusion Area			Assessment w/ Exclusion Area		
Oeiras	**Dry**	**Average**	**Wet**	**Dry**	**Average**	**Wet**
Area Coordinates	-9.30809º 38.67030º			-9.31151º 38.67030º		
Highest current velocity [m/s]	2.38	2.42	2.51	2.33	2.34	2.39
Average peak current velocity [m/s]	1.38	1.42	1.47	1.38	1.40	1.41
Belém	**Dry**	**Average**	**Wet**	**Dry**	**Average**	**Wet**
Area Coordinates	-9.20894º 38.68380º			-9.20894º 38.68110º		
Highest current velocity [m/s]	2.23	2.37	2.46	2.19	2.22	2.28
Average peak current velocity [m/s]	1.26	1.29	1.38	1.20	1.21	1.28
Cais do Sodré	**Dry**	**Average**	**Wet**	**Dry**	**Average**	**Wet**
Area Coordinates	-9.15354º 38.69460º			-9.15354º 38.69190º		
Highest current velocity [m/s]	2.00	2.01	2.03	1.82	1.79	1.85
Average peak current velocity [m/s]	1.17	1.19	1.22	1.14	1.18	1.25

By assessing the data, one can conclude that when considering different river discharges, the results in terms of water velocity remains largely unchanged. The reason for this is that the amount of water that flows into the estuary thanks to the tides is orders of magnitude larger than the amount of water that the Tagus River could possibly discharge. As was mentioned before, the average tidal range on the Portuguese coast implies the flow of roughly 26 850 m3/s into the estuary, which is vastly higher than the amount of water flow from the rivers that were considered on the different simulations.

This thesis methodology will then only highlight the assessment of energy production of a tidal turbine for the simulation with an average monthly river water discharge. The same methodology will also be applied for the other two simulations (with a low and high river water discharge), but only the final results of the two will be presented.

4.3.1. Assessment of the placement of the turbines

It is important to note that the boundary shear stress caused by the bottom friction of an open channel will cause a force that acts against the direction of the water flow, along the bottom water layer. This in turn causes the vertical distribution of water velocity to differ over the water depth (MIT, 2006).

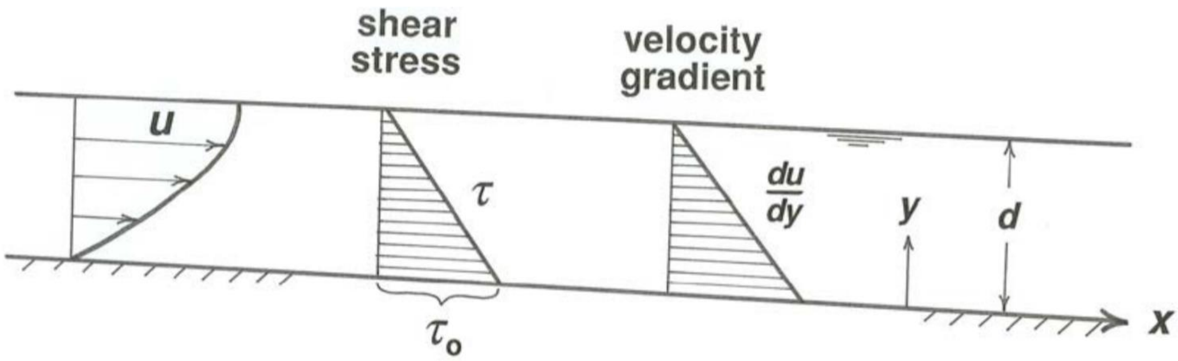

Figure 32 - Vertical distribution of velocity, shear stress, and velocity gradient in steady uniform open-channel flow (MIT, 2006)

This implies that the surface water velocities presented in Table 6 will differ over the water depth of each specific area. Considering that tidal turbines are submerged devices, this makes it necessary to determine the vertical distribution of the water velocity on the highlighted areas of interest. The purpose of this is not only to get a sense of the real current velocities that encompass a tidal turbine, but also to determine the optimal tidal diameter and the optimal depth at which to place it.

Consequently, three cross-sections of the channel were made, to visualize the spatial distribution of the average current velocities in the regions of interest of the month with the average river water discharges.

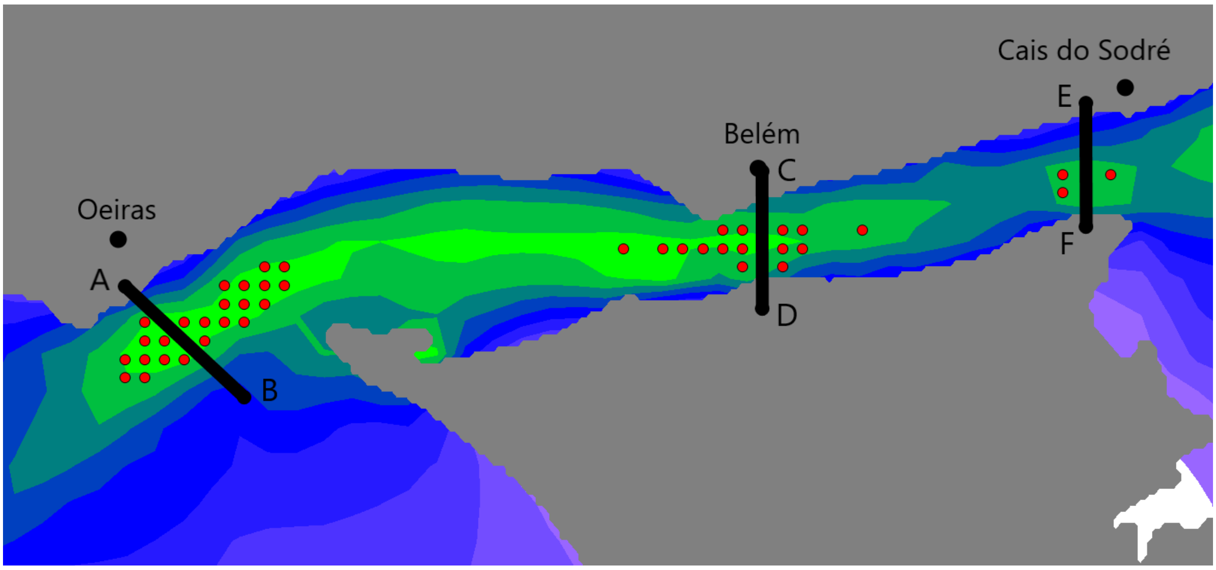

Figure 33 - Placement of the cross-sections of the regions of interest of the average water-discharge month

The following figures 31 to 33 represent the resulting values of the spatial distribution of the average current velocities along the different cross-sections.

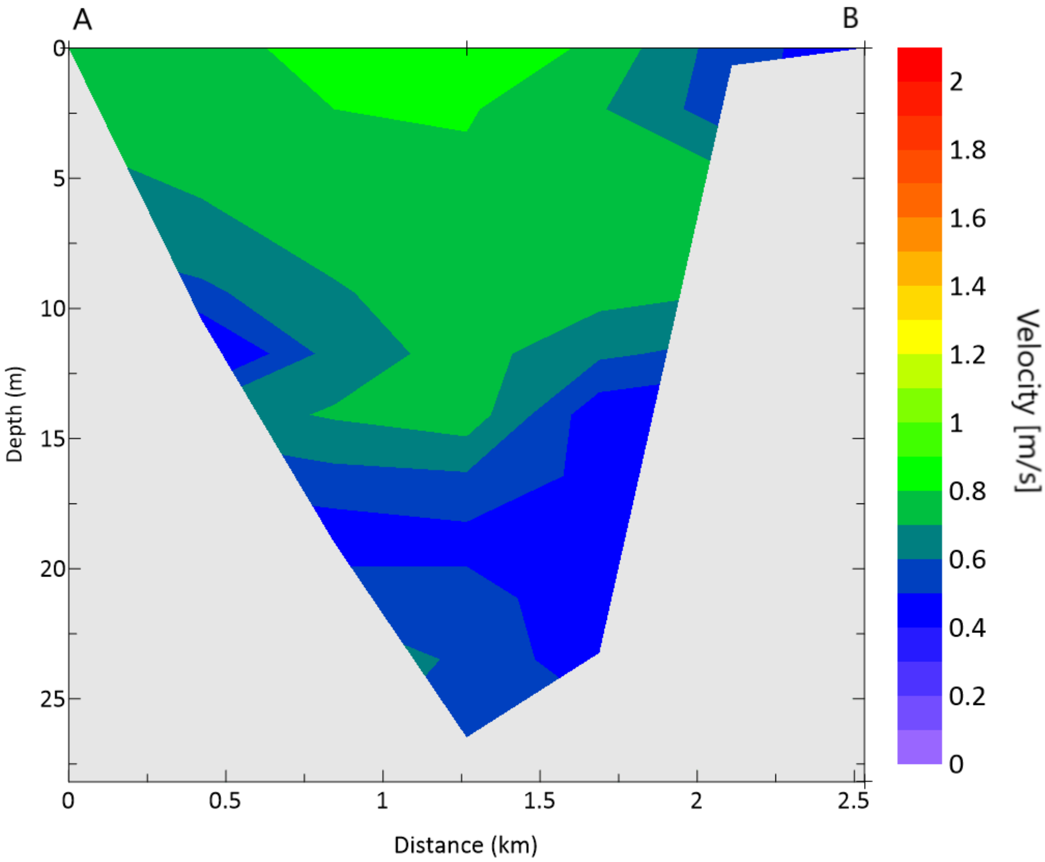

Figure 34 – Variation of the average water current in the Oeiras region on the average water discharge month

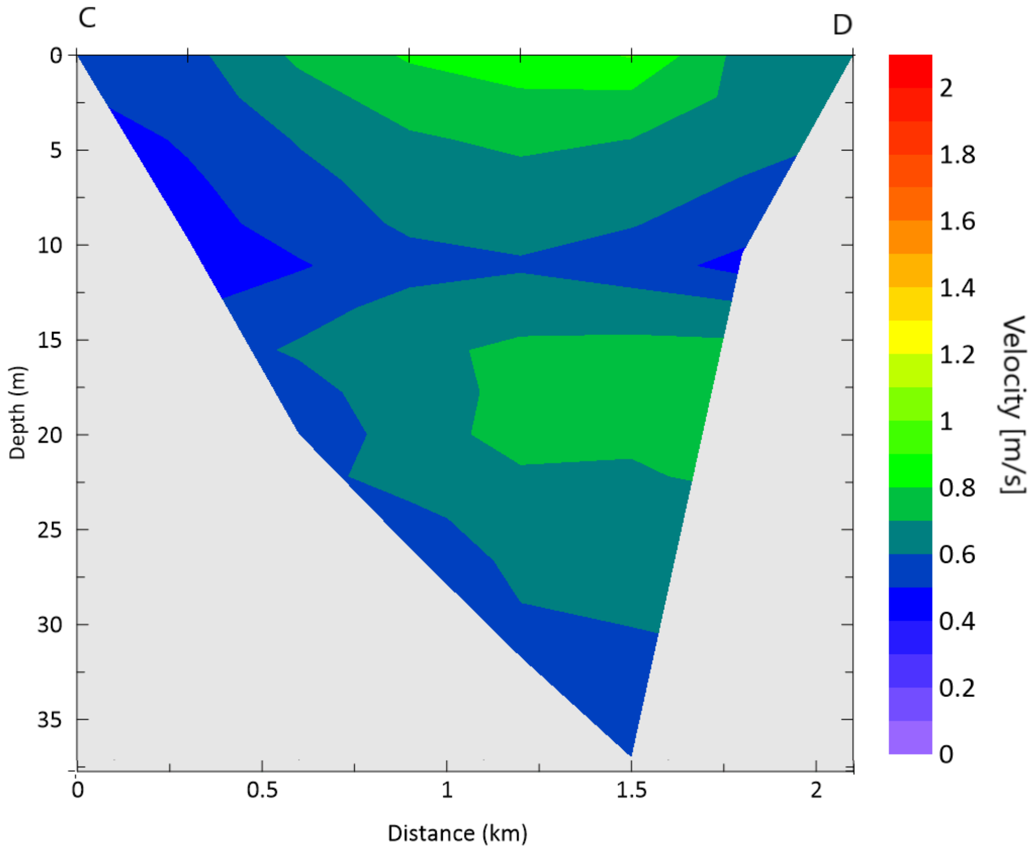

Figure 35 – Variation of the average water current in the Belém region on the average water discharge month

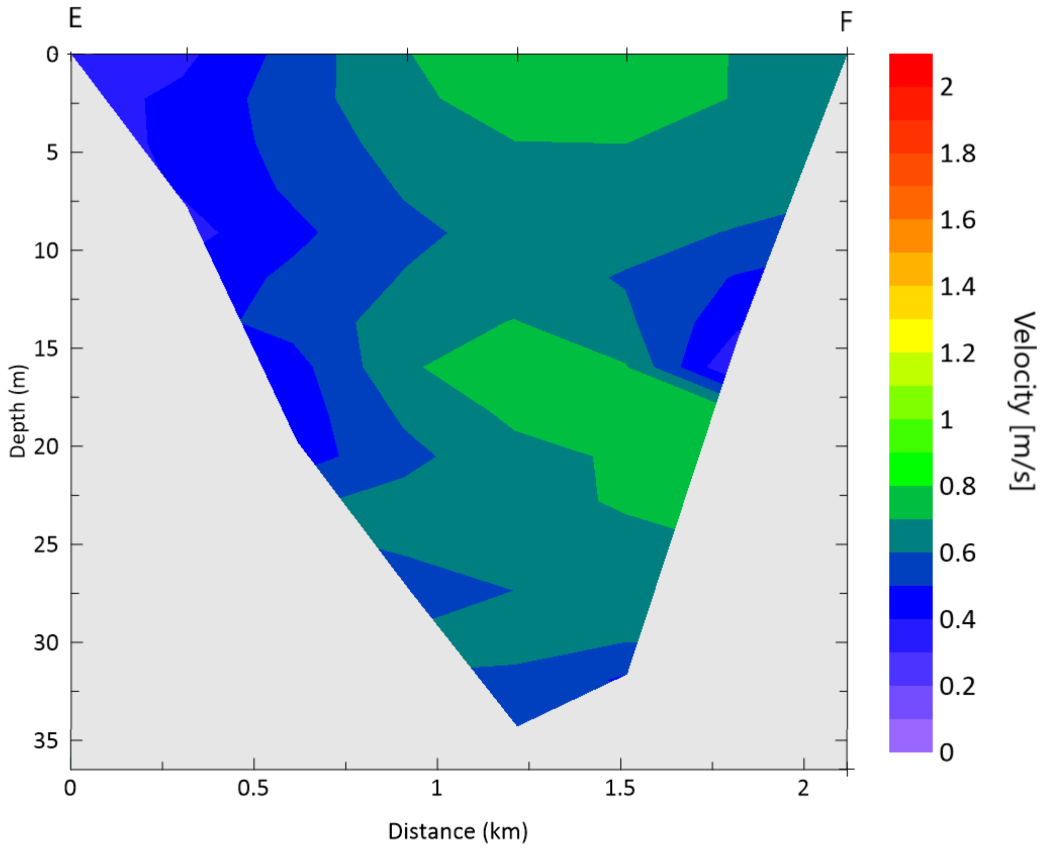

Figure 36 – Variation of the average water current in the Cais do Sodré region on the average water discharge month

Interestingly, both the *Belém* and *Cais do Sodré* regions show submerged areas with a higher average velocity than their surroundings. This suggests that there is high water displacement around 20 meters deep, likely a result of the tidal action, rather than the river action, otherwise the water velocity would decrease gradually from the surface all the way to the bottom, as shown in Figure 32. This, however, does not necessarily mean that these are the optimal regions to place a tidal turbine, as peak water velocities have a significant impact in the energy production of a turbine, as explained in Figure 25. For this reason, and due to the scale of the legend, it is hard to assess what the optimal depth at which to place a turbine is.

To solve this, the same three cross-sections were made. This time, however, the cross-sections were made making use of the results given by the equation of available kinetic energy of a water current (Equation (3)), so as to determine the depth with the highest available power:

$$P = \frac{1}{2} A\rho U^3 \tag{3}$$

Where ρ is the seawater density (=1025 kg/m^3), A is the specific area (=1m^2) and U is the value of the current velocity in any specific simulation cell, at any depth.

The following images illustrate the distribution of available power density along the cross-sections mentioned before:

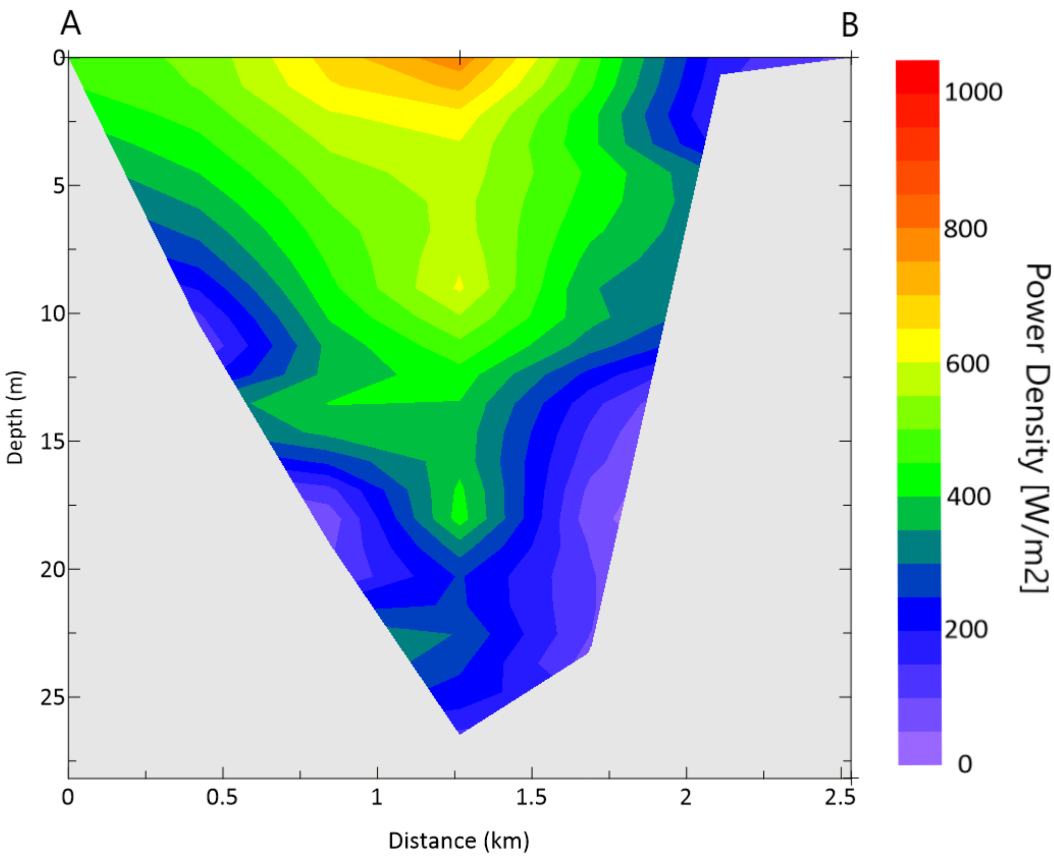

Figure 37 - Variation of the power density per square meter in the Oeiras region

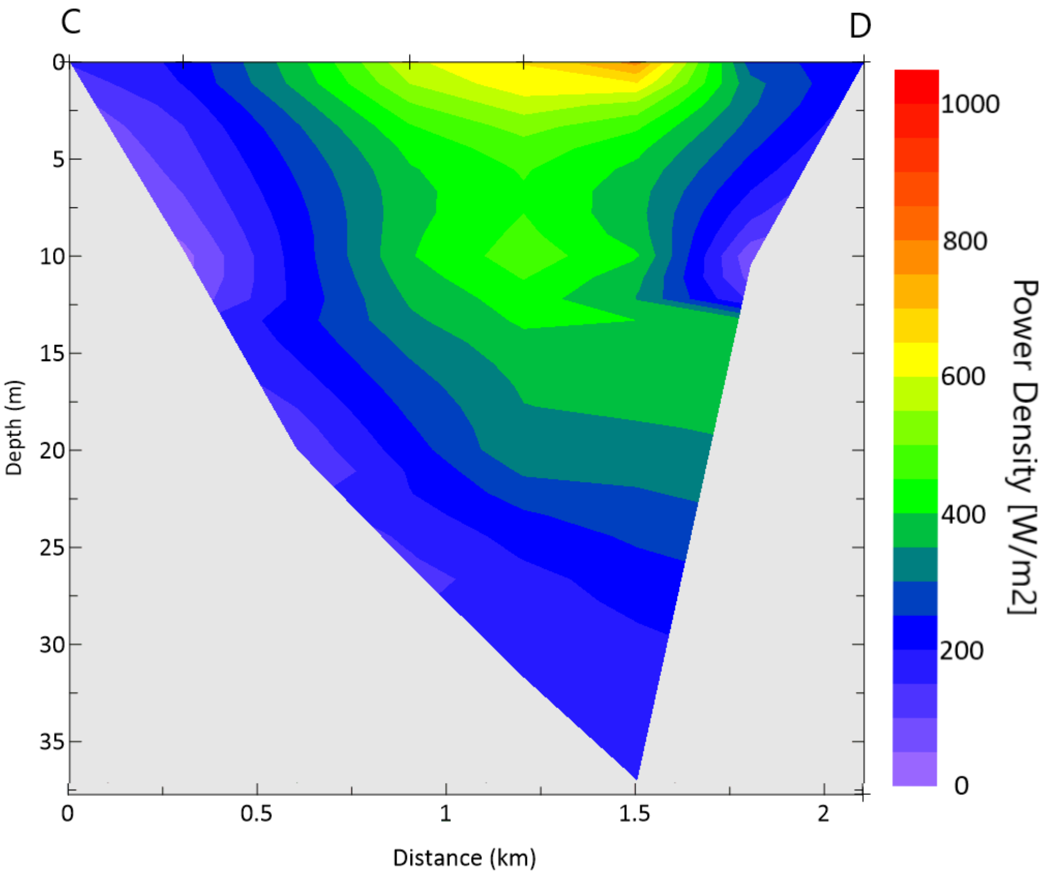

Figure 38 - Variation of the power density per square meter in the Belém region

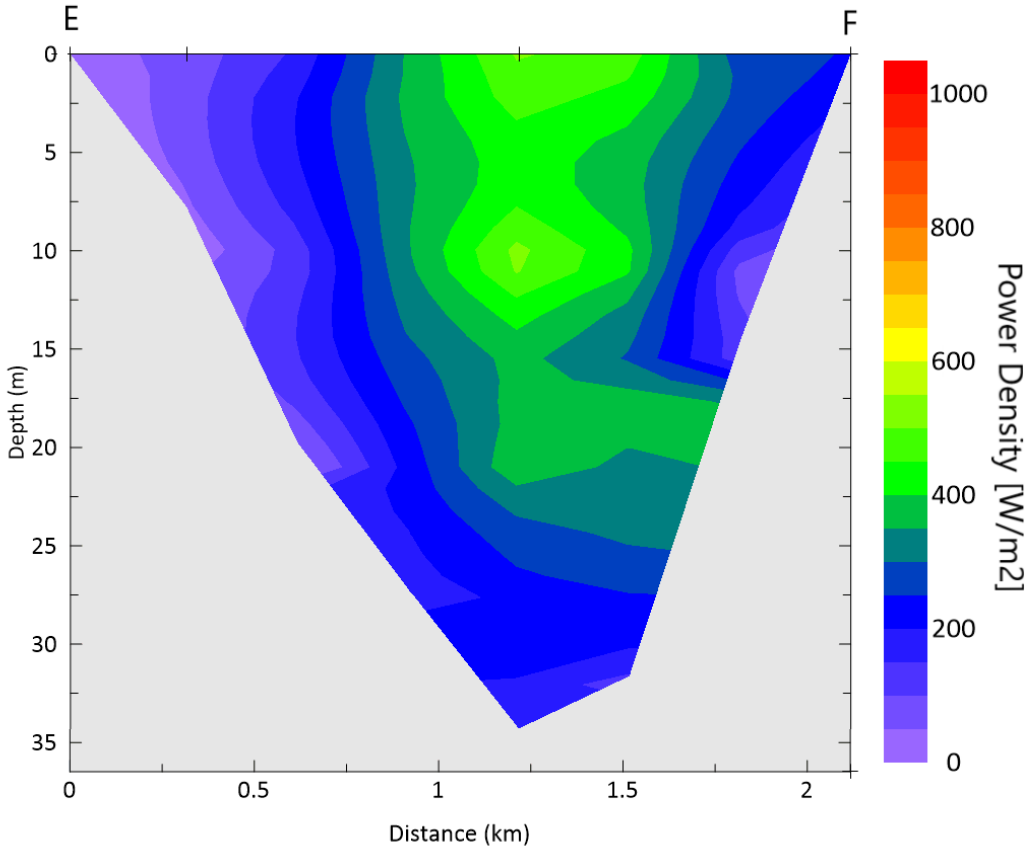

Figure 39 - Variation of the power density per square meter in the Cais de Sodré region

This time around, it is easily discernable that there is an area roughly 8-12 meters below the sea-level with a high power density, in all three regions of interest. As such, this is seen as the optimal depth at which to place the turbine axis, in order for the turbine to harness the largest amount of energy possible.

A cross-sectional assessment of the variation in power density for the three regions in the other two simulations (dry and wet river discharges) was also made, with the results presented in Annex 2.

4.3.2. Assessment of the dimensions of the turbines

Now that the optimal depth at which to place the turbines has been determined, it is time to assess its optimal dimensions. It has already been established, in subchapter 4.2.4, that the diameter of current tidal turbines is limited to 20-25 meters, and that they require a 5-meter top clearance and a bottom clearance of 25% of the water depth.

The following table defines the maximum theoretical diameter that a turbine could have in each of the different areas of interest, based on the limitations mentioned above.

Table 7 - Maximum theoretical turbine diameter for each region of interest

	Assessment w/o Exclusion Area	**Assessment w/ Exclusion Area**
Oeiras	-9.30809º 38.67030º	-9.31151º 38.67030º
Top clearance [m}	5	5
Water depth [m]	26.5	22.5
Bottom clearance [m]	6.63	5.63
Maximum theoretical diameter [m]	14.87	11.87
Belém	-9.20894º 38.68380º	-9.20894º 38.68110º
Top clearance [m}	5	5
Water depth [m]	31.7	37.0
Bottom clearance [m]	7.93	9.25
Maximum theoretical diameter [m]	18.77	22.75
Cais do Sodré	-9.15354º 38.69460º	-9.15354º 38.69190º
Top clearance [m}	5	5
Water depth [m]	34.3	31.6
Bottom clearance [m]	8.58	7.9
Maximum theoretical diameter [m]	20.72	18.7

Although the different locations have different sized turbines, this isn't necessarily a desirable solution, because rotors could start reaching into velocity fields that aren't necessarily relevant, energy density wise. Another argument against having a different-sized turbines solution is the fact that economies of scale would be lost, adding to the complexity and cost of implementation of such a solution, not only in terms of acquisition of the devices, but also in terms of their maintenance.

As such, this thesis considers a 15-meter wide tidal turbine for most assessments, except for the Oeiras zone assessment with an exclusion zone. For this case in particular, a 10-meter wide tidal turbine will be considered, due to water depth limitations.

4.3.3. Assessment of the velocity fields encompassed by the turbines

Given the dimensions of the turbines, it is easy to see that the rotors will be subject to various different current velocities, from various different layers in the modeling simulation.

Subchapter 3.3.2 gave a brief explanation of the role of the module Geometry in the simulation model. It states that the module Geometry allows for a subdivision of the vertical domain into different sub-domains, using different vertical coordinate systems. In this thesis' simulation model, it does so by dividing the water column into 50 layers, of which the 7 first are of Sigma coordinates and the other 43 are of Cartesian coordinates, similarly to the example portrayed in Figure 40.

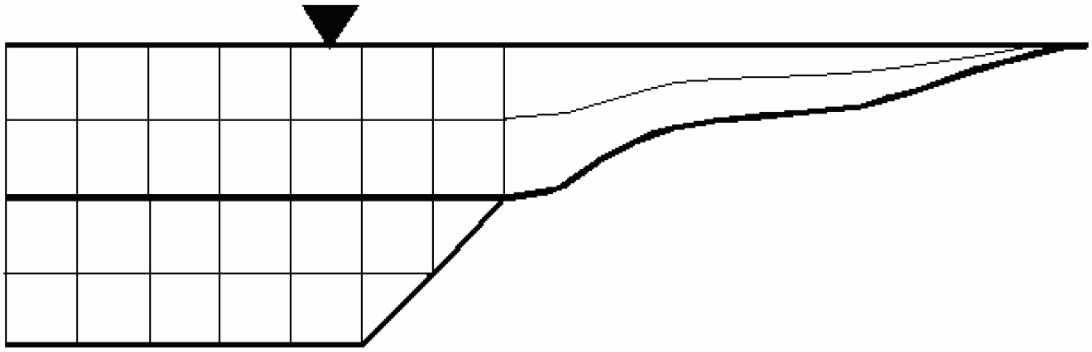

Figure 40 - Example of the sub-division of the water column in a Sigma domain (upper 2 layers) and a Cartesian domain (bottom 2 layers)

In the simulation model, the Sigma domain's 7 layers compute the first 8.68 meters of the water column, while the Cartesian domain's 43 layers compute the rest of the simulation's water column, all the way down to the bottom boundary layer.

Equation (9) states that in order to determine the energy produced by a turbine, one needs to know the turbine's swept area and the water velocity that goes through it. Given that the thesis' simulation model is composed of several layers, one needs to first ascertain the area occupied by the turbine in each layer and multiply it by the water velocity in said layer, in order to determine the average water velocity encompassed by a turbine.

Given the turbine placement's upper and lower restrictions, their horizontal axis is to be placed at a depth of 12.5m and 10m, for the 15-meter and 10-meter diameter turbines, respectively. This is done so in order to allow for a top clearance of 5 meters and in order for the turbines to encompass the layers with the highest velocity fields, as determined in 4.3.1.

Considering the height of each layer, and that the numbering starts at #50 on the surface layer, this means that the 15-meter diameter turbines encompass the velocity fields of layers 39 – 46, while the 10-meter diameter turbines encompass the velocity fields of layers 40 – 46.

By compiling the data of the velocity field for each layer and for each assessment area, in each simulated month, one can assess the turbine's swept area in each layer by using the following equation (Balsells Badia, 2017):

$$A_{Tk} = \frac{r^2}{2}\theta - r \cdot \sin\left(\frac{\theta}{2}\right) \cdot d - \sum_{k=1}^{k} A_{Tk-1} \tag{10}$$

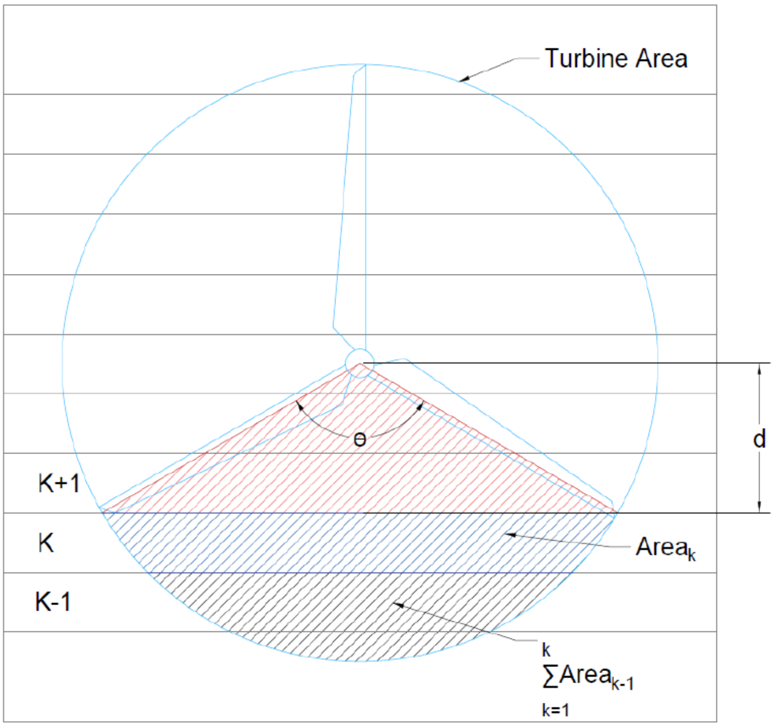

Figure 41 - Vertical discretization of the turbine area (Balsells Badia, 2017)

Where A_{Tk} represents the turbine's swept area in layer k. So, Equation (9) can be rewritten, for a turbine placed in a (i,j) coordinates cell, as:

$$P_T = \frac{1}{2} A \cdot \rho \cdot C_P \cdot \eta_{PT} \cdot U_{AV}^3 \tag{11}$$

Where U_{AV} is the average modulus velocity [m/s] of the k layers on the cell in the coordinates (i,j) that contain the turbine, calculated as:

$$U_{AV} = \frac{\sum_k A_{Tk} \cdot U_k}{\sum_k A_{Tk}} \tag{12}$$

The following tables sum up the average modulus water velocity encompassed by the turbines for each situation mention beforehand.

Table 8 - Average water current going through the turbine in highlighted areas of assessment

	Assessment w/o Exclusion Area			**Assessment w/ Exclusion Area**		
Oeiras	**Dry**	**Average**	**Wet**	**Dry**	**Average**	**Wet**
Area Coordinates	-9.30809º 38.67030º			-9.31151º 38.67030º		
Turbine diameter [m]	15			10		
Highest current velocity [m/s]	2.17	2.18	2.19	2.17	2.19	2.21
Average peak current velocity [m/s]	1.22	1.23	1.25	1.21	1.22	1.23

	Assessment w/o Exclusion Area			Assessment w/ Exclusion Area		
Belém	Dry	Average	Wet	Dry	Average	Wet
Area Coordinates	-9.20894º 38.68380º			-9.20894º 38.68110º		
Turbine diameter [m]	15			15		
Highest current velocity [m/s]	1.79	1.82	1.88	1.83	1.89	1.95
Average peak current velocity [m/s]	1.15	1.19	1.22	1.11	1.14	1.16
Cais do Sodré	Dry	Average	Wet	Dry	Average	Wet
Area Coordinates	-9.15354º 38.69460º			-9.15354º 38.69190º		
Turbine diameter [m]	15			15		
Highest current velocity [m/s]	1.87	1.92	1.97	1.74	1.77	1.80
Average peak current velocity [m/s]	1.20	1.22	1.24	1.12	1.15	1.17

The figures highlighting the discretization of the water velocity going through each turbine and for each situation are displayed in the Annex 3.

In order to determine the mean annual electrical power produced by a tidal turbine, a histogram analysis for the tidal current speed going through a turbine shall be carried out, using the results of the hydrodynamic model. The analysis has been performed by using an interval of 1 hour and a bin size of 0.1 m/s, so as to obtain the percentage of time at which the velocity falls within each bin. The following table presents the results obtain for the different areas of interest, for both assessments.

Table 9 - Total velocity histogram showing the percentage of time that the computed velocity falls within each velocity interval

Velocity bin [m/s]	Oeiras		Belém		Cais do Sodré	
	w/o channel	w/channel	w/o channel	w/channel	w/o channel	w/channel
0	0.64	0.84	0.40	0.64	0.17	0.27
0.1	6.34	6.01	5.07	7.05	5.64	7.28
0.2	5.17	6.07	7.55	7.52	6.74	7.18
0.3	5.13	5.34	6.58	6.98	5.77	6.64
0.4	6.34	5.67	5.81	6.14	5.94	6.14
0.5	6.07	6.88	5.91	6.14	6.98	6.64
0.6	6.21	6.91	6.38	7.89	6.17	7.62
0.7	8.52	8.79	8.76	9.09	8.02	8.56
0.8	11.17	10.91	9.46	10.47	9.03	10.23
0.9	8.93	10.10	10.23	9.56	8.93	9.06
1.0	8.69	7.48	7.95	8.32	7.48	6.81
1.1	7.99	6.48	7.89	7.08	8.02	8.39
1.2	4.53	5.57	6.58	4.26	6.07	4.97
1.3	3.62	1.78	4.53	3.22	4.93	4.43
1.4	2.05	2.01	2.89	1.61	3.99	2.48

Velocity bin [m/s]	Oeiras		Belém		Cais do Sodré	
	w/o channel	w/channel	w/o channel	w/channel	w/o channel	w/channel
1.5	2.35	2.62	1.31	1.44	2.55	1.11
1.6	1.98	1.24	1.54	1.17	1.24	1.54
1.7	1.48	1.98	0.81	0.91	1.24	0.54
1.8	0.84	1.38	0.34	0.37	0.81	0.10
1.9	0.64	0.50	0.03	0.10	0.23	
2.0	0.50	0.47		0.03	0.03	
2.1	0.54	0.70				
2.2	0.27	0.27				

By plotting the velocity distribution (or exceedance curves) with the data in the table above, it is easy to visualize that high-velocity water currents are more frequent in the instance of there being no approach channel into the Lisbon Port. This will then translate into a higher energy density and thus high electricity production on part of these turbines. Figures 42 to 44 showcase the comparison between the exceedance curves in all three regions of interest.

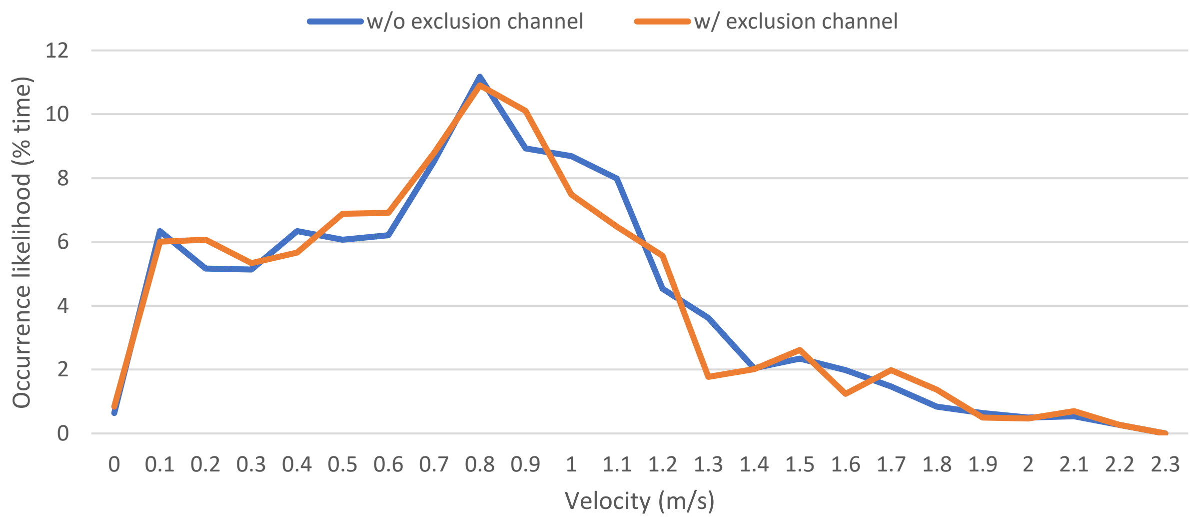

Figure 42 - Velocity distribution curves for the water flowing through the turbines in the Oeiras region

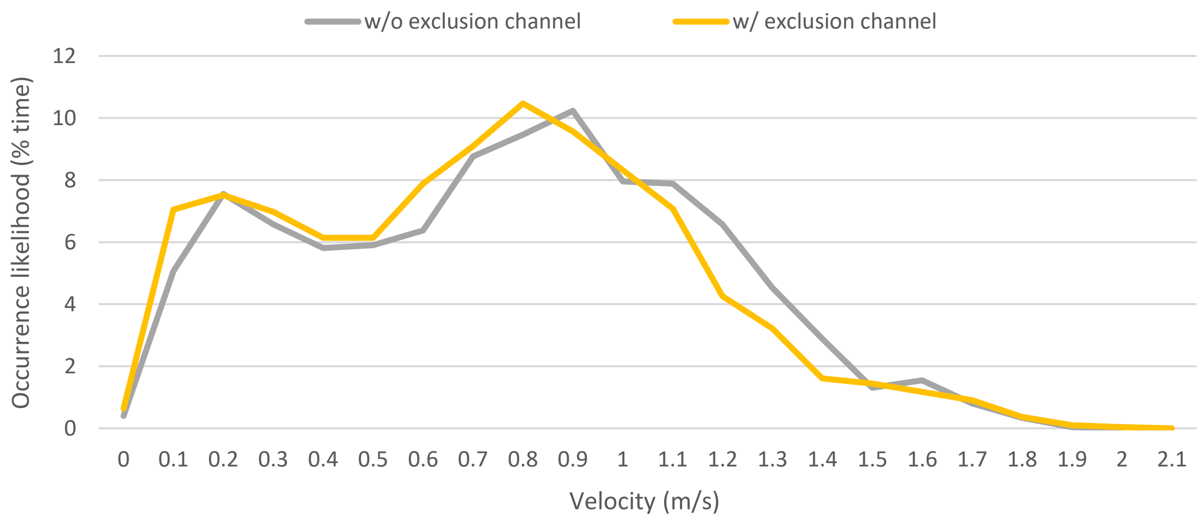

Figure 43 - Velocity distribution curves for the water flowing through the turbines in the Belém region

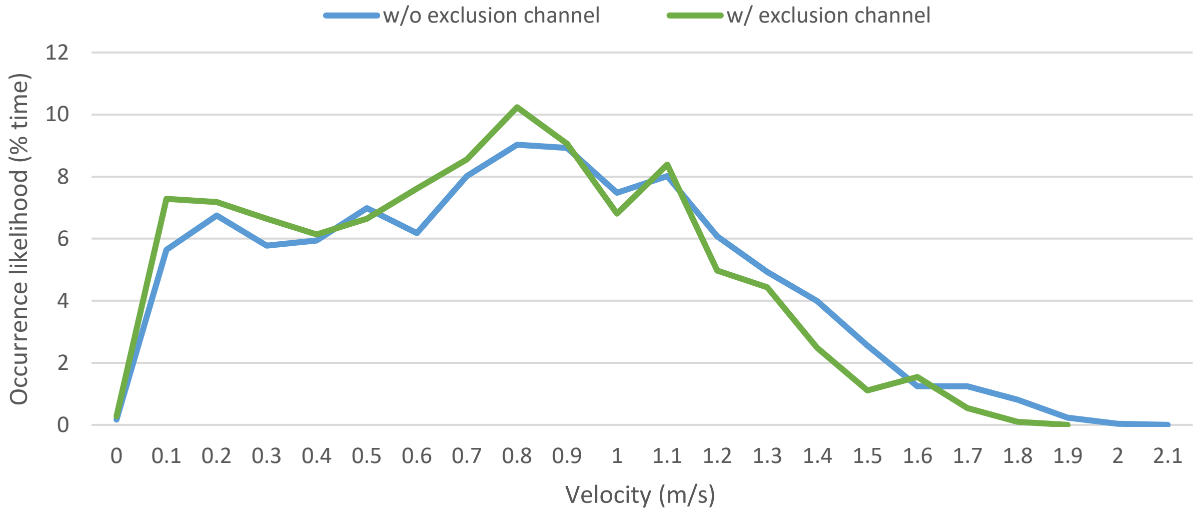

Figure 44 - Velocity distribution curves for the water flowing through the turbines in the Cais do Sodré region

Chapter 5

Analysis and Discussion of Results

5.1. General Overview

This chapter presents the obtained results for each simulated scenario, whilst making an assessment of said results. The simulation model presented beforehand serves as the basis to obtain the pretended results for each simulated scenario.

The different simulated scenarios are bound to present different characteristics, in such a way that different energy production simulations are analyzed. Given how similar the calculations made are from the different scenarios and the different locations, the full explanation will be made for a single scenario, in a single location, with the other scenarios' results simply being presented.

A generic system's economic analysis will also be provided.

5.2. Annual Energy Production (AEP)

Once the velocity distribution in the area of interest has been estimated, it can be applied to a TEC's power curve, in order to calculate its annual energy output.

Since no specific TEC device has been chosen, a generic device will be used for this purpose. Some of its generic characteristics have already been described in 4.2.4. There, it was established that a turbine's rotor power coefficient rises linearly from 0.38 at cut-in-velocity to 0.45 at rated velocity.

The cut-in speed is assumed constant at 0.5 m/s. This assumption greatly simplifies the analysis and, according to EMEC (2013), it does not call into question the accuracy of the results, since the available energy from tidal currents at speeds below 0.5m/s is usually less than 5% of the total available energy.

A turbine's rated velocity is the current velocity at which the power output reaches the limit that the electrical generator is capable of. EMEC (2013) states that the rated velocity can be taken as 71% of the Mean Spring Peak Velocity (V_{msp}), which is the peak tidal velocity observed at a mean spring tide. As such, the following table sums up the different rated velocities for the turbines throughout the different areas of interest.

Table 10 - Areas of interest's rated velocities, or limit that the turbine's electrical generators are capable of

	Oeiras		Belém		Cais do Sodré	
	w/o channel	w/channel	w/o channel	w/channel	w/o channel	w/channel
V_{msp} [m/s]	2.2	2.2	1.9	2.0	2.0	1.8
Rated Velocity [m/s]	1.56	1.56	1.35	1.42	1.42	1.28

Finally, the average powertrain efficiency (η_{PT}) can be considered 90% for a no specific TEC device (EMEC, 2013).

All the parameters necessary to assess the electrical power generated by a tidal turbine over the course of one year have now been determined. Table 11 presents the calculation of the electrical power and of the mean electrical power for each velocity bin used in the velocity distributions computation for the Oeiras region without considering an approach channel. The rotor diameter considered here is of 15 meters, meaning the turbine has a swept area of 177 m².

Table 11 - Mean annual electrical power (kW) in the assessment area w/o channel in the Oeiras region

Velocity bin	Occurrence likelihood	Available power	Rotor power coefficient	Electrical power per bin	Mean annual electrical power per bin
U_i [m/s]	$f(U_i)$ [%]	$P_{AV(i)} = 0.5\rho A U_i^3$ [kW]	C_P [-]	$P(U_i) = P_{AV(i)} \cdot C_P$ [kW]	$P(U_i) \cdot f(U_i)$ [kW]
0	0.64	0.00	0	0.00	0.00

Velocity bin	Occurrence likelihood	Available power	Rotor power coefficient	Electrical power per bin	Mean annual electrical power per bin
U_i [m/s]	$f(U_i)$ [%]	$P_{AV(i)} = 0.5\rho A U_i^3$ [kW]	C_P [-]	$P(U_i) = P_{AV(i)} \cdot C_P$ [kW]	$P(U_i) \cdot f(U_i)$ [kW]
0.1	6.34	0.09	0	0.00	0.00
0.2	5.17	0.72	0	0.00	0.00
0.3	5.13	2.45	0	0.00	0.00
0.4	6.34	5.80	0	0.00	0.00
0.5	6.07	11.32	38	4.30	0.26
0.6	6.21	19.56	39	7.56	0.47
0.7	8.52	31.06	39	12.21	1.04
0.8	11.17	46.37	40	18.54	2.07
0.9	8.93	66.02	41	26.83	2.39
1.0	8.69	90.57	41	37.40	3.25
1.1	7.99	120.54	42	50.57	4.04
1.2	4.53	156.50	43	66.69	3.02
1.3	3.62	198.97	43	86.10	3.12
1.4	2.05	248.51	44	109.18	2.23
1.5	2.35	305.66	45	136.30	3.20
1.6	1.98	370.96	45	155.32	3.08
1.7	1.48	444.95	X	155.32	2.29
1.8	0.84	528.18	X	155.32	1.30
1.9	0.64	621.19	X	155.32	0.99
2.0	0.50	724.53	X	155.32	0.78
2.1	0.54	838.73	X	155.32	0.83
2.2	0.27	964.35	X	155.32	0.42
				$\boldsymbol{P_{mean}}$	**34.80 kW**

By adding up the mean annual electrical power of the different velocity bins, it can be determined that a turbine with a diameter of 15 meters placed in the highest energy density area of the Oeiras region has a mean annual electrical power of 34.80 kW. As for the annual energy production (AEP) of said turbine, it can be obtained by multiplying the P_{mean} computed above by the available hours per year and the powertrain efficiency, as follows:

$$AEP = 8760 \cdot \eta_{PT} \cdot P_{mean} \tag{13}$$

All things considered, the turbine described would have an annual energy production of roughly 274.4 MWh.

According to PORDATA (n.d.), there are (in 2017) roughly 86 487 houses (villas and apartments) in Oeiras. When considering the county's domestic electrical energy consumption of 192.586,6 MWh in that same year (PORDATA, n.d.), we can conclude that an average house in Oeiras has an annual electrical energy consumption of 2.2 MWh.

As such, a single tidal turbine with a diameter of 15 meters placed in the area with the highest energy density near Oeiras has the potential to power nearly 125 houses there.

The same assessment was done for all other areas of interest, and the results for their annual energy production and the number of houses they can power are presented in the following table:

Table 12 - AEP for a single turbine in the different assessment areas, and number of houses powered

	Oeiras		Belém		Cais do Sodré	
	w/o channel	**w/channel**	**w/o channel**	**w/channel**	**w/o channel**	**w/channel**
Turbine diameter [m]	15	10	15	15	15	15
P_{mean} [kW]	34.80	15.06	28.94	25.52	32.83	25.48
AEP [MWh]	**274.37**	**118.69**	**228.18**	**201.20**	**258.83**	**200.84**
Annual energy consumption [MWh/house]	2.2		2.1		2.1	
# houses powered	**124.73**	**53.95**	**108.66**	**95.81**	**123.25**	**95.64**

5.3. Monthly Energy Production (MEP)

Although knowing a tidal turbine's annual energy production is important, it is also relevant to know how this electric energy is produced throughout the course of one month. This time around, instead of grouping the velocity data into different velocity bins, Equation (11) was used directly for the values of water velocity throughout one month instead.

Figure 45 shows the variation in the current velocity going through the turbine in the area with the highest energy in the Oeiras region, for the different simulated months

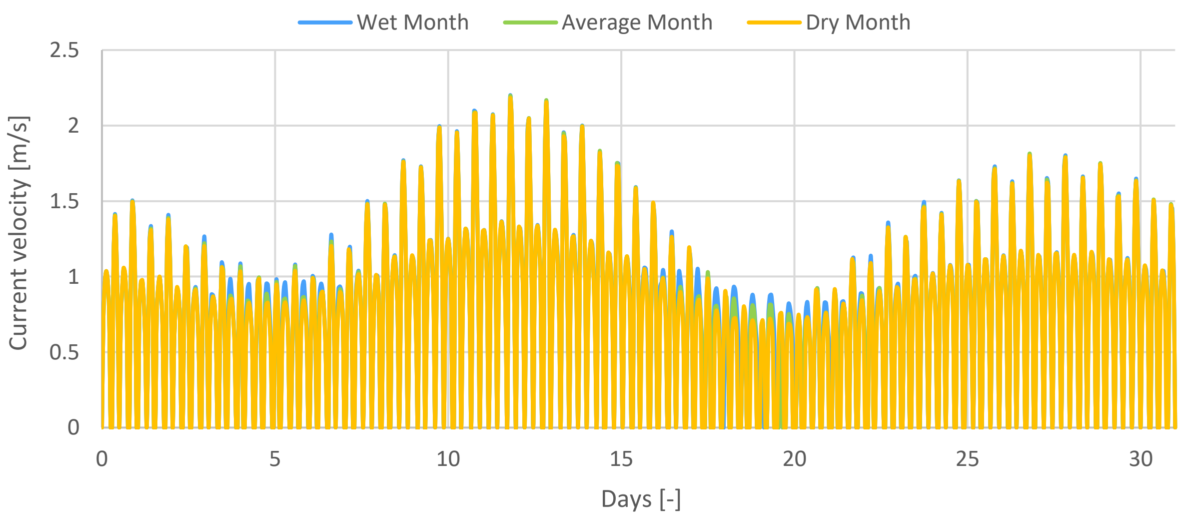

Figure 45 - Discretization of the water velocity going through the turbine in the Oeiras region with the highest energy density

It is easily discernable that the different river discharges (computed in the different model simulations), have very little impact of the current velocities that occur during the spring tides, as the water coming into the estuary from the tidal action is the determinant factor in the current velocities.

The same cannot be said during the neap tides, as river discharges have a greater ponderosity in the water that builds up in the estuary, meaning greater current velocities during a wet month rather than on an average and on a dry month.

When using these values for the current velocity in Equation (11) (and also bearing in mind the resulting rotor power coefficient), we can assess the turbine's power generation at any given instance during the month, as is shown in Figure 46.

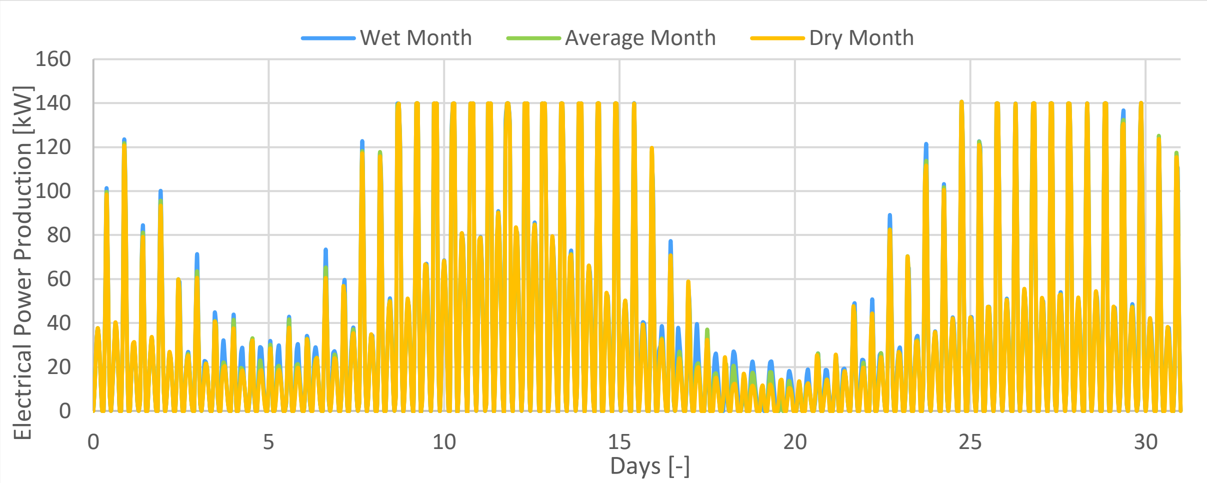

Figure 46 - Discretization of the turbine's electrical power output throughout the month

It can be concluded that the only instances where the turbine reaches its rated velocity is during the spring tides, as there is a limit to how much power a turbine can produce. That being said, it is possible to add-up the electrical power that is output throughout the month to get a sense of the turbine's total monthly energy production.

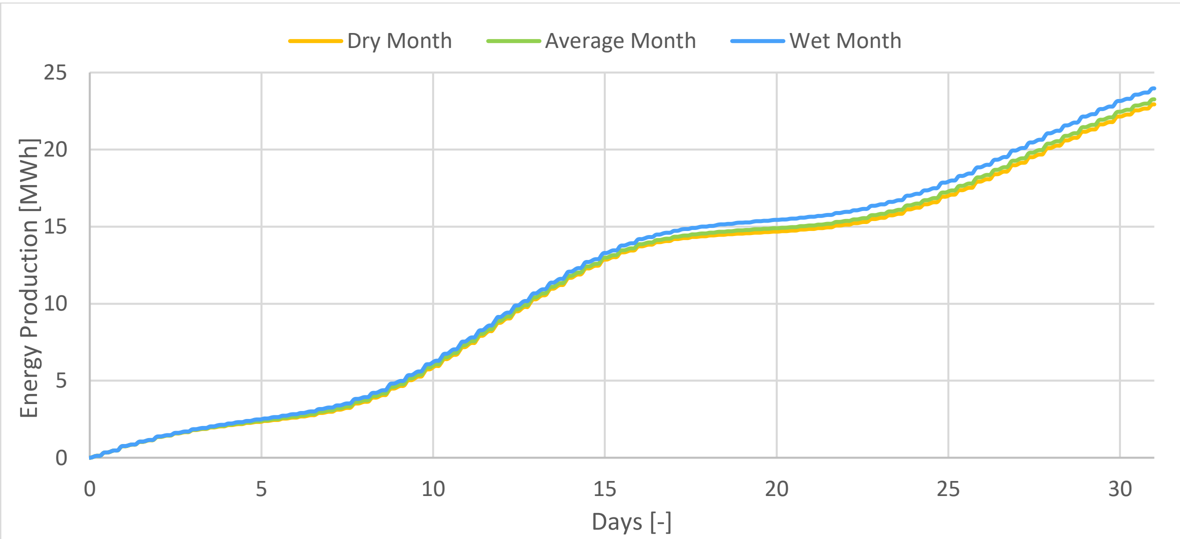

Figure 47 - Cumulative energy produced by the turbine over the course of the month

As can be seen in Figure 47, the energy production pattern from a tidal turbine placed in the Tagus estuary remains largely unchanged over the course of the year, as different simulations with different river discharges show similar amounts of electrical energy produced.

In the case of a 15-meter diameter turbine placed in the area with the highest energy density in the Oeiras region, this amounts to roughly 22.93 MWh during a dry month, 23.26 MWh during an average month, and 23.97 MWh during a wet month. By assuming that a year is composed of 6 dry months, 3 average months and 3 wet months, we can estimate that the turbine's annual energy production is 279.30 MWh, which is a bit over the value determined in subchapter 5.2, of 274.37 MWh. The reason for this discrepancy is likely linked to the fact that the values for the current velocity in the assessment of the AEP were rounded in order to be grouped into velocity bins, instead of using the actual values, which gave rise to a slightly more conservative estimate.

The same can be said for the other areas of assessment, whose results are presented in the following table:

Table 13 - MEP for a single turbine in the different assessment areas

Region	Assessment (Turbine diameter)	River discharge	Monthly Energy Production [MWh]	Annual Energy Production [MWh]	AEP [MWh] (Assessed in 5.2)
Oeiras	w/o exclusion area (15m)	**Dry**	**22.93**	**279.30**	274.37
		Average	**23.26**		
		Wet	**23.97**		
	w/ exclusion area (10m)	**Dry**	**9.86**	**120.64**	118.69
		Average	**10.10**		
		Wet	**10.39**		
Belém	w/o exclusion area (15m)	**Dry**	**18.49**	**232.54**	228.18
		Average	**19.71**		
		Wet	**20.82**		
	w/ exclusion area (15m)	**Dry**	**16.41**	**204.26**	201.20
		Average	**17.30**		
		Wet	**17.97**		
Cais do Sodré	w/o exclusion area (15m)	**Dry**	**21.18**	**261.86**	258.83
		Average	**22.19**		
		Wet	**22.75**		
	w/ exclusion area (15m)	**Dry**	**16.64**	**203.45**	200.84
		Average	**17.08**		
		Wet	**17.46**		

Compared to the AEP values assessed in 5.2, the AEP values determined from the turbine's MEP is slightly higher. The reason for this is that the water velocities in that assessment were grouped into velocity bins, which can give rise to inaccuracies due to rounding. Nonetheless, the results determined in subchapter 5.2 present a more conservative estimate of a turbine's electric energy production, which is why these will be the values assumed for the remainder of the thesis.

The figures referent to the assessment of the turbines' monthly energy production in the other areas of interest are presented in the Annex 4.

5.4. AEP comparison with the Module Turbine

Besides the three different model simulations that were done for the assessment described beforehand, a 4th simulation was also computed. The difference between this and the other simulations, is that this time, the MODULE TURBINE was engaged in the simulation model.

The Module Turbine is a MOHID module that was coded recently into the programming software by an IST's Masters student (Balsells Badia, 2017). This module serves to determine the impact that a tidal turbine has on a water current's flow, and how much power it can draw from it.

This simulation comes to show how good of an approximation to the industry's guidelines way of assessing a tidal turbine's electrical energy production this Module is, or not, and how it can be perfected. This module was done in order to instantly assess a potential tidal farm's electric energy production, when using MOHID.

The differences between the MOHID's Module Turbine and the assessment done in this thesis come mainly in three forms:

1. It considers a constant rotor power coefficient (C_P) from a turbine's cut-in speed to its rated velocity, rather than having it rise linearly;
2. It assumes a security factor of 15% of the cut-in speed, meaning that once a turbine rotor starts spinning, it won't stop producing electric energy until the current velocity falls below 85% of the turbine's cut-in speed. Once it decreases below this value, the water current needs to increase again over the cut-in speed in order to kick-start the turbine rotor;
3. It does not take into account the powertrain efficiency.

This simulation has the exact same specifications as the one for the month with the average river discharge, so as to offer a point of comparison between the two. The difference here is that 6 turbines were placed in the simulation model: one for each of the areas of interest. All of them have the exact same specifications as the ones in the turbines determined above, in terms of location, diameter, cut-in speed, rated velocity and depth at which they are placed.

The sole difference in the turbine's characteristics, is that they were set to have a constant rotor power coefficient of 0.40 from the cut-in speed, to the rated velocity.

As such, the following table sums up the different turbine's annual energy production (for a simulated month with an average river discharge) assessed through the MOHID's Module Turbine and compares them to the values assessed earlier. However, given that only an average water discharge month was simulated this time, the turbine's AEP was calculated considering that one year consists of 12 average water discharge months, instead of the previous assumption of it being composed of 6 dry months, 3 average months and 3 wet months

Table 14 - Comparison of the AEP assessment for both methods

	Oeiras		Belém		Cais do Sodré	
	w/o channel	**w/channel**	**w/o channel**	**w/channel**	**w/o channel**	**w/channel**
Turbine diameter [m]	15	10	15	15	15	15
AEP [MWh] (Module Turbine)	**274.95**	**111.08**	**239.18**	**137.91**	**255.28**	**173.88**
AEP [MWh] (assessed in 5.2)	274.37	118.69	228.18	201.20	258.83	200.84
AEP [MWh] (1 year = 12 average months)	**279.11**	**121.18**	**236.50**	**207.64**	**266.24**	**205.00**
Similarity [%]	**98.51**	**91.66**	**101.13**	**66.42**	**95.88**	**84.82**

It is easy to see that the Module Turbine that was coded into MOHID offers, for most situations, a good approximation to a turbine's electrical energy production, even without taking into account the powertrain efficiency.

Where it falls short is when the assessment is made in less energy dense locations. One possible explanation for this is the fact that the turbine's electrical output is stifled by the imposition of a fixed value for the rotor power coefficient, whereas this value varies from 0.38 (at cut-in speed) to 0.45 (at the rated velocity), according to the industry's guidelines (EMEC, 2013).

Figure 25 (Page 40) showed how important the water current velocity is when determining a turbine's electrical power output, meaning that the highest water currents are the most determinant in a location's power generation. By placing a cap of 0.40 on the turbine's rotor power coefficient, this means that the turbine isn't harnessing as much energy as it could during peak currents. This is especially relevant for the areas of assessment when considering a navigation channel, where the peak water currents are paramount in those areas' electrical energy potential.

This could be rectified by raising the rotor power coefficient to the guideline's limit of 0.45, but that would only result in an overestimation of the electrical energy generated by a turbine.

As a result, having a variable rotor power coefficient is important when trying to assess a turbine's energy potential, thus being a good correction to be made in the Module Turbine, coded into the MOHID software. Another easy, and yet relevant correction would be to consider the turbine's powertrain efficiency.

The figures with the comparison of the monthly cumulative energy production for both assessment methods are presented in Annex 5.

5.5. Annual Energy Production of a Potential Tidal Farm

Now that a single turbine's electrical energy output when placed in different locations of the Tagus river has been established, it is time to determine how much energy a tidal farm could generate.

When considering that a grid cell on the estuary's lower section (see Figure 19) in the simulated model is roughly 300x300m, one can assess how many tidal turbines can be fit in such an area, given EMEC's guidelines, presented in Figure 24. As such, the following table sums up the number of tidal turbines that can be placed in each grid cell section on the assessment areas, and what their annual electrical production would be, when considering the values assessed in 5.2 for a single turbine:

Table 15 – Annual Energy Production of a Potential Tidal Farm in each of the interest areas, and the #houses each powers

	Oeiras		**Belém**		**Cais do Sodré**	
	w/o channel	**w/channel**	**w/o channel**	**w/channel**	**w/o channel**	**w/channel**
Turbine diameter [m]	15	10	15	15	15	15
Grid Cell size [mxm]	300x300	300x300	300x300	300x300	300x300	300x300
# Turbines	**24**	**48**	**24**	**24**	**24**	**24**
AEP [GWh]	**6.58**	**5.70**	**5.48**	**4.83**	**6.21**	**4.82**
Annual energy consumption [MWh/house]	2.2		2.1		2.1	
# houses powered	**2 991**	**2 591**	**2 610**	**2 300**	**2 957**	**2 295**

Considering this, it is safe to assume that any tidal farm that is 300 meters long by 300 meters wide and that is placed in one of Tagus' river most energy density areas (while considering a vessel approach channel) can generate enough electricity to power on average 2 400 houses.

According to EDP (2017), 1 kWh of electrical energy requires roughly 269 grams of CO_2 emissions to be generated. Given the table above, this means that the average considered tidal farm placed in the Tagus river is capable of removing 1 360 metric tons of atmospheric CO_2 emissions every year, which is the equivalent to removing 296 passenger vehicles from the streets, as a typical one emits about 4.6 metric tons of carbon dioxide per year (US EPA, 2016).

Comparatively to the number of houses that a tidal farm can power, or the equivalent number of car-emissions it curbs, one can also look into the amount of power that is consumed in order to light up the public streets, through the light poles.

According to PORDATA (n.d.), the amount of electric energy consumed by the city of Lisbon in order to power the street lighting, in 2017, was 66.09 GWh. The *Oeiras* county, on the other hand, consumed a total of 13.11 GWh for the same purpose, and during the same year. When considering placing the assessed tidal farms in the different areas of interest, one can be used to power the *Oeiras* county, while the other two can power the city of Lisbon.

As such, a 48-turbine tidal farm, placed in the most energy dense area in the *Oeiras* region (while allowing the normal functioning of the Port of Lisbon) has the potential to power roughly 44% of the county's entire electric energy used to light the street lights on. By using the same principle for the other two 24-turbine tidal farms placed in the *Belém* and *Cais do Sodré* regions, they would have the potential to power up to 15% of the city's entire energy use for public lighting.

5.5.1. Tidal Farm Economic Analysis

All in all, when considering the LCOE value of 0.15 €/kWh determined in 2.3.2, it would cost roughly €16.8 million over the course of 20 years in order to implement the average considered tidal farm in the Tagus estuary.

This cost can be further broken into CAPEX and OPEX costs, based on what was said in 2.3.2. The following table breaks down the LCOE cost of an average 24-turbine tidal farm producing 5.6 GWh of electric energy annually over the course of 20 years:

Table 16 - LCOE breakdown of an average 24-turbine tidal farm in the Tagus River over the project's lifetime

Cost Category	Total Cost
CAPEX [€]	**10.080.000**
Project development [€]	672.000
Grid connection [€]	1.176.000
Device [€]	4.872.000 (€203.000/turbine)
Moorings and foundation [€]	1.680.000
Installation [€]	1.512.000
OPEX [€]	**6.720.000**
Material costs [€/year]	23.520
Transport costs [€/year]	215.040
Labour costs [€/year]	6.720
Production losses costs [€/year]	6.720
Insurance costs and Fixed expenses [€/year]	191.520

When considering that the actual electric energy supply cost in Portugal sits at 0.22 €/kWh (PORDATA, n.d.), this makes the pursuit of cheaper and cleaner alternatives more attractive. With an expected LCOE cost of 0.15 €/kWh, the solution of a tidal farm in the Tagus estuary could be seen as a legitimate alternative to power a good part of the nearby county's electric energy consumption in order to illuminate the public streets. Such a project would reach its break-even point after 11.25 years and show a €7.84M profit after its 20 years lifetime, provided that the electric energy supply cost in Portugal sits at 0.22€/kWh.

It has already been shown that a tidal farm placed in the Tagus estuary has the potential to power a good part of the nearby coastline's public lighting. The estuary's reduced wave action when compared to offshore conditions, coupled with its close proximity to the power grid and maintenance infrastructures means that few funds would be spent in expensive underwater powerlines, nor complex mooring solutions. The following subchapter looks into possible solutions that can be adopted in order to achieve the desired solution.

5.5.2. Technical Solutions

The presented technical solutions follow a theoretical approach, whilst relying on the estuary's morphological conditions, referencing some environmental issues and restrictions relative to the installation of a tidal farm.

By being in close proximity to the power grid and to the necessary infrastructures – such as ports and marinas – in order to provide the tidal farm with technical support, such a project would have great operational potential if it were to be placed in the Tagus estuary. The fact that it would be implemented in an estuary rather than a water channel in the middle of the ocean, also means that installation and maintenance operations should be considerably easier than the ones performed in offshore locations, due to reduced wave action.

The horizontal-axis turbines present a greater variability in their dimensions and installation methods: they can be anchored to the ocean floor through a mono-pile, a gravity-based foundation, or even installed in floating structures, in modules capable of being grouped.

As was mentioned, the estuary's reduced wave action makes it unnecessary for a mono-pile anchorage to be used, as these are characterized as being more technically challenging to install and maintain, and thus more expensive. This issue is mitigated when considering a floating structure that supports the turbines, which would be itself moored to the sea floor via cables. These turbines' main advantage over the other solutions is their easy access to maintenance operations and insurance that the turbines would always be submersed, as they accompany the water level. Another inherent advantage is their mobility, as they can be moved to wherever the highest energy potential area is at any given moment. The fact that there is a floating structure, however, implies that an exclusion zone would have to be created for other vessels, as these would not be able to navigate through the turbines. The fact that they are placed in an estuary also makes them more susceptible to being hit by debris flowing from the river, such as tree logs, which could damage these structures. As such, the ideal solution to be adopted for a tidal farm placed in the Tagus estuary is expected to be composed of bi-directional tidal turbines moored by a gravity-based solution.

As such, any of the gravity-based horizontal tidal turbine solutions presented in Annex 1 is a viable solution to be implemented in the Tagus estuary, provided that they are properly dimensioned given the estuary's bathymetry. Such solutions are as follows:

Table 17 - Possible tidal turbine solutions to be implemented in the Tagus Estuary

Company	Device name	Mooring solution	Rotor Diameter [m]	Rated Power [MW]	Ref.
Andritz Hydro Hammerfest	HS1000	Gravity-based	21	1.0	[2]
Atlantis Resources Corp.	AR-1500	Gravity-based	18	1.5	[6]
Marine Current Turbines	SeaGen U	Gravity-based	3x(16-20)	1.8-3.0	[57]
Nova Innovation Ltd	Nova M100	Gravity-based	9	0.1	[64]
Oceana Energy Company	TIDES	Gravity-based	2-18	>3	[68]
SABELLA SAS	D03	Gravity-based	3	0.03	[86]
Tidal Energy Ltd	DeltaStream	Gravity-based	-	0.4	[59]
Verdant Power	Free Flow System	Gravity-based	3x5	-	[102]

Chapter 6

Conclusions and Future Work

6.1. Achievements

The implementation of renewable energy sources in city centers is of paramount importance given the current state of needing to reduce the greenhouse gas emissions, by relying less on fossil fuels and diversifying on several different clean energy sources.

The energy sector is dominated by finite and polluting energy sources, where 80% of the world's primary energy produced is non-renewable. As such, it is vital to increase the proportion of energy produced through renewable sources, namely hydro, wind and solar, without them having negative impacts in the countries' economies. Unlike fossil fuels, however, renewable energy sources are not available on demand, meaning that when there is a peak in power demand, the wind might not be blowing, or the sun might not be shining. Since there is currently no economically viable way of storing electric energy, one way of mitigating this issue is by diversifying the renewable energy sources. This is where tidal energy comes in.

Unlike solar and wind power, tidal energy is cyclical and predictable to a degree of months in advance, giving it a strong advantage over the other two sources of energy. By having the Tagus estuary next to it the city of Lisbon (and the adjacent coastline), it would benefit tremendously if tidal energy were to be drawn from the estuary's water currents.

The scope of the purpose of this work was to get an overall idea of whether or not the water currents found on the Tagus estuary are strong enough to power a small tidal farm composed of an array of submerged tidal turbines. This was done by resorting to the estuary's hydrodynamic modeling, with the aid of the software MOHID. After countless hours of computing power for the four different simulations made, and after dozens of hours in data analysis, this early assessment proves that the Tagus estuary holds a lot of potential if a tidal farm were to be built in it.

It has been shown that a small tidal farm composed of only 24 turbines over an area 300x300 meters in one of Tagus' river most energy density areas (while considering a vessel approach channel) is able to power on average 2 400 homes for a period of 20 years. Such a project is predicted to cost €17 million and it would remove the equivalent of 29 thousand tons of CO_2 emissions from the atmosphere.

When considering that the actual electric energy supply cost in Portugal sits at 0.22 €/kWh (PORDATA, n.d.), this makes the pursuing of cheaper and cleaner alternatives more attractive. With an expected LCOE cost of 0.15 €/kWh, the solution of a tidal farm in the Tagus estuary could be seen as a legitimate alternative to power a good part of the nearby county's electric energy consumption in order to illuminate the public streets. Being in close proximity to the power grid and to several ports that can be used to aid in O&M services turns the Tagus estuary as an ideal location to implement a tidal farm, as these would imply lesser costs and logistics in order to maintain such an infrastructure. Its close proximity to the power grid also translates into a less extensive underwater power cable, further reducing the tidal farm's CAPEX costs.

It has also been shown that the Module Turbine that was coded into the MOHID software is a good approximation to the industry's guidelines of a tidal turbine's electrical energy output, based on a location's hydrodynamic characteristics, namely the water current speed. This proves that using it in a MOHID simulation model for assessing any area of interest's energy potential will provide with a good estimate of the amount of electrical energy that a tidal farm would generate, if it were placed there. This is only true however if the project's resource assessment is at its feasibility stage, as the design development stage requires a fuller account of a turbine's electric energy output.

6.2. Limitations

This work, however, does not come without its limitations, as it is but a mere simple assessment of the Tagus' tidal energy. One of its limitations is the fact that it does not consider the energy output of a specific tidal turbine on the Tagus estuary. What is does instead is consider the characteristics of a generic, bi-directional tidal turbine, but that might not be entirely representative of what energy a concrete turbine solution of one of the countless alternatives presented in the Annex 1 would generate.

Another limitation comes in the form of the simulation model itself, both in terms of its resolution and also the output data time. Being a pre-feasibility assessment of the site characteristics and not a full design development project meant that the simulation model resolution needn't be less than 500 meters, according to the industry's guidelines. Despite that, a resolution of 300 meters was used for each grid cell, but that is still a far cry from the 50-meter grid cell resolution needed for a design development project assessment. As such, the values presented in this works do not paint the full picture when it comes to a tidal farm electric energy output, when placed on the Tagus estuary. As for the output data time, the fact that it was set to one hour in order to reduce the amount of data needed to analyze meant that specific critical instances might have been missed, such as the time when the tides reach their peak ebb speed or the time when they reach their turning point.

Another thing that was lacking was the consideration of multiple turbines in the simulation for a single cell. This stems from the fact that the way the Turbine Module was computed means that there can only be one turbine per cell. As such, the assessment of a tidal farm's energy production was made by multiplying the energy production of a single turbine with the number of turbines that were to be placed there. This means that the influence that some turbines might have on other's energy production (due to physical phenomenon such as the wake effect) weren't taken into account.

6.3. Future Work

Following the study carried out, some opportunities and suggestions for the making of future works are presented, in order to complement and develop upon the results obtained in this study. Some opportunities highlighted are related to the limitations of the study itself, while others can expand the scope of this study to other, more comprehensive ones, and with the prospect of identifying more opportunities. As such, the following points are enumerated:

With respect to the simulation model itself, it would benefit from having not only a higher grid cell resolution, but also from outputting data in more instances, in order to have a clearer picture of a site's hydrodynamics and energy potential. This can be easily solved through the use of a higher-resolution nested model in the simulation model used and by setting a lower output time so as to get more time instances from the simulation model. The assessment made would also benefit from determining the dynamics of multiple tidal turbines together, so as to see the influence they have on each other's energy production. These are bound to cause some sediment transport from the seafloor, which also wasn't assessed in this work and would be interesting to see. The effect that waves might have on these structures also wasn't determined, both in terms of stability and of energy production, since waves can increase the turbine's local water velocity.

Another interesting variation would be the use of a specific tidal turbine technology – hopefully one that has already been developed and is higher up on the readiness scale. That could add to the validation of a feasibility of the implementation of such a technology in settings beside urban environments, such as the Tagus estuary is to the city of Lisbon.

Finally, the Module Turbine that was coded into the MOHID software can be perfected into mimicking better a tidal turbine's reaction to a water current, namely taking into account the powertrain efficiency and considering a variating rotor power coefficient, based on the water current velocity. Such improvements would likely result in a more trustworthy result for a tidal turbine's electric energy output potential, on a specific assessment site.

References

[1] Abreu, André. (2010). Avaliação Do Potencial Energético Das Marés No Estuário Do Rio Douro. Faculdade de Engenharia da Universidade do Porto.

[2] ANDRITZ HYDRO Hammerfest. (2012). Renewable energy from tidal currents. https://www.andritz.com/resource/blob/61614/cf15d27bc23fd59db125229506ec87c7/hy-hammerfest--1--data.pdf, accessed May 20, 2019.

[3] APL. (2018). Publicação Estatística 2018. http://www.portodelisboa.pt/portal/page/portal/PORTAL_PORTO_LISBOA/ESTATISTICAS/ACTIVIDADE_PORTUARIA/TAB_PUBLICACOES/pub%20ano2018-PT%20ING%20-%20VF.pdf, accessed March 19, 2019.

[4] APL. (N.d.). CANAL DA BARRA SUL. http://www.portodelisboa.pt/portal/page/portal/PORTAL_PORTO_LISBOA/HIDROGRAFIA/REGULAMENTO_CANAIS/ANEXOS/BARRA%20SUL.htm, accessed March 19, 2019.

[5] ARH Tejo. (2011). Plano de Gestão Da Região Hidrográfica Do Tejo. Ministério da Agricultura, Mar, Ambiente e Ordenamento do Território. https://www.apambiente.pt/_zdata/Politicas/Agua/ParticipacaoPublica/Documentos/ARHTejo/PGRH/2_PGRHTejo_versoextensa.pdf.

[6] Atlantis Resources. (n.d.). AR1500 Tidal Turbine. https://simecatlantis.com/wp/wp-content/uploads/2016/08/AR1500-Brochure-Final-1.pdf, assessed May 21, 2019

[7] AVISO+. (N.d.). Description FES99. https://www.aviso.altimetry.fr/en/data/products/auxiliary-products/global-tide-fes/description-fes99.html, accessed September 28, 2018.

[8] Balsells Badia, Óscar. (2017) Implementation of the Effect of Turbines on Water Currents in MOHID Modelling System. https://upcommons.upc.edu/handle/2117/112828, accessed March 25, 2019.

[9] Boyle, Godfrey. (2012) Renewable Energy: Power for a Sustainable Future (3rd Ed.). Godfrey Boyle, ed. Oxford: Oxford University Press and Open University. http://ukcatalogue.oup.com/product/9780199545339.do, accessed September 5, 2018.

[10] Braunschweig, Frank, and Luís Fernandes. (2005). MOHID Graphical User Interfaces User Manual. Lisbon: Instituto Superior Técnico. http://www.mohid.com/PublicData/Products/Manuals/MOHID%20UInterface.pdf.

[11] Braunschweig, Frank, Luís Fernandes, and Filipe Lourenço. (2012). MOHID Studio User Guide. Action Modulers. http://wiki.actionmodulers.com/wiki/index.php?title=MOHID_Studio_-_User_Guide_-_v.2.0.

[12] Braunschweig, Frank, Flávio Martins, Paulo Chambel, and Ramiro Neves. (2003). A Methodology to Estimate Renewal Time Scales in Estuaries: The Tagus Estuary Case. Ocean Dynamics 53(3): 137–145.

[13] Brito, David. (2005). Integração de Detecção Remota, Dados in-Situ e Modelos Numéricos No Estudo Do Transporte de Sedimentos Coesivos No Estuário Do Tejo. Instituto Superior Técnico.

[14] Campuzano, F J, R Fernandes, P C Leitão, et al. (2012). Implementing Local Operational Models Based on an Offline Downscalling Technique: The Tagus Estuary Case. 2as Jornadas de Engenharia Hidrográfica, 20-22 June 2012, Lisbon, Portugal. Extended abstracts: 105-108

[15] Campuzano F (2018). Coupling watersheds, estuaries and regional seas through numerical modelling for Western Iberia. PhD Thesis, Instituto Superior Técnico, Universidade de Lisboa, Portugal.

[16] Capricorn Marine. (n.d.). Capricorn Marine. http://www.capricornmarine.com/, assessed May 20, 2019

[17] Castro-Santos, Laura, Geuffer Prado Garcia, Ana Estanqueiro, and Paulo A. P. S. Justino. (2015). The Levelized Cost of Energy (LCOE) of Wave Energy Using GIS Based Analysis: The Case Study of Portugal. International Journal of Electrical Power & Energy Systems 65: 21–25.

[18] Charlier, R.H., and J.R. Justus. (1993). Ocean Energies: Environmental, Economic and Technological Aspects of Alternative Power Sources. Elsevier Oceanography Series. Amsterdam, The Netherlands.

[19] Copping, Andrea, Courtney Smith, Luke Hanna, et al. (2013). Tethys: Developing a Commons for Understanding Environmental Effects of Ocean Renewable Energy. International Journal of Marine Energy 3–4. Special Issue – Selected Papers - EWTEC2013: 41–51.

[20] Corsatea, Teodora Diana, and Davide Magagna. (2014). Overview of European Innovation Activities in Marine Energy Technology. European Commission, Brussels, Belgium: Joint Research Centre (JRC). http://publications.jrc.ec.europa.eu/repository/bitstream/JRC90901/jrc-14-marinereport-online-dm.pdf.

[21] Det Norske Veritas AS. (2014). Design of Offshore Wind Turbine Structures. Norway: DNV. https://rules.dnvgl.com/docs/pdf/DNV/codes/docs/2014-05/Os-J101.pdf.

[22] EDP. (2017). Origem da Energia - Particulares | EDP. edp - eletricidade e gás no mercado livre. https://www.edp.pt/origem-energia/, accessed April 9, 2019.

[23] EIA. (2018). Levelized Cost and Levelized Avoided Cost of New Generation Resources in the Annual Energy Outlook 2018. U.S. Energy Information Administration. https://www.eia.gov/outlooks/aeo/pdf/electricity_generation.pdf.

[24] EMEC. (2013). Assessment of Tidal Energy Resource - Marine Renewable Energy Guides. European Marine Energy Centre Ltd (EMEC). http://www.emec.org.uk/assessment-of-tidal-energy-resource/.

[25] EMEC. (N.d.). Tidal Devices: EMEC: European Marine Energy Centre. http://www.emec.org.uk/marine-energy/tidal-devices/, accessed September 7, 2018, a.

[26] EMEC. (N.d.). Tidal Developers: EMEC: European Marine Energy Centre. http://www.emec.org.uk/marine-energy/tidal-developers/, accessed March 18, 2019, b.

[27] Energy XPRT. (n.d.). Model TidalStar - Power System. https://www.energy-xprt.com/products/model-tidalstar-power-system-245103#headerSite, assessed May 20, 2019.

[28] EU. (2014). Blue Energy Action Needed to Deliver on the Potential of Ocean Energy in European Seas and Oceans by 2020 and Beyond. http://eur-lex.europa.eu/legal-content/EN/TXT/?qid=1396419828231&uri=CELEX:52014DC0008, accessed May 23, 2018.

[29] Eurostat. (2013). Coastal Regions - Population Statistics. http://ec.europa.eu/eurostat/statistics-explained/index.php/Archive:Coastal_regions_-_population_statistics.

[30] FCUL. (2018). FCUL - Previsão de Marés. http://webpages.fc.ul.pt/~cmantunes/hidrografia/hidro_mares.html, accessed September 5, 2018.

[31] Fernandes, L. (2005). Modelling of Arsenic Dynamics in the Tagus Estuary. Instituto Superior Técnico.

[32] Fernandes, Rodrigo. (2001). Modelação de Derrames de Hidrocarbonetos. Instituto Superior Técnico. http://www.mohid.com/PublicData/Products/Thesis/TFC_RodrigoFernandes.pdf.

[33] Free Flow Power. (2011). Mississippi River Hydrokinetics Project Development. https://pianc.us/wp-content/uploads/2016/07/11_guidroz_Free-Flow-Power-Smart-Rivers-Conference-Public-Presentation-9_2011.pdf, assessed May 20, 2019.

[34] Frost, Ciaran, David Findlay, Ewen Macpherson, Philip Sayer, and Lars Johanning. (2018). A Model to Map Levelised Cost of Energy for Wave Energy Projects. Ocean Engineering 149: 438–451.

[35] Hammons, T.J. (2011). Tidal Power in the UK and Worldwide to Reduce Greenhouse Gas Emissions. International Journal of Engineering Business Management 3(2): 16–28.

[36] Hydra Tidal. (n.d.). The Technology MORILD. https://hydratidal.wordpress.com/the-technology/, assessed May 20, 2019

[37] ICNF. (2018). Geologia | Hidrologia | Clima. Página. Geologia, hidrologia e clima da Reserva Natural do Estuário do Tejo. http://www2.icnf.pt/portal/ap/r-nat/rnet/geo, accessed September 19, 2018.

[38] IEA. (2016). World Energy Outlook 2016. International Energy Agency. https://www.iea.org/media/publications/weo/WEO2016SpecialFocusonRenewableEnergy.pdf.

[39] Instituto Hidrográfico. (2000). Marés | Instituto Hidrográfico. http://www.hidrografico.pt/glossario-cientifico-mares.php, accessed May 23, 2018.

[40] Instituto Hidrográgico. (2018). Tabela de Marés. Tabela de Marés. http://www.hidrografico.pt/tabelamares, accessed December 27, 2018.

[41] IRENA. (2014). Tidal Energy - Technology Brief. http://www.irena.org/DocumentDownloads/Publications/Tidal_Energy_V4_WEB.pdf, accessed September 4, 2018.

[42] IRENA. (2014a). Ocean Energy - Technology Readiness, Patents, Deployment Status and Outlook.

[43] IRENA. (2018). Renewable Power Generation Costs in 2017. Abu Dhabi: International Renewable Energy Agency. https://www.irena.org/-/media/Files/IRENA/Agency/Publication/2018/Jan/IRENA_2017_Power_Costs_2018.pdf.

[44] Jenne, Scott, Yi-Hsiang Yu, and Vincent Neary. (2015). Levelized Cost of Energy Analysis of Marine and Hydrokinetic Reference Models: Preprint: 9.

[45] Krohn, David, Mike Woods, Jenny Adams, et al. (2013). Wave and Tidal Energy in the UK Conquering Challenges, Generating Growth. Renewable UK. https://cdn.ymaws.com/www.renewableuk.com/resource/resmgr/publications/reports/Wave&Tidal_SOI.pdf.

[46] Leitão, Paulo. (2003). Integração de Escalas e de Processos Na Modelação Do Ambiente Marinho. Instituto Superior Técnico.

[47] Lewis, A., S. Estefen, J. Huckerby, et al. (2011). Ocean Energy. In IPCC Special Report on Renewable Energy Sources and Climate Change Mitigation. Cambridge, United Kingdom and New York, NY, USA: Cambridge University Press. http://www.ipcc-wg3.de/report/IPCC_SRREN_Ch06.pdf.

[48] Lopes de Almeida, Catarina. (2008). Aproveitamento Da Energia Da Onda de Maré No Estuário Do Tejo. Universidade de Aveiro.

[49] López, Iraide, Jon Andreu, Salvador Ceballos, Iñigo Martínez de Alegría, and Iñigo Kortabarria. (2013). Review of Wave Energy Technologies and the Necessary Power-Equipment. Renewable and Sustainable Energy Reviews 27: 413–434.

[50] Lyon, Katrina, Mark Rayner, Philip Jennings, and Christine Creagh. (2004). Tidal Energy. Australian Institute of Energy: 1–5.

[51] Macedo, Maria Emília. (2006). Caracterização de Caudais Do Rio Tejo. Lisbon: Ministério do Ambiente, do Ordenamento do Território e do Desenvolvimento Regional. http://www.ccdr-lvt.pt/files/fab372a0a4525eddaf1c20e1ab852a25.pdf.

[52] Magagna, Davide, Andrew MacGillivray, Henry Jeffrey, et al. (2014). Wave and Tidal Energy Strategic Technology Agenda. SI Ocean. http://www.marineenergywales.co.uk/wp-content/uploads/2016/01/SI-Ocean-WaveTidal-Strategic-Technology-Agenda.pdf.

[53] Magallanes Renovables. (n.d.). Generating future. http://www.magallanesrenovables.com/en/proyecto, assessed May 20, 2019

[54] Mako Energy. (n.d.). Mako Tidal Turbines. https://www.mako.energy/, assessed May 20, 2019

[55] Manwell, J.F., J.G. McGowan, and A.L. Rogers. (2009). Wind Energy Explained: Theory, Design and Application. 2nd edition. http://ee.tlu.edu.vn/Portals/0/2018/NLG/Sach_Tieng_Anh.pdf.

[56] MARETEC. (2003). MOHID Description: Description of the 3D Water Modelling System. http://www.mohid.com/PublicData/Products/Manuals/Mohid_Description.pdf.

[57] Marine Current Turbines. (n.d.). Marine Current Turbines. http://www.sinclair-consultants.com/cms/data/files/documents/Marine-Current-Turbines-leaflet.pdf, assessed May 20, 2019

[58] Marine Energy Corporation. (n.d.). Open Ocean Current Catchers. http://www.marineenergycorp.com/marine-energy/open-ocean-current-catchers.shtml, assessed May 20, 2019

[59] Mehmood, Nasir, Liang, Zhang, and Khan, Jawad. (2012). Diffuser Augmented Horizontal Axis Tidal Current Turbines. Vol.4. Research Journal of Applied Sciences, Engineering and Technology.

[60] MIT. (2006). Introduction to Fluid Motions, Sediment Transport and Current-Generated Sedimentary Structures - Chapter 4: Flow in Pipes and Channels. Massachusetts Institute of Technology. https://ocw.mit.edu/courses/earth-atmospheric-and-planetary-sciences/12-090-introduction-to-fluid-motions-sediment-transport-and-current-generated-sedimentary-structures-fall-2006/course-textbook/ch4.pdf, accessed March 20, 2019.

[61] MOHID Wiki. (2018). MOHID Wiki. http://wiki.mohid.com/index.php?title=Main_Page, accessed September 17, 2018.

[62] MOHID Wiki. (N.d.). Module Geometry. http://wiki.mohid.com/index.php?title=Module_Geometry, accessed September 26, 2018.

[63] Neves R. (2013). The Mohid concept. Case studies with MOHID, M. Mateus & R. Neves (eds.), IST Press. pp 1-11.

[64] Nova Innovation. (n.d.). Nova M100. https://www.novainnovation.com/nova-m100, assessed May 21, 2019

[65] O Rourke, Fergal, Fergal Boyle, and Anthony Reynolds. (2010). Tidal Energy Update 2009. Applied Energy 87(2): 398–409.

[66] Ocean Energy Forum. (2016). Ocean Energy Strategic Roadmap 2016, Building Ocean Energy for Europe. https://webgate.ec.europa.eu/maritimeforum/sites/maritimeforum/files/OceanEnergyForum_Roadmap_Online_Version_08Nov2016.pdf.

[67] Ocean Flow Energy. (n.d.). Evopod Technology. http://www.oceanflowenergy.com/Evopod-Technology.html, assessed May 21, 2019

[68] Oceana Energy Company. (n.d.). Design. https://www.oceanaenergy.com/design, assessed May 20, 2019

[69] OES. (2015). International Levelised Cost Of Energy for Ocean Energy Technologies. Ocean Energy Systems. https://www.ocean-energy-systems.org/publications/oes-documents/market-policy-/document/international-levelised-cost-of-energy-for-ocean-energy-technologies-2015-/, accessed April 15, 2019.

[70] Orbital Marine Power. (n.d.). SR2000. https://orbitalmarine.com/technology-development/sr2000, assessed May 20, 2019.

[71] Owen, Alan. (2008). Chapter 7 - Tidal Current Energy: Origins and Challenges. *In* Future Energy. Trevor M. Letcher, ed. Pp. 111–128. Oxford: Elsevier. http://www.sciencedirect.com/science/article/pii/B9780080548081000077, accessed September 5, 2018.

[72] Panwar, N. L., S. C. Kaushik, and Surendra Kothari. (2011). Role of Renewable Energy Sources in Environmental Protection: A Review. Renewable and Sustainable Energy Reviews 15(3): 1513–1524.

[73] Physical Oceanography Group. (2010). Assessment of Tidal Energy Resource in the Strait of Gibraltar. University of Málaga: 25.

[74] Pina, Pedro. (2001). An Integrated Approach to Study the Tagus Estuary Water Quality. Instituto Superior Técnico.

[75] Pina, Pedro, L Fernandes, Frank Braunschweig, P. C. Chambel, and R Neves. (2004). Modelling Estuarine Systems: The Tagus Application.

[76] Pinto, L, F J Campuzano, R Fernandes, L Fernandes, and R Neves. (2012). An Operational Model for the Portuguese Coast: 4.

[77] PORDATA. (N.d.). Custo da eletricidade para utilizadores. https://www.pordata.pt/Europa/Pre%C3%A7os+da+electricidade+para+utilizadores+dom%C3%A9sticos+e+industriais+(Euro+ECU)-1477, accessed May 1, 2019.

[78] PORDATA. (N.d.). Alojamentos Familiares Clássicos. https://www.pordata.pt/Municipios/Alojamentos+familiares+cl%C3%A1ssicos-92, accessed March 27, 2019.

[79] PORDATA. (N.d.). Consumo de Energia Eléctrica: Total e Por Tipo de Consumo https://www.pordata.pt/Municipios/Consumo+de+energia+el%c3%a9ctrica+total+e+por+tipo+de+consumo-25-123, accessed March 27, 2019.

[80] Portela, L. I. (1996). Modelação matemática de processos hidrodinâmicos e da qualidade da água no estuário do Tejo. http://repositorio.lnec.pt:8080/xmlui/handle/123456789/8737, accessed September 18, 2018.

[81] Prandle, D. (1984). Simple Theory for Designing Tidal Power Schemes. Advances in Water Resources 7(1): 21–27.

[82] Rebordão, Ilina. (2008). Análise Do Potencial Energético Dos Fluxos de Maré No Estuário Do Rio Lima. Instituto Superior Técnico.

[83] REUK. (N.d.). Betz Limit. Renewable Energy UK. http://www.reuk.co.uk/wordpress/wind/betz-limit/, accessed March 18, 2019.

[84] REUK. (n.d.). TidEl Tidal Turbines. http://www.reuk.co.uk/wordpress/tidal/tidel-tidal-turbines/, assessed May 20, 2019

[85] Rourke, Fergal O., Fergal Boyle, and Anthony Reynolds. (2009). Renewable Energy Resources and Technologies Applicable to Ireland. Renewable and Sustainable Energy Reviews 13(8): 1975–1984.

[86] Sabella. (n.d.). D03. https://www.sabella.bzh/en/projects/d03, assessed May 20, 2019

[87] Santos, Madalena, Adélio Silva, Paulo Leitão, Henrique Coelho, and Ramiro Neves. (2004). Aplicação de Um Modelo Hidrodinâmico (MOHID) Como Ferramenta Na Avaliação Da Qualidade Da Lagoa de Óbidos. http://maretec.mohid.com/projects/FozdoArelho/Confer%C3%AAncias/01_1%C2%BA%20Semin%C3%A1rio%20SLC%202004-Vila%20Nova%20de%20Santo%20Andr%C3%A9,%20Portugal.pdf.

[88] Schottel Tidal Generator. (n.d.). Cost-Effective Power from Currents. http://www.blackrocktidalpower.com/fileadmin/data_BRTP/pdf/STG-datasheet.pdf, assessed May 20, 2019

[89] Segura, Eva, Rafael Morales, and José A. Somolinos. (2017). Cost Assessment Methodology and Economic Viability of Tidal Energy Projects. Energies 10(11): 1806.

[90] SI Ocean. (2013). Ocean Energy: Cost of Energy and Cost Reduction Opportunities. https://energiatalgud.ee/img_auth.php/1/10/SI_OCEAN._Ocean_Energy_-_Cost_of_Energy_and_Cost_Reduction._2013.pdf.

[91] Smart, Gavin, and Miriam Noonan. (2018). Tidal Stream and Wave Energy Cost Reduction and Industrial Benefit. UK: Catapult - Offshore Renewable Energy. https://www.marineenergywales.co.uk/wp-content/uploads/2018/05/ORE-Catapult-Tidal-Stream-and-Wave-Energy-Cost-Reduction-and-Ind-Benefit-FINAL-v03.02.pdf, accessed April 9, 2019.

[92] Sustainable Marine Energy. (2017). Tidal Energy Platforms, PLAT-O (Offshore). https://s3-eu-west-1.amazonaws.com/assets-sustainablemarine-com/downloads/SME_TidalEnergyPlatforms_V3.0.pdf, assessed May 20, 2019

[93] Tethys. (n.d.) Nautricity at EMEC. https://tethys.pnnl.gov/annex-iv-sites/nautricity-emec, assessed May 20, 2019

[94] Tidal Stream. (2014). Trition T3 - Medium Platform 3 - 5 MW. http://www.tidalstream.co.uk/html/triton_t3.html, assessed May 20, 2019

[95] Tocardo Tidal Power. (n.d.). Offshore solutions. https://www.tocardo.com/solutions/offshore/, assessed May 21, 2019

[96] United Nations. (2007). PERCENTAGE OF TOTAL POPULATION LIVING IN COASTAL AREAS. http://www.un.org/esa/sustdev/natlinfo/indicators/methodology_sheets/oceans_seas_coasts/pop_coastal_areas.pdf.

[97] United Nations. (2012). Energy – UN-Habitat. https://unhabitat.org/urban-themes/energy/, accessed July 11, 2018.

[98] United Nations. (2017). World Population Prospects: The 2017 Revision, Key Findings and Advance. Working Paper No. ESA/P/WP/248. https://esa.un.org/unpd/wpp/publications/Files/WPP2017_KeyFindings.pdf, accessed May 21, 2018.

[99] US Energy Information Administration. (2017a). International Energy Outlook. https://www.eia.gov/outlooks/ieo/, accessed May 21, 2018.

[100] US Energy Information Administration. (2017b). Tidal Power - Energy Explained, Your Guide To Understanding Energy - Energy Information Administration. https://www.eia.gov/energyexplained/index.php?page=hydropower_tidal, accessed May 23, 2018.

[101] US EPA, OAR. (2016). Greenhouse Gas Emissions from a Typical Passenger Vehicle. Overviews and Factsheets. US EPA. https://www.epa.gov/greenvehicles/greenhouse-gas-emissions-typical-passenger-vehicle, accessed April 9, 2019.

[102] Verdant Power. (n.d.). Free Flow System. https://www.verdantpower.com/free-flow-system, assessed May 21, 2019

[103] Willemsen, Diederik. (2018). Spring and Neap Tides - Astronomical Origin of Tides. http://www.sailingissues.com/navcourse6.html, accessed September 5, 2018.

[104] World Energy Council. (2016). World Energy Resources - Marine Energy. https://www.worldenergy.org/wp-content/uploads/2017/03/WEResources_Marine_2016.pdf.

[105] WWTurbine. (2017). Outreach Report - Water Wall Turbine Inc. https://wwturbine.com/assets/docs/WWT%20CEF%20Outreach%20Final%20Report.pdf, assessed May 21, 2019

Annexes

Annex 1: Tidal Developers

The following table contains a list of the tidal energy concepts known to EMEC.

Table A1-1 – Known existing horizontal axis tidal turbine solutions. (EMEC n.d.)

Company	Country	Device Name	Device Type
Andritz Hydro Hammerfest	Norway	HS1000	Horizontal Axis Turbine
Aquantis Ltd	USA	AQ Series	
Atlantis Resources Corp	UK	AR-1500	Horizontal Axis Turbine
Atlantis Resources Corp	UK	AR-1000	Horizontal Axis Turbine
Atlantisstrom	Germany	Atlantisstorm	Horizontal Axis Turbine
Balkee Tide and Wave Electricity	Mauritius	Tidal and Wave Power Electrical Generator (TWPEG)	Horizontal Axis Turbine
BioPower System Pty Ltd	Australia	bioStream	Other
Bluewater	Netherlands	BlueTEC (Bluewater Tidal Energy Converter)	Other
Bosch Rexroth	Germany		Horizontal Axis Turbine
Bourne Energy	USA	CurrentStar	Horizontal Axis Turbine
Bourne Energy	USA	TidalStar	Horizontal Axis Turbine
Bourne Energy	USA	OceanStar	Horizontal Axis Turbine
Centro Tecnologico SOERMAR	Spain	PROCODAC	
Cetus Energy	Australia	Cetus Turbine	Horizontal Axis Turbine
Current Power AB	Sweden	Current Power	Vertical Axis Turbine
Current2Current	UK	Tidal Turbine	Vertical Axis Turbine

Company	Country	Device Name	Device Type
Deepwater Energy BV	Netherlands	Oryon Watermill	Vertical Axis Turbine
EC-OG	UK	Subsea Power Hub	Vertical Axis Turbine
EEL Energy	France	EEL Energy	Oscillating Hydrofoil
Elemental Energy Technology Limited	Australia	SeaUrchin	Other
Flex Marine Power Ltd	UK	Swimmer Turbine	
Flumill	Norway	Flumill Power Tower	Archimedes Screw
Free Flow 69	UK	Osprey	Vertical Axis Turbine
Free Flow Power Corporation	USA	SmarTurbine	Horizontal Axis Turbine
GCK Technology	USA	Gorlov Turbine	Vertical Axis Turbine
Guinard Energies SAS	France	MagaWattBlue	
Hales Water Turbines Ltd	UK	Hales Turbine	Other
Hydra Tidal AS	Norway	Morild II	Horizontal Axis Turbine
Hydro Alternative Energy	USA	OCEANUS	
Hydro-Gen	France	Hydro-Gen	Horizontal Axis Turbine
HydroQuest	France	Hydroquest Tidal	Vertical Axis Turbine
Hydrovolts Inc	USA	C-12 Canal Turbine	Horizontal Axis Turbine
Hydrovolts Inc	USA	WF-10-15 Waterfall Turbine	Other
Hyundai Heavy Industries	Korea		
IHC Tidal Energy	Netherlands	OceanMill	Vertical Axis Turbine
InCurrent Turbines Ltd	Canada	Vortex Power Drive	
Instream Energy Systems	Canada	Vertical Axis Hydrokinetic Turbines	Vertical Axis

Company	Country	Device Name	Device Type
		(VAHT)	Turbine
Integrated Power Technology Corporation	USA	TURBOFOIL	Oscillating Hydrofoil
Jupiter Hydro Inc	Canada		Archimedes Screw
Kawasaki Heavy Industries, Ltd	Japan		Horizontal Axis Turbine
Kepler Energy	UK	Kepler Turbine	Other
Leading Edge	US		Oscillating Hydrofoil
Lucid Energy Technologies	USA	Gorlov Helical Turbine (GHT)	Vertical Axis Turbine
Lunar Energy	UK	Rotech Tidal Turbine (LTT)	Enclosed tips (Venturi)
Magallanes Renovables	Spain	Magallanes Project	Horizontal Axis Turbine
Mako Tidal Turbines	Australia	MAKO Tidal Turbines	Horizontal Axis Turbine
Marine Current Turbines	UK	SeaGen S	Horizontal Axis Turbine
Marine Current Turbines	UK	SeaGen U	Horizontal Axis Turbine
Marine Energy Corporation	USA	Current Catcher	Horizontal Axis Turbine
Minesto	Sweden	Deep Green	Tidal Kite
Modec	Japan	Savonius Keel & Wind Turbine Darrieus (SKWID)	Other
Natural Currents	USA	Red Hawk	Other
Nautricity Ltd	UK	CoRMaT	Horizontal Axis Turbine
New Energy Corporation	Canada	EnviroGen/EnviroCurrent	Vertical Axis Turbine
Norwegian Ocean Power	Norway	H300	Vertical Axis Turbine
Nova Innovation Ltd	UK	Nova M100	Horizontal Axis Turbine

Company	Country	Device Name	Device Type
Ocean Flow Energy	UK	Evopod	Horizontal Axis Turbine
ORPC	USA	RivGen Power System	Horizontal Axis Turbine
Ocean Renewable Power Company (ORPC)	USA	TidGen Power System	Horizontal Axis Turbine
Ocean Renewable Power Company (ORPC)	USA	OCGen	Horizontal Axis Turbine
Oceana Energy Company	USA	TIDES	Horizontal Axis Turbine
Offshore Islands Ltd	USA	Current Catcher	Horizontal Axis Turbine
Open Ocean Energy Ltd	Ireland	Tidal Junior Flyer	
OpenHydro	Ireland	Open-Centre Turbine	Enclosed tips (Venturi)
QED Naval	Scotland	Subhub	Other
REAC Energy GmbH	Germany	StreamCube	Vertical Axis Turbine
Renewable Devices Marine Ltd	UK	Capricon 5	Horizontal Axis Turbine
Renewable Devices Marine Ltd	UK	River Otter	
Renewable Devices Marine Ltd	UK	Capricon 125	Horizontal Axis Turbine
Renewable Devices Marine Ltd	UK	Sea Otter	
Repetitive Energy Company	UK	REPEN6	Vertical Axis Turbine
ResHydro	USA	Hydrofoil Cascade Resonator (HCR)	Oscillating Hydrofoil
SABELLA SAS	France	D03	Horizontal Axis Turbine
SCHOTTEL group	Germany	STG (SCHOTTEL Tidal Generator)	Horizontal Axis Turbine
Scotrenewables	UK	SR2000	Horizontal Axis Turbine

Company	Country	Device Name	Device Type
SeaCurrent	The Netherlands	SeaCurrent TidalKite™	Tidal Kite
SeaPower Gen	UK	SPG	
Seapower scrl	Italy	GEM	Tidal Kite
SMD Hydrovision	UK	TiDEL	Horizontal Axis Turbine
Straum AS	Norway	Hydra Tidal	Horizontal Axis Turbine
Suanders Energy Ltd	UK	Power-Frame	Horizontal Axis Turbine
Sustainable Marine Energy (SME)	UK	PLAT-O	Horizontal Axis Turbine
Tidal Energy Ltd	UK	DeltaStream	Horizontal Axis Turbine
Tidal Energy Pty Ltd	Australia	Davidson Hill Venturi (DHV) Turbine	Enclosed tips (Venturi)
Tidal Sails AS	Norway	Tack Reach	Other
TidalStream Limited	UK	Triton 6 (Tidal Turbine Platform System)	Horizontal Axis Turbine
TidalStream Limited	UK	Triton 3 (Tidal Turbine Platform System)	Horizontal Axis Turbine
Tidalys	France	ELECTRImar 4200	Horizontal Axis Turbine
Tidalys	France	ELECTRImar 1800	Horizontal Axis Turbine
Tocardo Tidal Turbines	Netherlands	T2	Horizontal Axis Turbine
Verdant Power	USA	Free Flow Kinetic Hydropower System (KHPS)	Horizontal Axis Turbine
Vortex Hydro Energy	USA	VIVACE (Vortex Induced Vibrations Aquatic Clean Energy)	Other
Vortex Power Drive	USA	Vortex Power Drive	
Water Wall Turbine Inc	Canada	Water Wall Turbine - In-Flow Water Current Technology	Horizontal Axis Turbine

Annex 2: Variation in Power Density

In this Annex, the Figures referent to the variation in power density throughout the different simulated months are shown, and for every assessment area.

<u>Oeiras Region</u>:

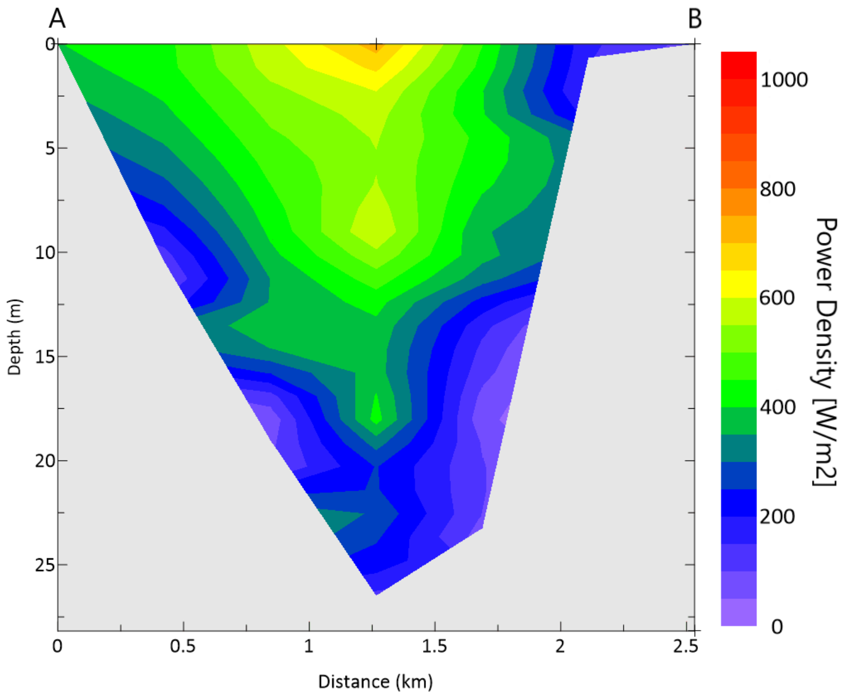

Figure A2 - 1 – Average Power Density distribution over the course of the dry month

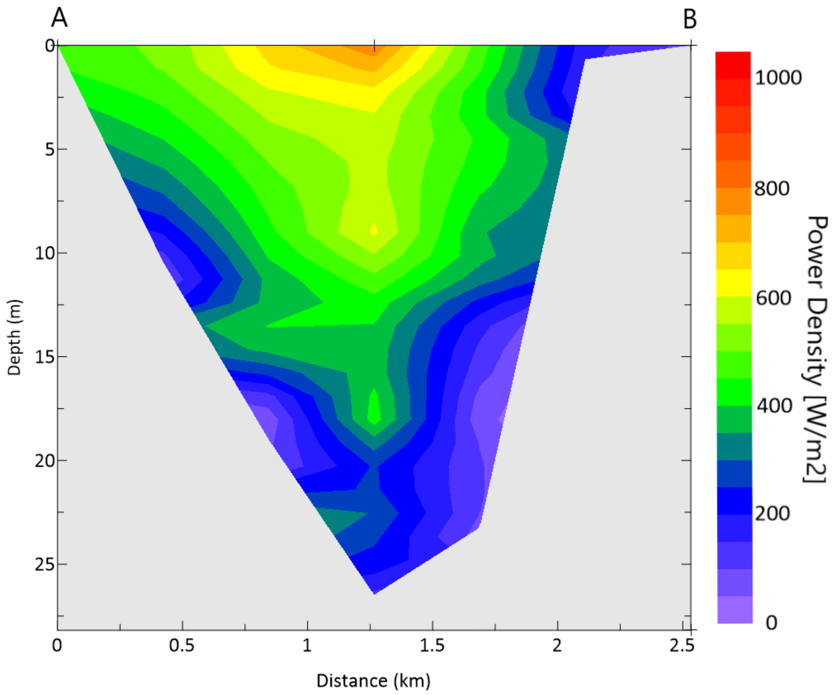

Figure A2 - 2 - Average Power Density distribution over the course of the average month

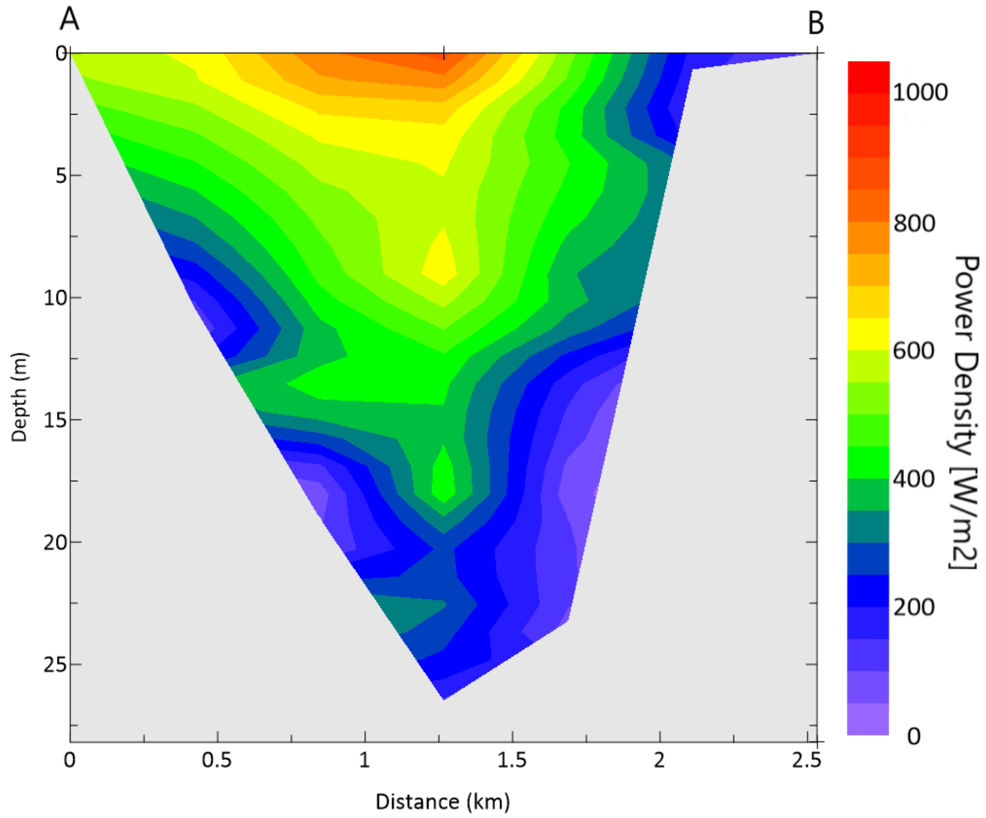

Figure A2 - 3 - Average Power Density distribution over the course of the wet month

<u>Belém Region</u>:

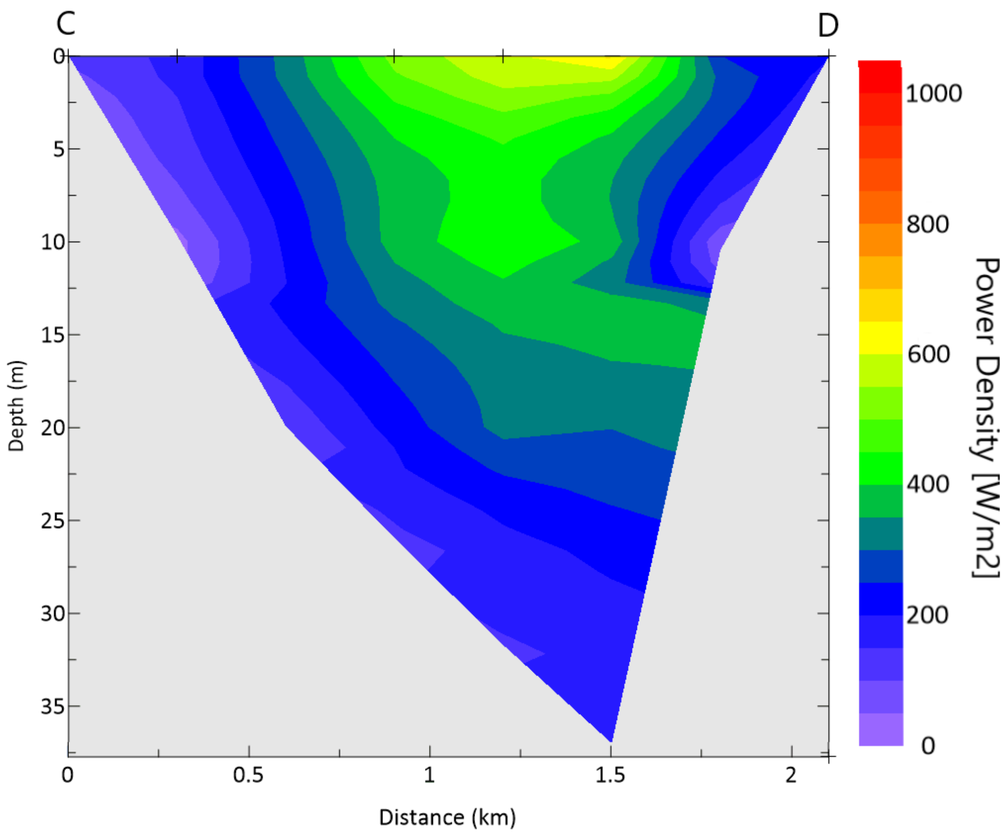

Figure A2 - 4 - Average Power Density distribution over the course of the dry month

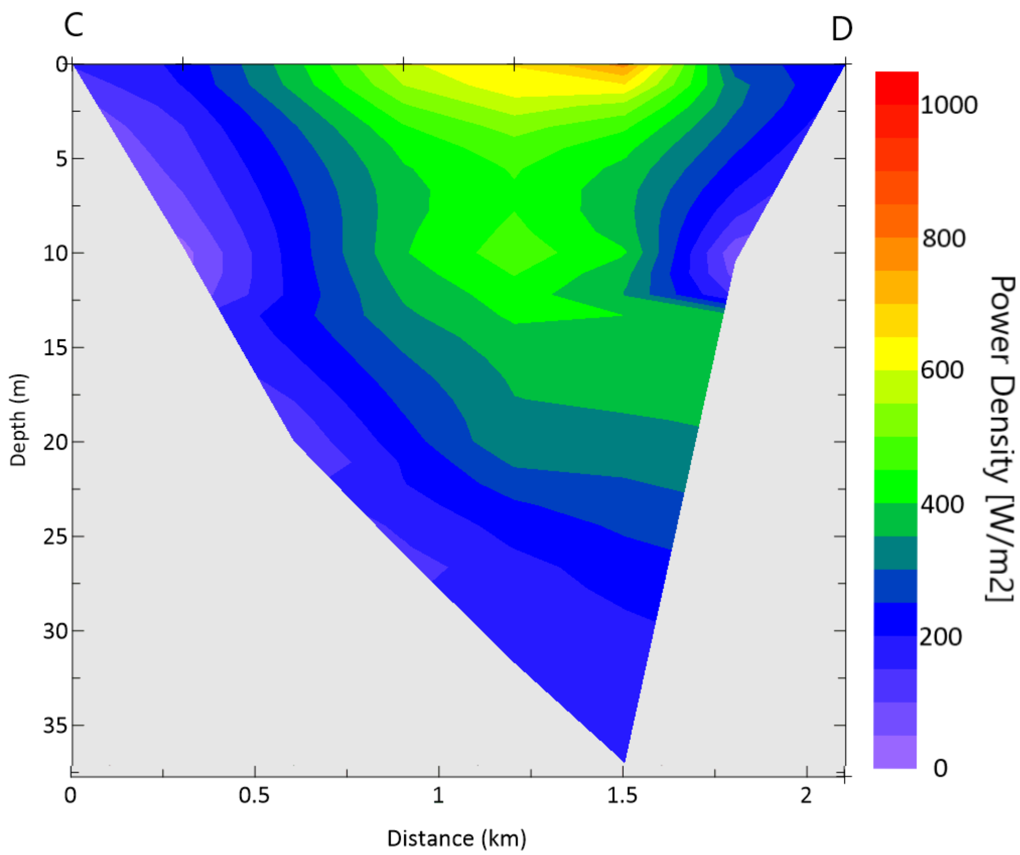

Figure A2 - 5 - Average Power Density distribution over the course of the average month

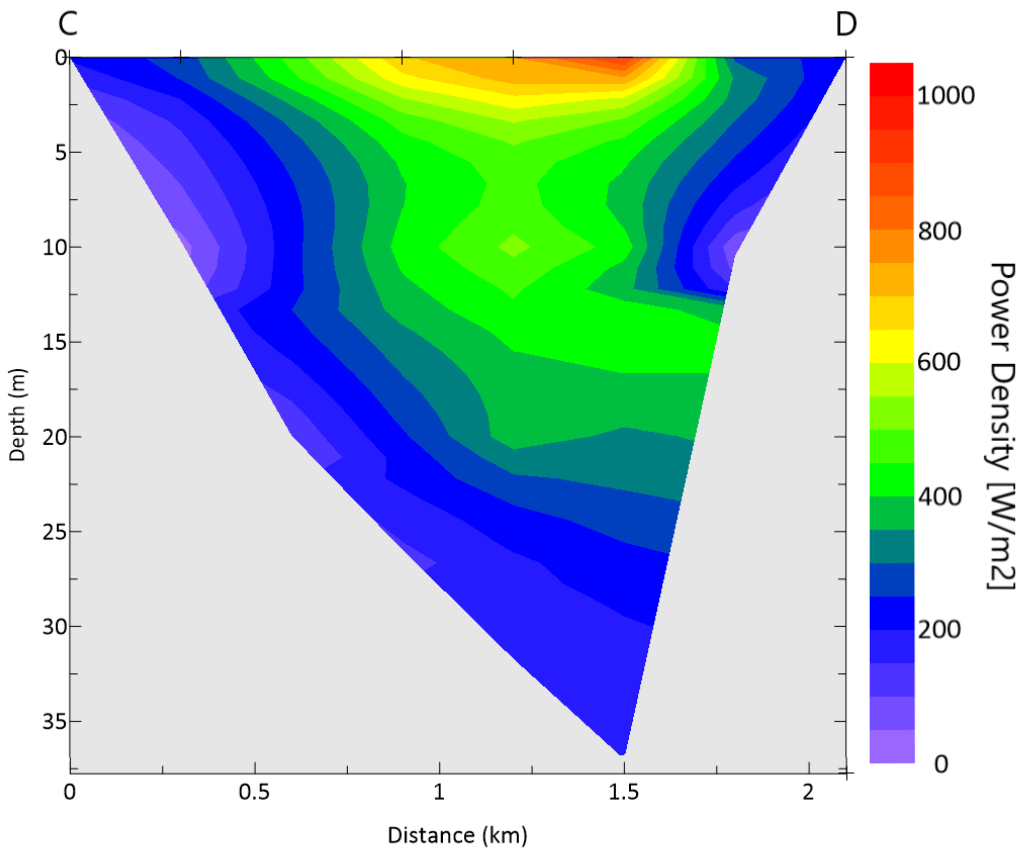

Figure A2 - 6 - Average Power Density distribution over the course of the wet month

Cais do Sodré Region:

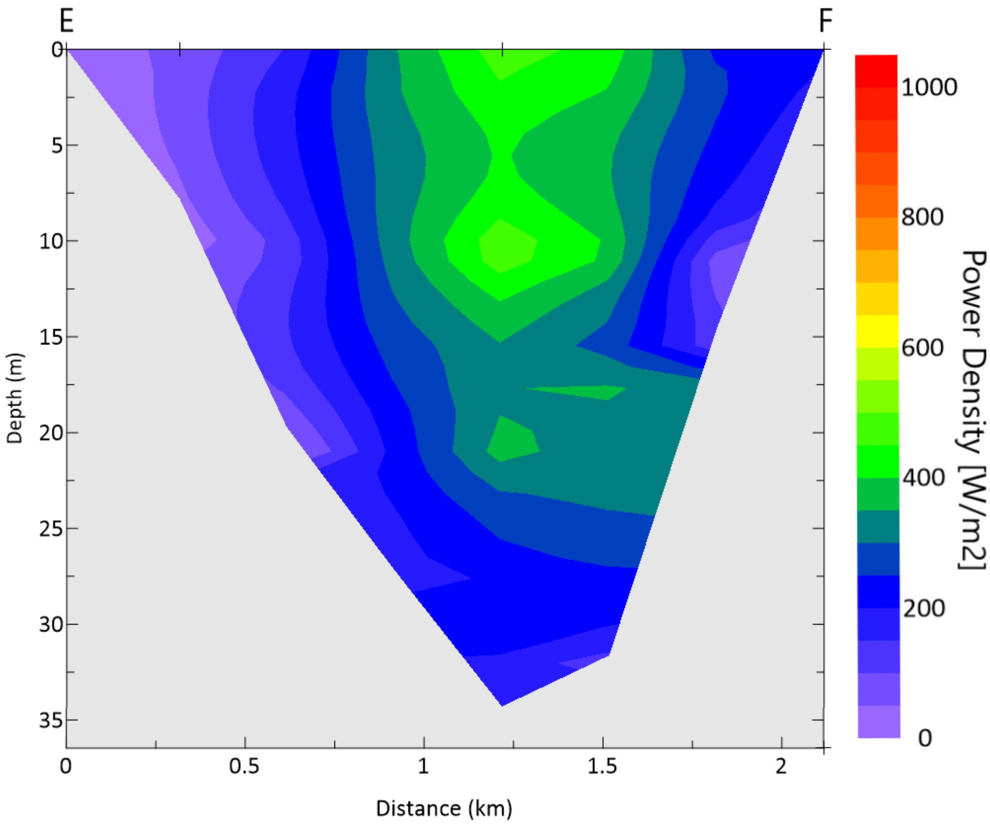

Figure A2 - 7 - Average Power Density distribution over the course of the dry month

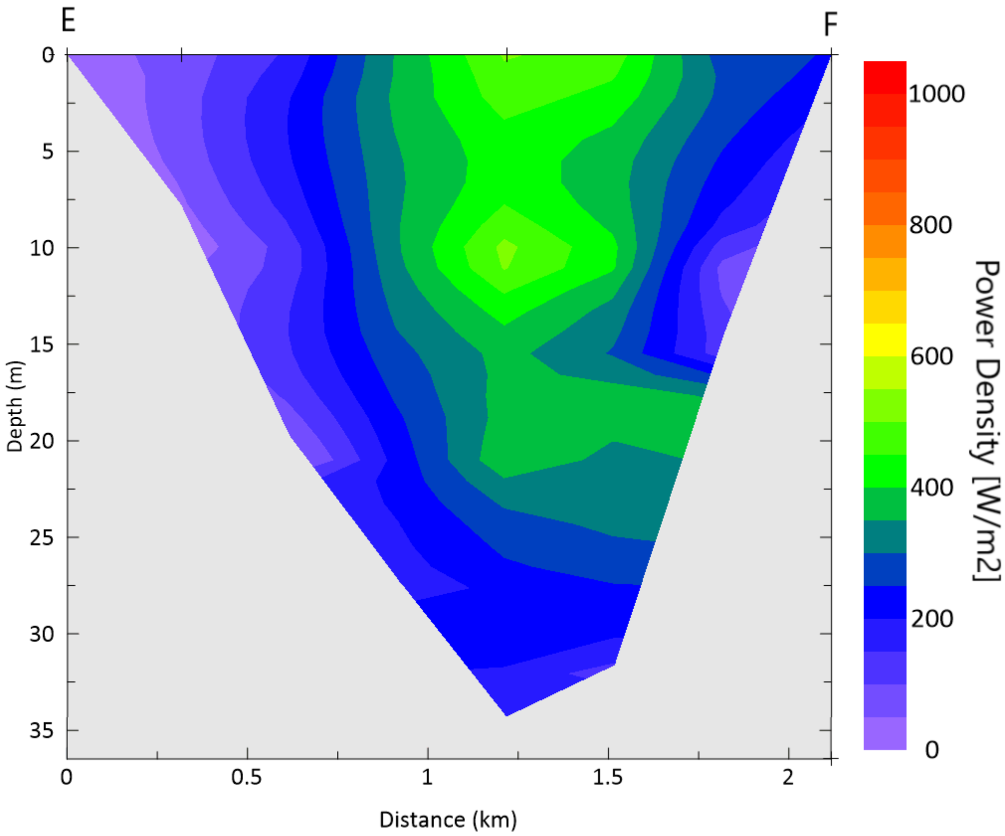

Figure A2 - 8 - Average Power Density distribution over the course of the average month

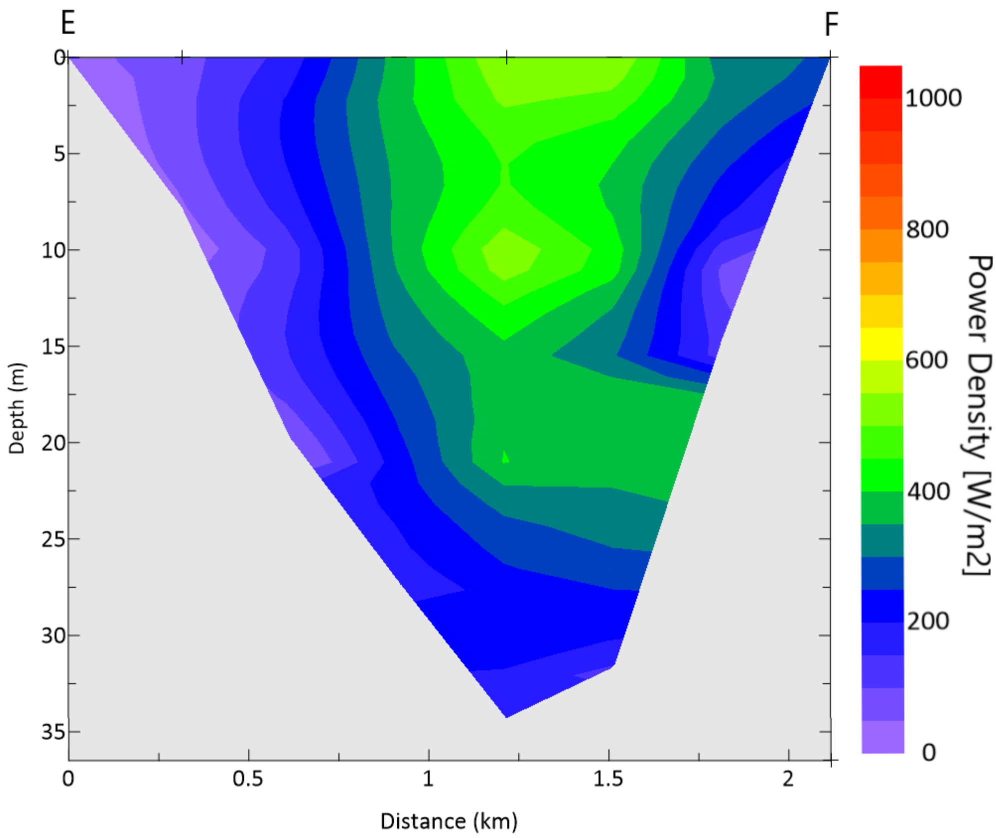

Figure A2 - 9 - Average Power Density distribution over the course of the average month

Annex 3: Detailing of the Water Velocity going through each turbine

This annex presents the figures with the discretization of the water velocity going through each turbine and for each simulated month.

Oeiras Region:

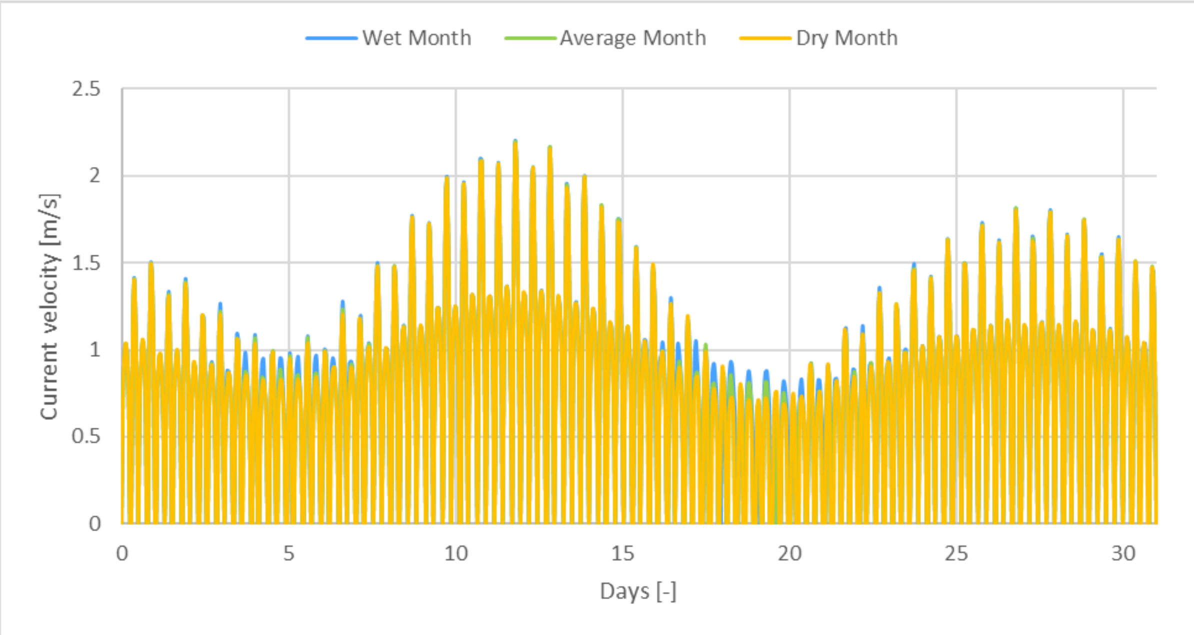

Figure A3 - 1 -Water velocities through a turbine on the highest energy density site of the simulated months

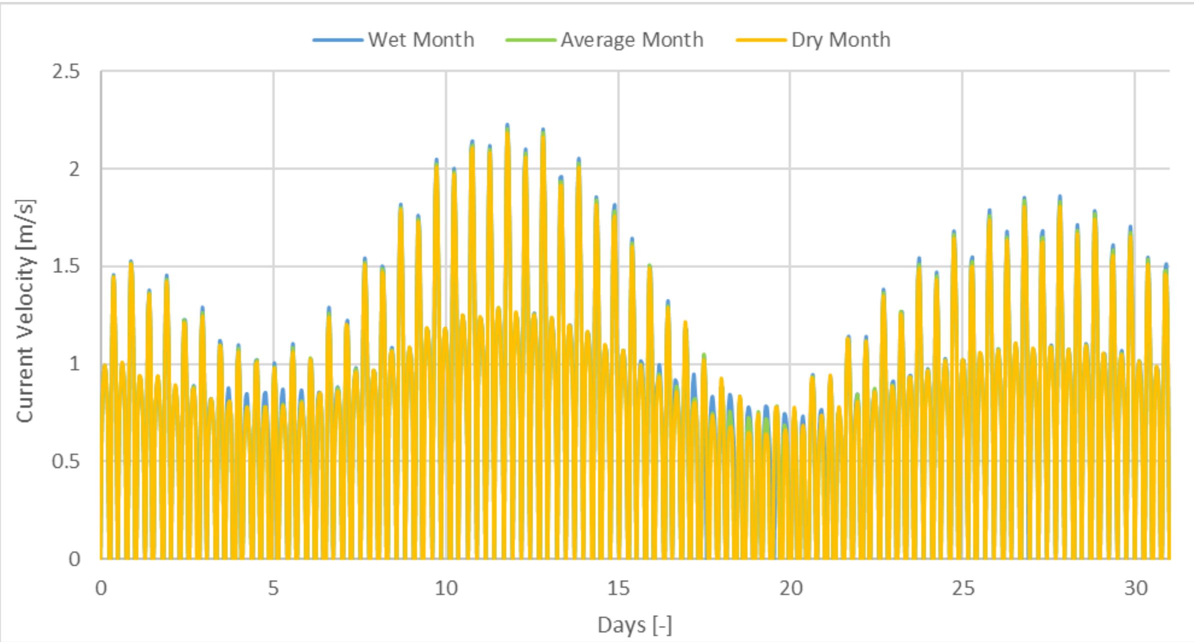

Figure A3 - 2 -Water velocities through a turbine on the highest energy density site (with an exclusion zone) of the simulated months

Belém Region:

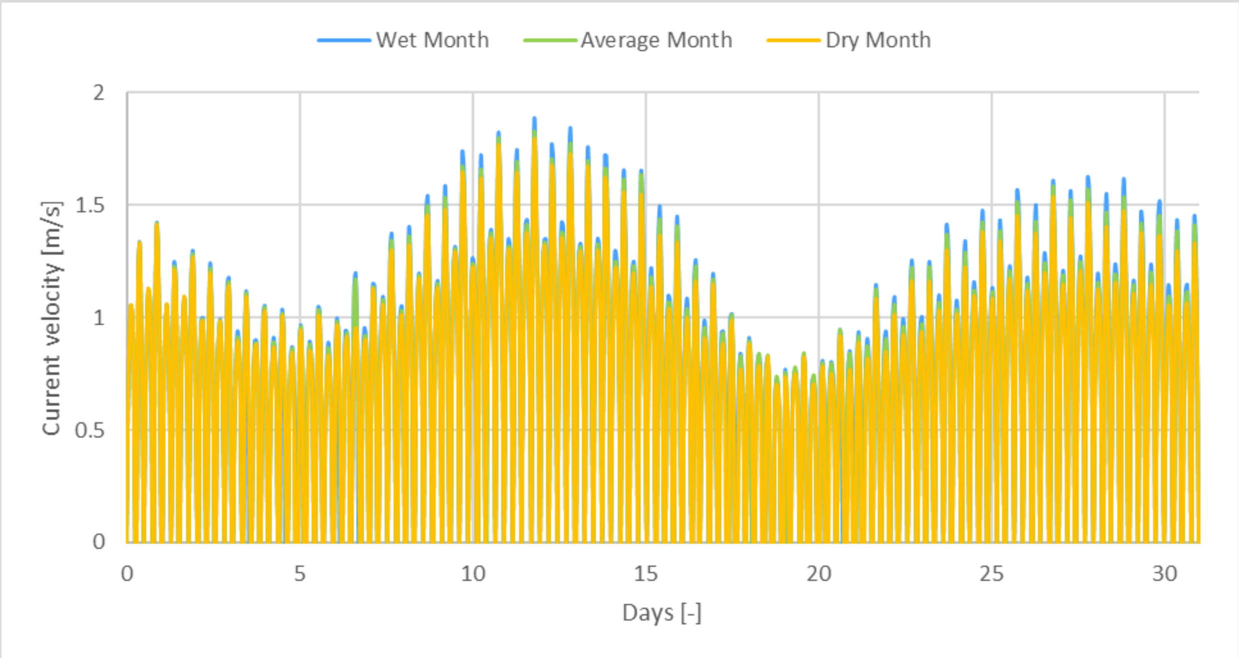

Figure A3 - 3 -Water velocities through a turbine on the highest energy density site of the simulated months

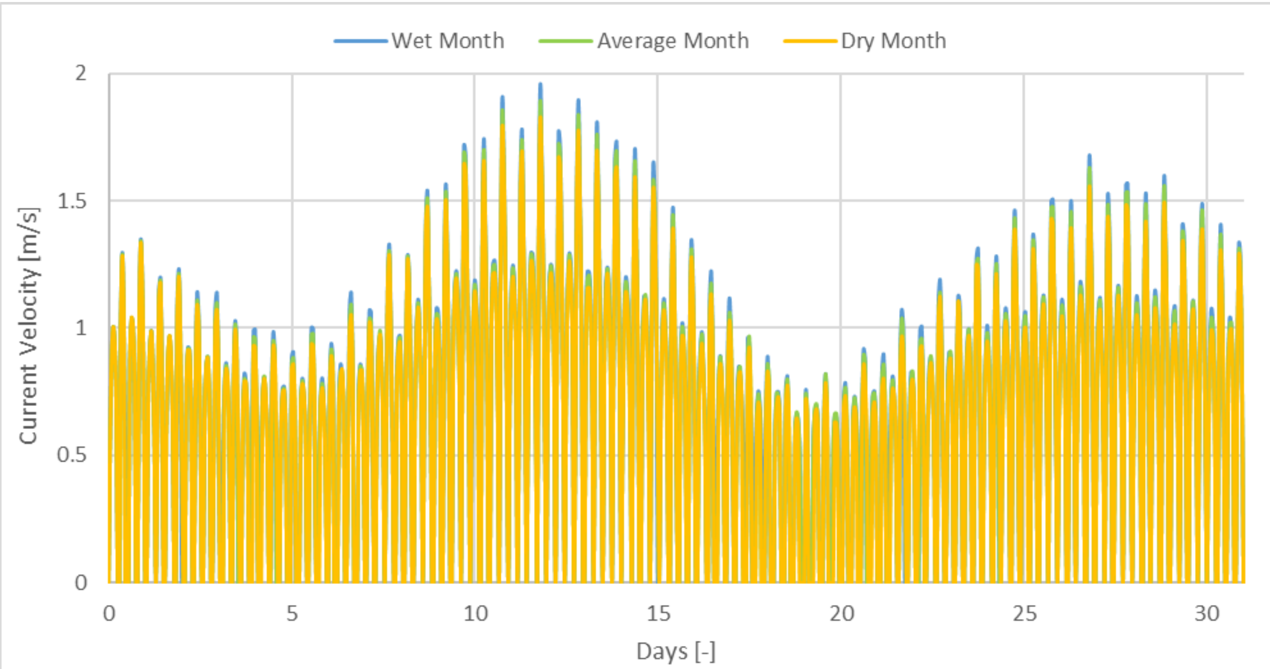

Figure A3 - 4 -Water velocities through a turbine on the highest energy density site (with an exclusion zone) of the simulated months

Cais do Sodré Region:

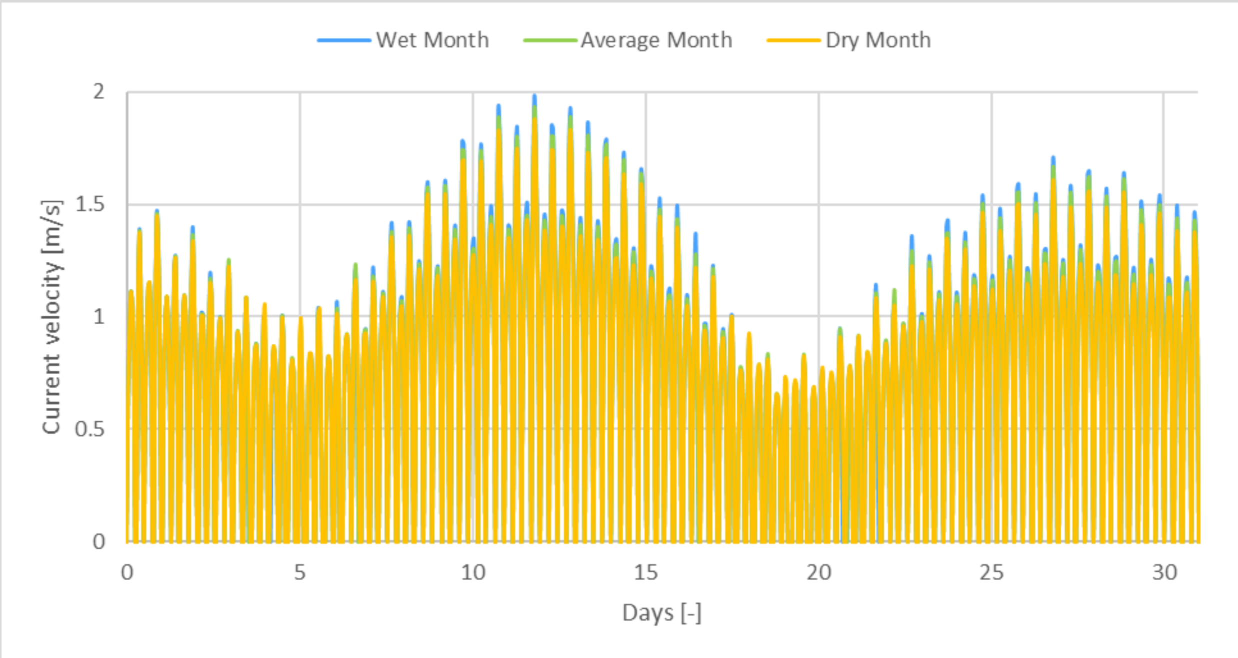

Figure A3 - 5 -Water velocities through a turbine on the highest energy density site of the simulated months

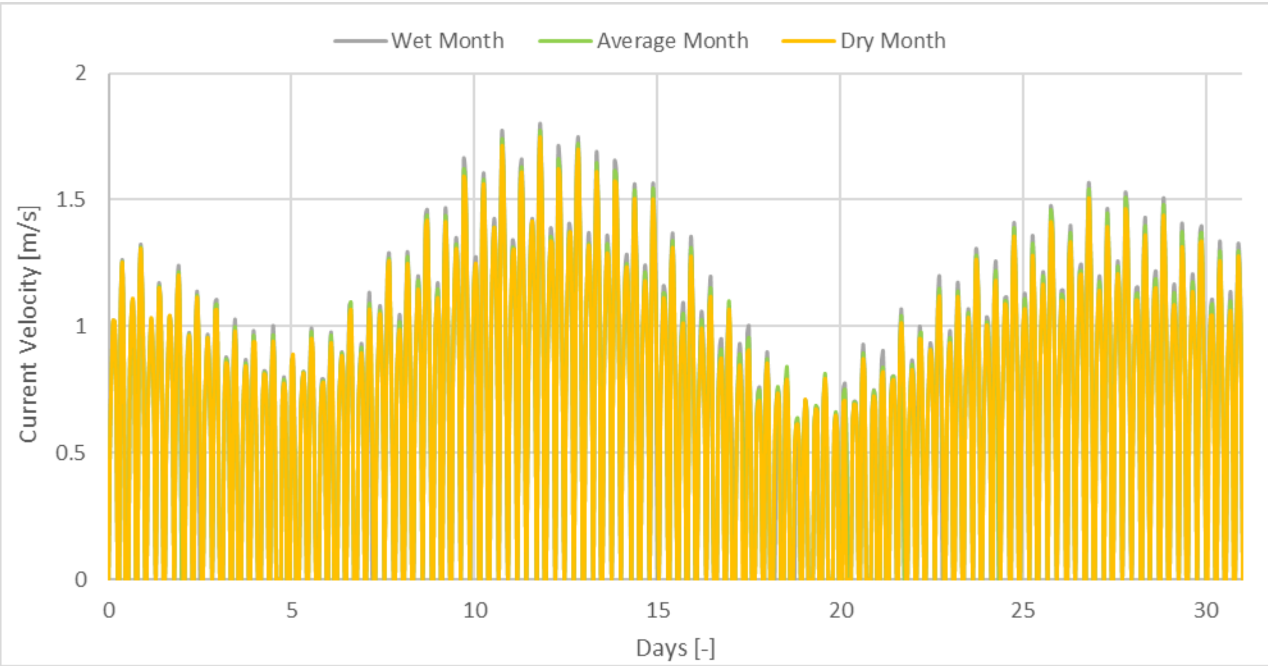

Figure A3 - 6 -Water velocities through a turbine on the highest energy density site (with an exclusion zone) of the simulated months

Annex 4: Turbine's Monthly Energy Production

This annex presents the figures with the monthly energy production of each turbine and for each simulated month.

Oeiras Region:

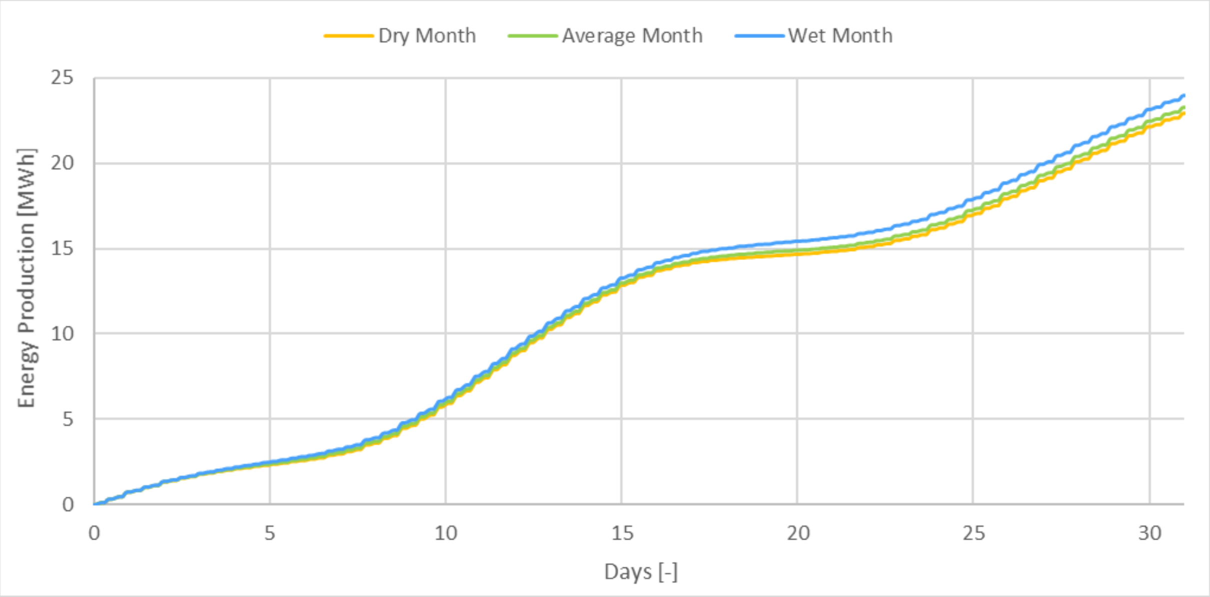

Figure A4 - 1 -A single turbine's monthly energy production on the highest energy density area

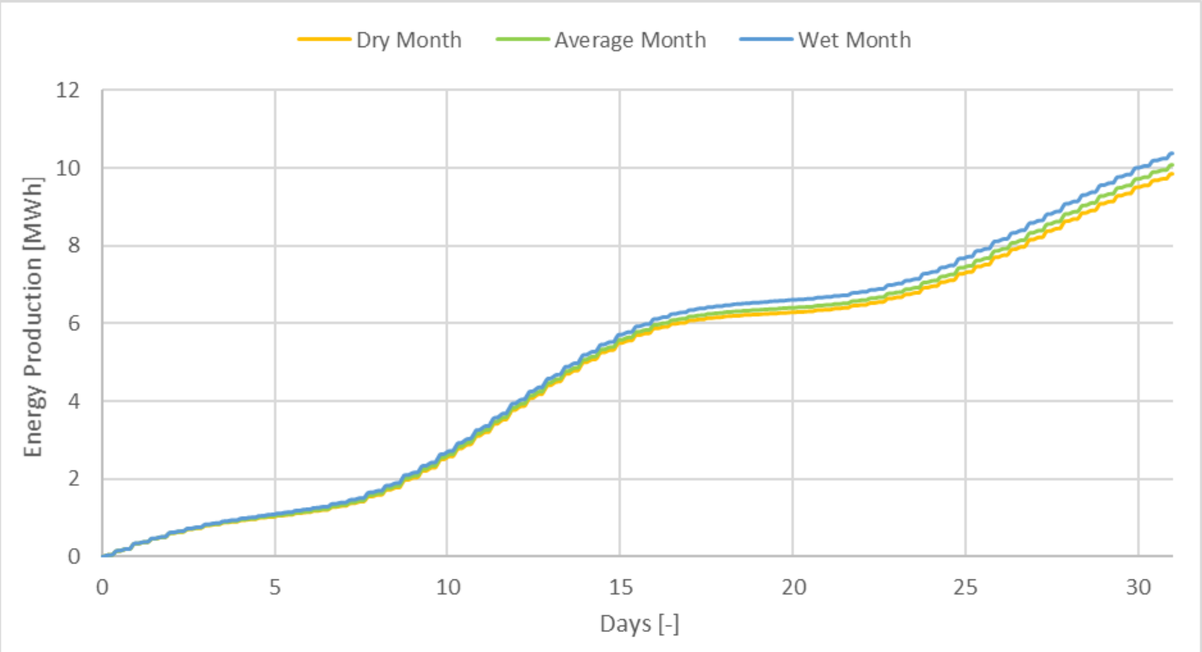

Figure A4 - 2 -A single turbine's monthly energy production on the highest energy density area (with an exclusion zone)

Belém Region:

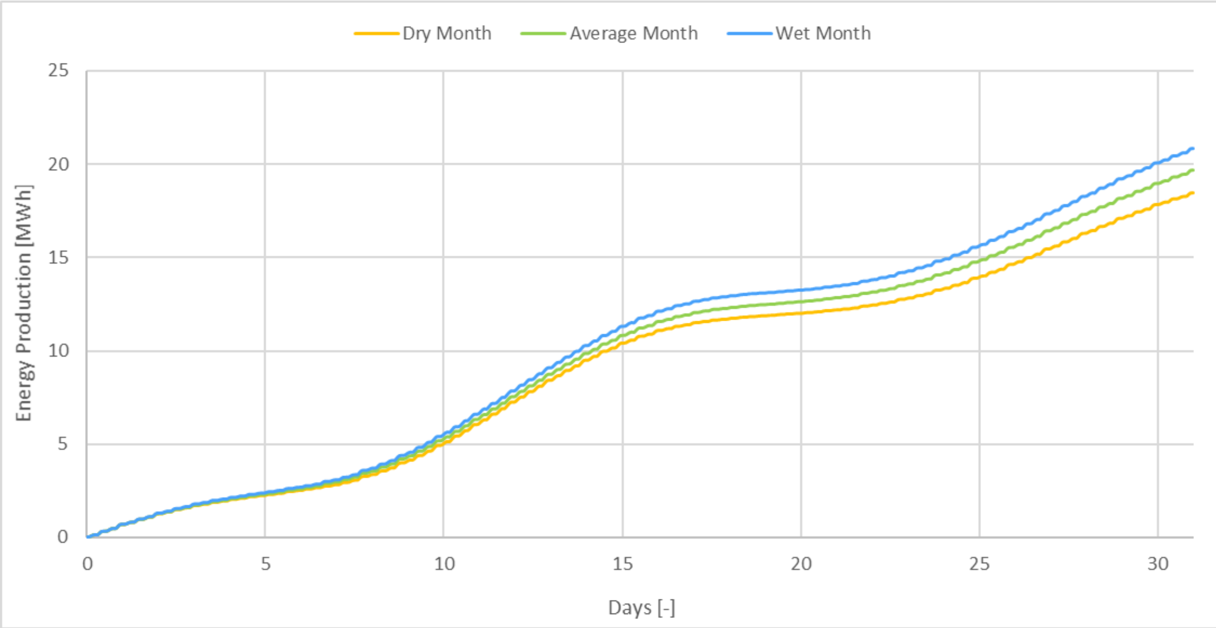

Figure A4 - 3 -A single turbine's monthly energy production on the highest energy density area

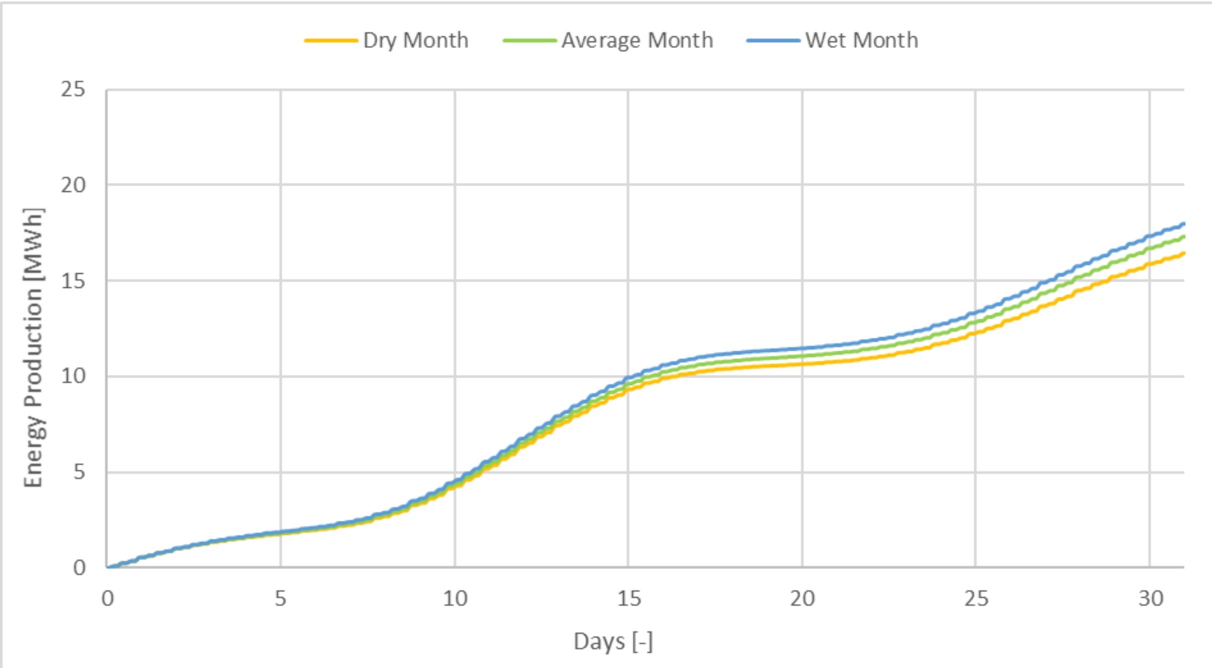

Figure A4 - 4 -A single turbine's monthly energy production on the highest energy density area (with an exclusion zone)

Cais do Sodré Region:

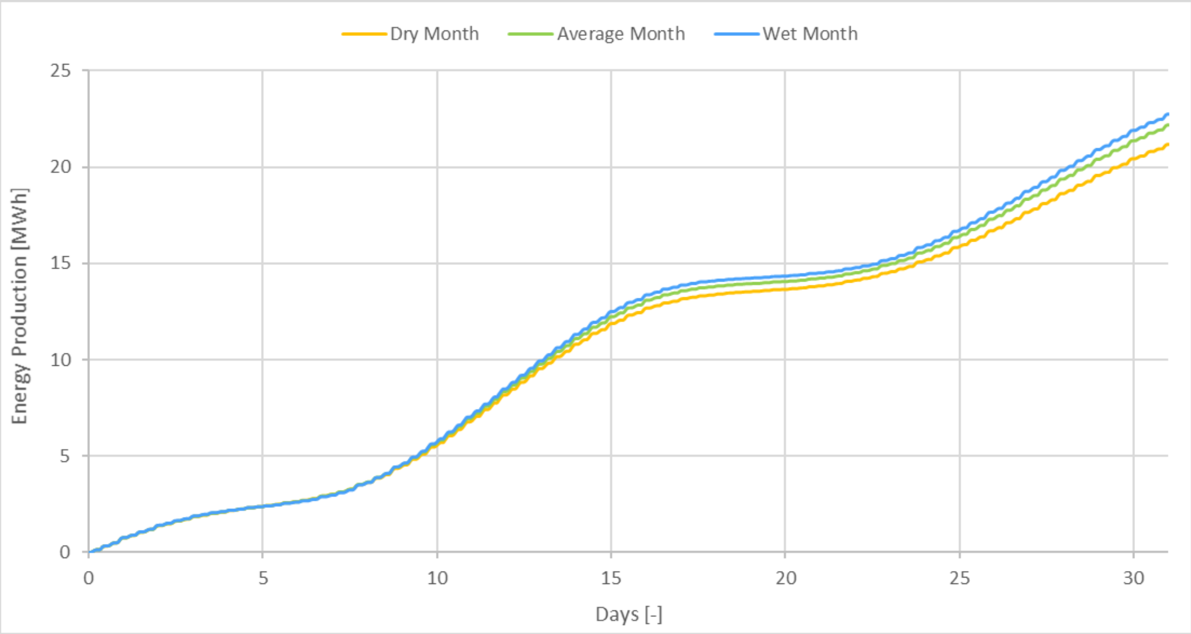

Figure A4 - 5 -A single turbine's monthly energy production on the highest energy density area

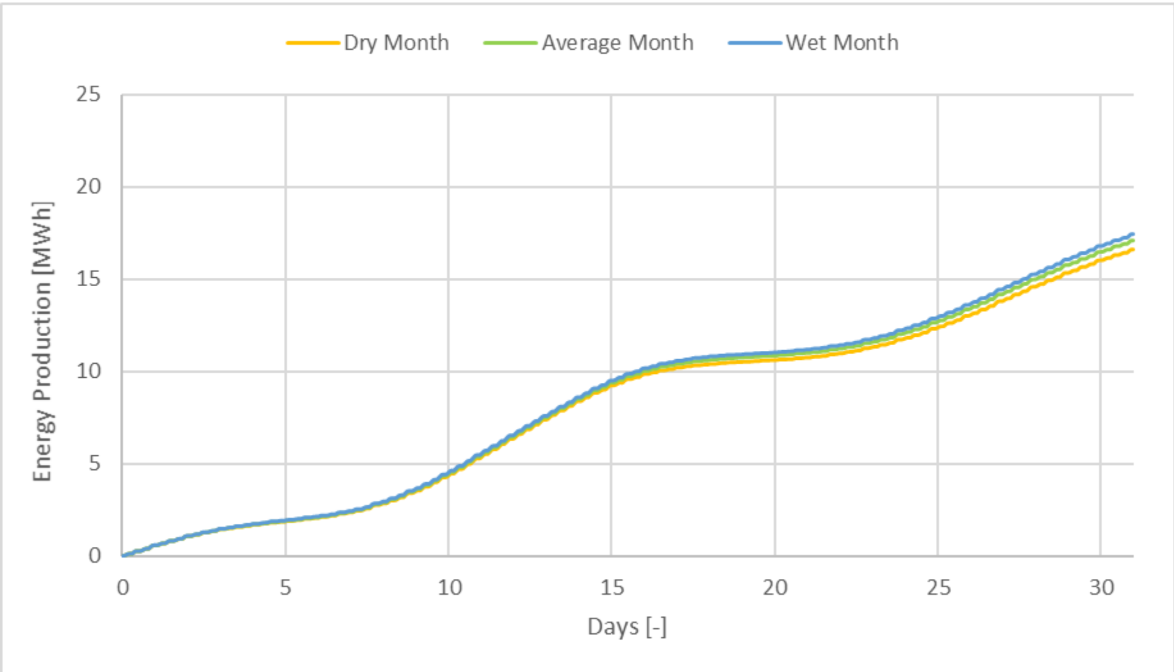

Figure A4 - 6 -A single turbine's monthly energy production on the highest energy density area (with an exclusion zone)

Annex 5: Comparison between the Turbines' MEP Assessment Methods

This annex presents the figures with the comparison between the turbines' monthly energy production assessment methods, for an average water discharge simulated month.

Oeiras Region:

Figure A5 - 1 -Comparison of assessment methods of a single turbine's monthly energy production on the highest energy density area

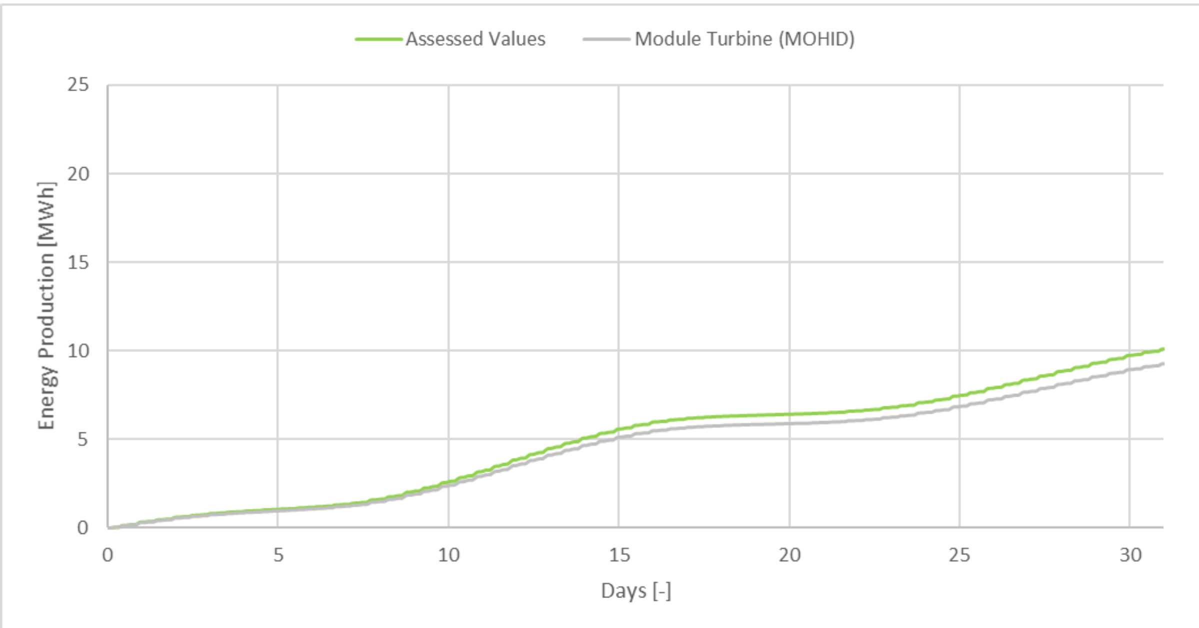

Figure A5 - 2 -Comparison of assessment methods of a single turbine's monthly energy production on the highest energy density area (with an exclusion zone)

Belém Region:

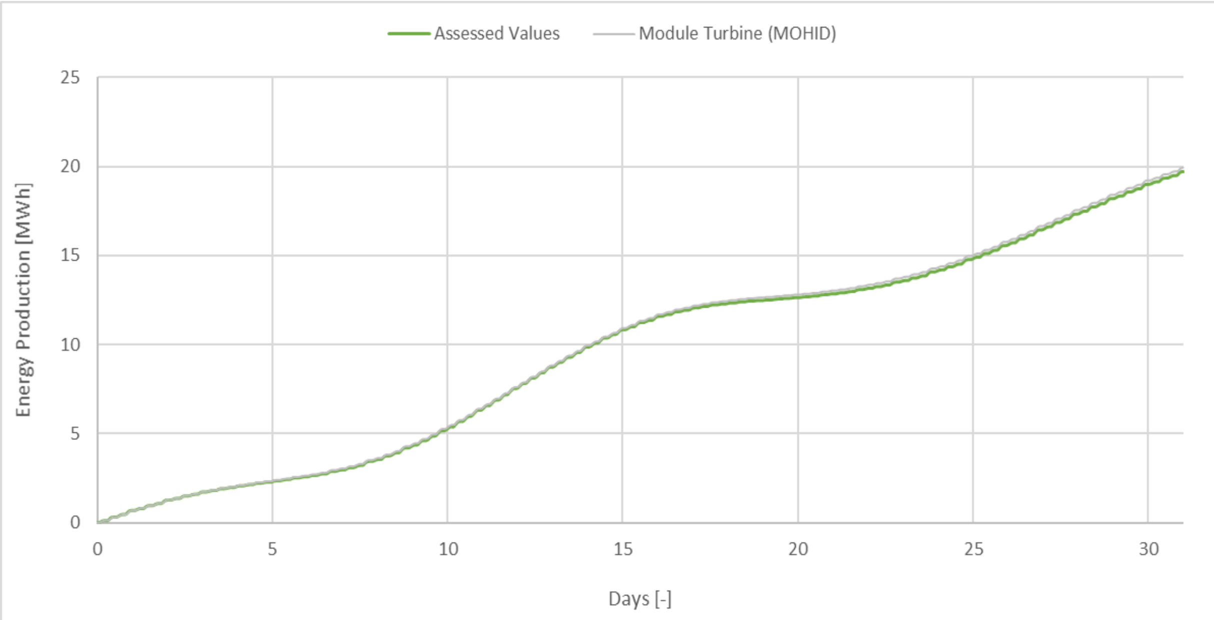

Figure A5 - 3 -Comparison of assessment methods of a single turbine's monthly energy production on the highest energy density area

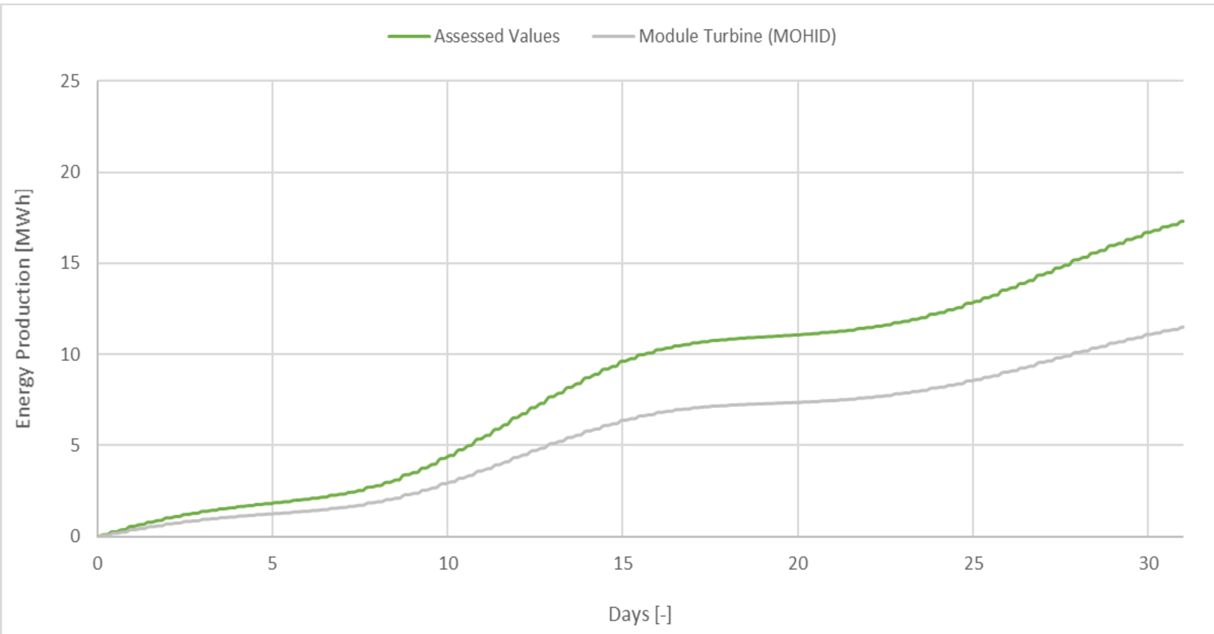

Figure A5 - 4 -Comparison of assessment methods of a single turbine's monthly energy production on the highest energy density area (with an exclusion zone)

Cais do Sodré Region:

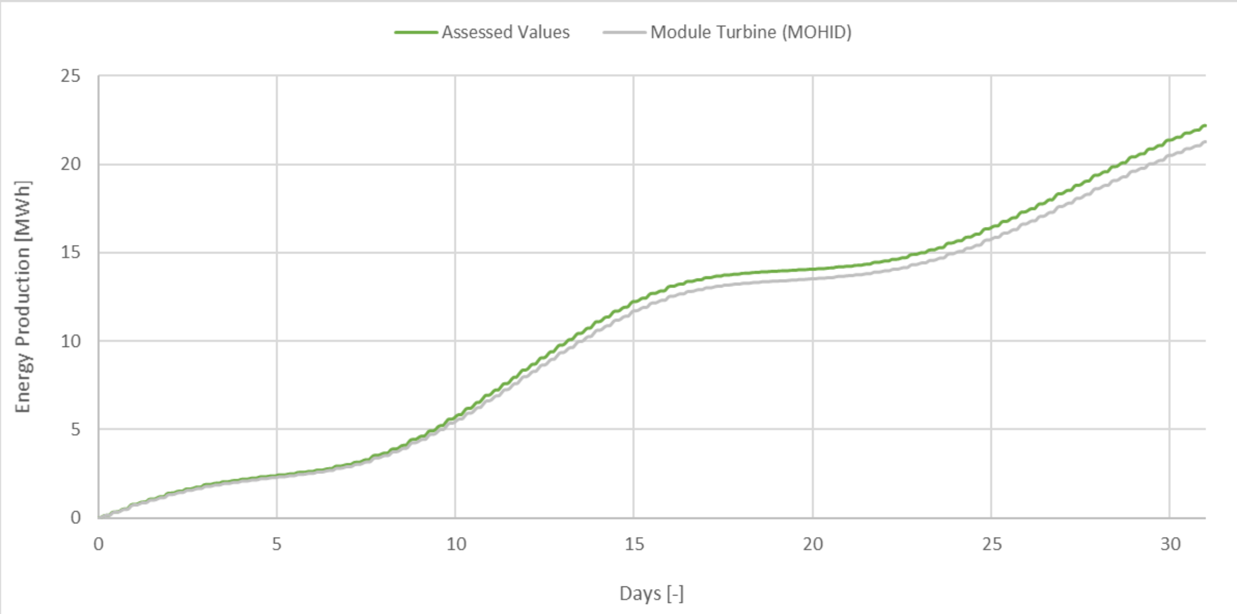

Figure A5 - 5 -Comparison of assessment methods of a single turbine's monthly energy production on the highest energy density area

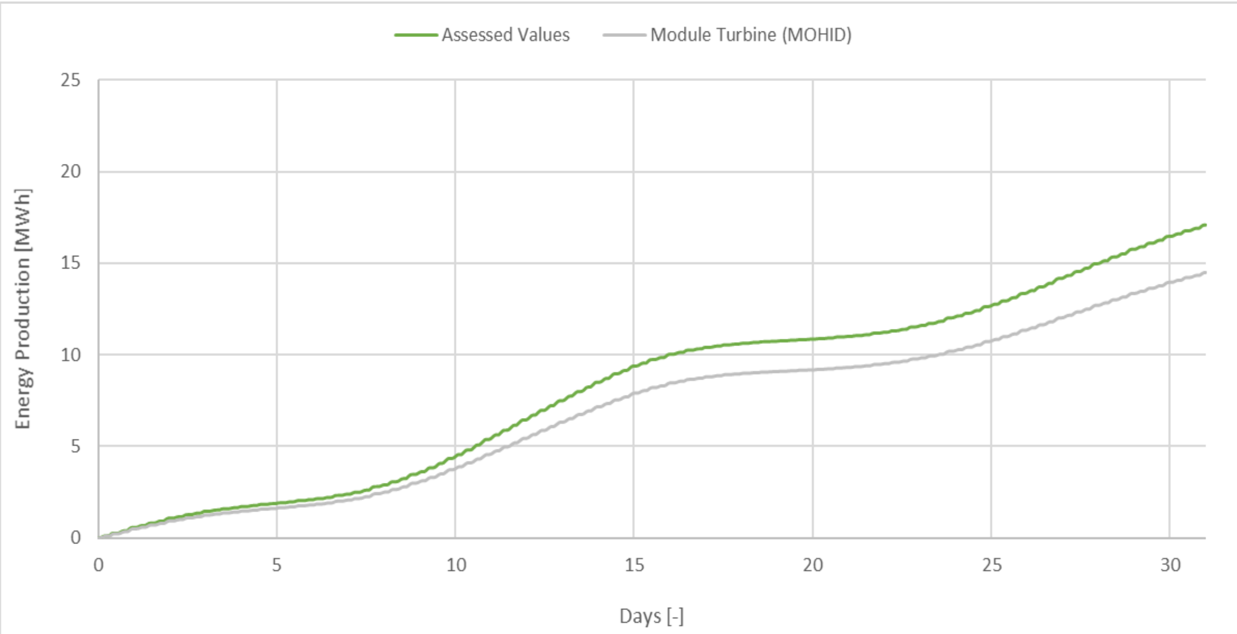

Figure A5 - 6 -Comparison of assessment methods of a single turbine's monthly energy production on the highest energy density area (with an exclusion zone)